

A SENSITIVE SPECTRAL SURVEY OF INTERSTELLAR FEATURES IN THE NEAR-UV [3050-3700Å].

N. H. BHATT¹ AND J. CAMI^{1,2}

¹Department of Physics and Astronomy, The University of Western Ontario, London, ON N6A 3K7, Canada

²SETI Institute, 189 Bernardo Avenue, Suite 100, Mountain View, CA 94043, USA

Accepted for publication in ApJS

ABSTRACT

We present a comprehensive and sensitive unbiased survey of interstellar features in the near-UV range (3050-3700 Å). We combined a large number of VLT/UVES archival observations of a sample of highly reddened early type stars – typical diffuse interstellar band (DIB) targets – and unreddened standards. We stacked the individual observations to obtain a reddened “superspectrum” in the interstellar rest frame with a signal-to-noise (S/N) ratio exceeding 1500. We compared this to the analogous geocentric and stellar rest frame superspectra as well as to an unreddened superspectrum to find interstellar absorption features. We find 30 known features (11 atomic and 19 molecular) and tentatively detect up to 7 new interstellar absorption lines of unknown origin. Our survey is sensitive to narrow and weak features; telluric residuals preclude us from detecting broader features. For each sightline, we measured fundamental parameters (radial velocities, line widths, and equivalent widths) of the detected interstellar features. We also revisit upper limits for the column densities of small, neutral polycyclic aromatic hydrocarbon (PAH) molecules that have strong transitions in this wavelength range.

Subject headings: ISM: atoms – ISM: molecules – line: identification – methods: observational – stars: early-type

1. INTRODUCTION

The interstellar medium (ISM) is chemically rich: almost 200 molecular carriers have been detected in space (see e.g. Müller et al. 2001, 2005; Tielens 2013) as well as many atomic species. In addition, there remains an unidentified class of gas phase molecular carriers thought to be responsible for a series of over 400 interstellar features - the diffuse interstellar bands (DIBs) - that are observed in lines of sight that intersect interstellar clouds (see Herbig 1995; Sarre 2006 for reviews; for DIB surveys, see Jenniskens & Desert 1994; Tuairisg et al. 2000; Hobbs et al. 2008, 2009). The DIB carriers are presumably a collection of stable, carbonaceous molecules that are widespread and abundant in space. They are most likely related to carbon chains, polycyclic aromatic hydrocarbons (PAHs) or fullerene compounds.

Many molecular species – including some of these proposed DIB carriers – could be in principle detected and identified in the UV and the near-UV. For instance, laboratory measurements of small neutral PAHs show strong transitions in the near-UV. Recently, Salama et al. (2011) and Gredel et al. (2011) therefore compared their laboratory data to near-UV archival data of reddened targets. No PAH features were reliably detected, but Gredel et al. (2011) found several other molecular absorption lines in this range (due to CH, CH⁺, NH, CN, and even OH⁺).

However, while the ISM has been extensively studied in the optical and infrared ranges, the near-UV remains relatively unexplored in comparison, and thus our inventory of interstellar spectral features may be incomplete. Indeed, to the best of our knowledge, an unbiased search for interstellar features and possible DIBs in this wave-

length range has not yet been presented in the literature. This lack of detailed studies reflects the challenges of observing in the near-UV such as generally poor instrumental sensitivity and significant telluric ozone absorption. Here, we present such an unbiased survey using archival data from the UVES instrument mounted on the VLT. UVES is one of the few instruments that has a good sensitivity in the near-UV; we furthermore increase our sensitivity by co-adding a large number of spectra.

This paper is organized as follows. We begin by detailing our data set and processing steps in §2. §3 then describes the methodology we used to search for interstellar features, our sensitivity limits and results. We discuss our results in § 4, and also revisit upper limits on the column densities of small, neutral PAHs. We summarize our work in § 5.

2. OBSERVATIONS AND DATA REDUCTION

Our goal is to search in the near-UV for interstellar lines, and those are often weak and narrow. We thus require at the same time high spectral resolution and good sensitivity. Very few instruments offer both at the same time in the near-UV. The UVES instrument (Dekker et al. 2000) mounted on the Very Large Telescope (VLT) is ideally suited since it covers the range \sim 3000Å–11000Å at high spectral resolution. For the near-UV range of interest, we only need data using the standard 346 setting (centered around 346 nm) on the blue arm of the instrument, covering the range 3030Å–3880Å at a maximum resolving power of 82,000. The ESO archive contains a large data set of UVES 346 observations (both raw and fully reduced data) for many targets that are suitable for our study here, and we thus exclusively use UVES archival data in this paper.

2.1. Sample Selection

The ideal targets for our survey are stars that sample a sight line with significant amounts of interstellar material, that exhibit few confusing stellar lines, and that are bright enough to have sufficient flux in the near-UV. Reddened, early-type (O and B) stars are thus ideal targets – criteria that are also characteristic for DIB targets. We searched the UVES archive for such targets, and not surprisingly, a significant fraction of the data we use here stems indeed from observational DIB programs or from programs studying translucent clouds. Our study here includes 185 observations of 51 reddened targets (see Table 3).

In addition to our reddened targets, we also searched for a large number of unreddened comparison stars. Such standards are important to better establish the nature (instrumental, telluric, stellar or interstellar) of spectral features. We found these targets by searching SIMBAD for all stars with spectral type O or B with $B - V < 0.1$ and with at least 100 literature references. Using this list of ~ 1000 targets, we searched the UVES archives and obtained 300 observations corresponding to 50 unreddened targets. From this collection, we then visually inspected each observation, discarding observations that showed a clear interstellar Na I line, or exhibited either possible reduction problems or instrumental residuals. After this filtering, 166 observations corresponding to 39 unreddened targets remained.

Our final data set thus consists of 351 spectra, obtained with a resolving power between 58,000–71,000 for the reddened targets, and 40,000–71,000 for the unreddened targets. The full list of targets, along with basic data and the corresponding ESO programs are listed in Table 3.

2.2. Data Reduction

For most of our targets, we obtained fully reduced spectra from the UVES-ESO reprocessed archive¹. However, for some targets, clear artefacts were present in these standard pipeline products (due to e.g. incorrect order merging). For these targets, we obtained the raw data² and carried out the data reduction ourselves. We similarly retrieved the raw data from the archive for those targets for which fully reduced data were not yet available in the reprocessed archive.

We processed the raw data using the Gasgano³ file organizer with the UVES pipeline (version 5.0.9), and followed the `uvess_obs_scirec` recipe to reduce the raw observations. This recipe performs bias and dark frame subtraction, flat-fielding, wavelength calibration, automated order detection, background subtraction, optimal extraction, and optimal merging. We retrieved the necessary observation-specific calibration files (bias, dark, flat and arc lamp frames) from the ESO archive. Other calibration files (catalog of arc lines, arc lamp frame, atmospheric extinction table, standard star, format check frame) are provided with Gasgano. The final product is a full, calibrated spectrum, similar to what is provided in the reprocessed archive.

A visual inspection of all reduced spectra revealed systematic artefacts in some observations, showing up as

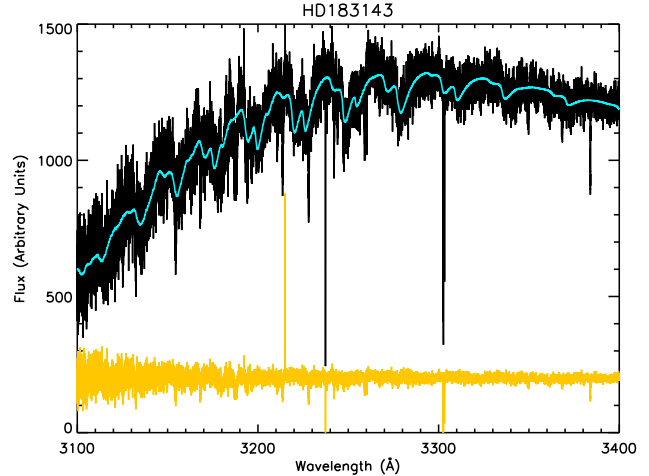


FIG. 1.— An example of the telluric ozone correction, where we have divided the UVES spectrum of HD 183143 (top; black) by the best fit telluric ozone spectrum (top; cyan), resulting in the corrected spectrum (bottom; gold; shown here $\times 200$ for clarity).

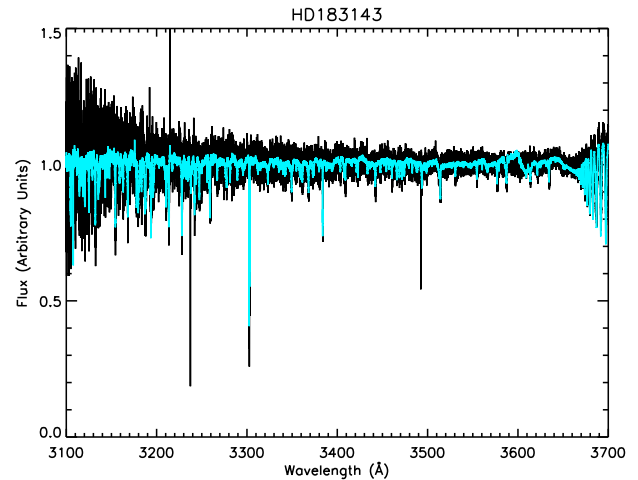


FIG. 2.— An example of the gain in quality obtained from co-adding observations. A single, processed spectrum of HD 183143 is shown in black, and the co-added spectrum (including four observations) is shown in cyan.

repeating undulations with a period of one echelle order. This issue is well documented⁴, but is not easily corrected. In the most severe cases, we excluded the spectra from our study. We kept some of the mildly affected spectra, reasoning that the artefacts are much broader than the typical features we will be searching for and thus should not interfere much with our goals. The signal-to-noise ratio is variable across the spectrum. The spectra are quite noisy at the shortest wavelengths (around 3040 Å) due to the low sensitivity of the instrument at these wavelengths, but the quality improves at longer wavelengths; Table 3 gives some indication of how the quality varies across our sample.

2.3. Further Processing

We carried out some additional processing steps to facilitate further analysis and improve the sensitivity of our search. First, we flagged bad pixels and cosmic ray

¹ http://archive.eso.org/eso/eso_archive_adp.html

² http://archive.eso.org/wdb/wdb/eso/eso_archive_main/query

³ <http://www.eso.org/sci/software/gasgano/>

⁴ <http://www.eso.org/observing/dfo/quality/reproUVES/processing.html>

hits, and replaced the flux values at these points with interpolated values while assigning a large uncertainty.

Next, we corrected our spectra for the strong contamination due to telluric ozone in the near-UV. In our spectra, absorption in the Huggins band is clearly present in the range 3100–3400 Å (see Fig. 1). Ideally, one would divide the spectrum of a reddened target by the spectrum of an unreddened, broad-lined reference star of the same spectral type observed at a similar airmass and close in time to the target. Good pairwise reference observations however are not available in the archive for most of our targets. Furthermore, dividing by a standard decreases the S/N in the bluest parts of the spectrum where sensitivity is already low. We therefore opted for an alternative approach to remove the ozone signature, similar to Herbig (2000). We used O₃ absorption cross sections from Burrows et al. (1999) and determined the ozone column density for each observation that provides the best match to the spectrum in that range. We then divided out the ozone spectrum from the observations. As can be seen from Fig. 1, this removes all of the broad structure visible in the spectrum. However, since the cross sections are sampled at a much lower spectral resolution than our observations, narrow telluric features may still be left in the spectra (see § 3.2). We also compared our spectra to the absorption cross-sections of several other atmospheric species (e.g. BrO, ClO₂, H₂CO, and SO₂)⁵ but did not find evidence for any of them in our spectra. Note that narrow telluric residuals remain, but will not pose insurmountable problems for our work (see Sect. 3).

Next, we determined the broad-band continuum for each our spectra by fitting a cubic spline through a small number of anchor points that were iteratively determined to best reproduce the observed stellar continuum. The resulting curve reproduces all broad-band spectral variations, including many (broad) artefacts remaining from the data reduction process. Our routine has some difficulties near the Balmer discontinuity, resulting in artefacts in the spectrum. However, these will not affect our further analysis much. After inspection, we normalized our observations to this continuum.

We then applied a heliocentric correction to all individual observations, and determined the signal-to-noise ratio of each spectrum from the mean flux and standard deviation in a wavelength range devoid of obvious spectral features (3450Å–3452Å). For each target, we then co-added the individual spectra by calculating the weighted mean flux at each wavelength where the weights are inversely proportional to the variance in the data. For the remainder of this paper, we will refer to this weighted average spectrum of a target as the *optimal spectrum*. Fig. 2 illustrates the dramatic gain in quality that results from this operation. For our survey described below, we thus start from a single, high-quality optimal spectrum for each of our 90 reddened and unreddened targets.

3. A SEARCH FOR INTERSTELLAR FEATURES

3.1. Methods

Interstellar spectral features can have different appearances. For lines of sight that intersect only one interstellar cloud, atomic (ionic) and simple molecular lines are

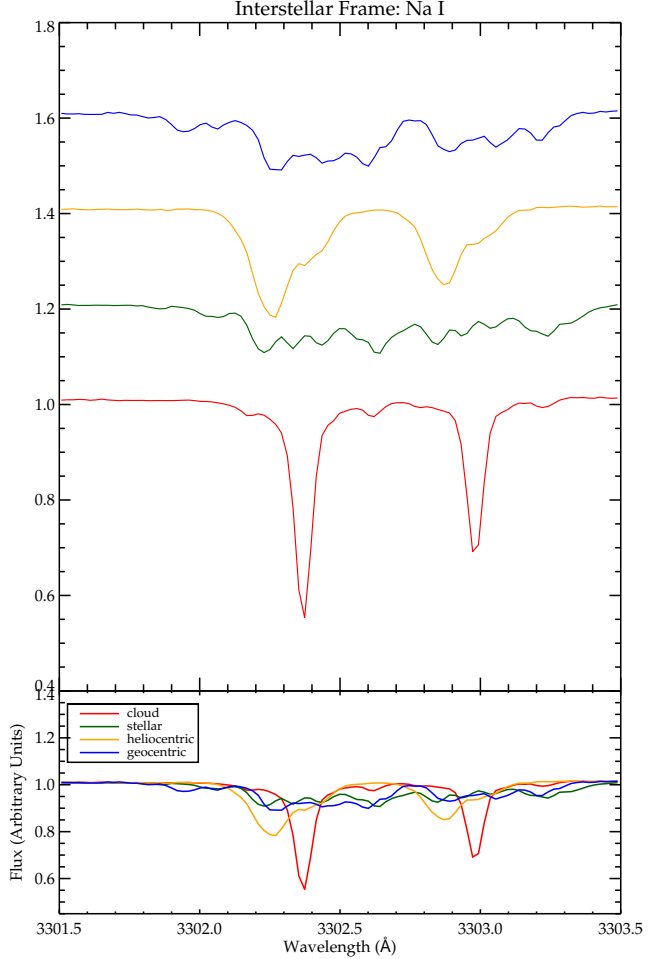


FIG. 3.— The four superspectra in the spectral region around the Na I 3302.368/3302.987 Å doublet for respectively the geocentric (top; blue), heliocentric (yellow), stellar (green) and interstellar (bottom; red) rest frame. The bottom panel shows all four spectra on top of each other.

generally very narrow since their intrinsic line width is determined primarily by the velocity dispersion in the cloud. Such lines are generally easy to detect and recognize. DIBs on the other hand have a wide range of intrinsic widths and profiles (see e.g. Westerlund & Krelowski 1988; Ehrenfreund & Foing 1996; Kerr et al. 1996; Krelowski & Schmidt 1997; Galazutdinov et al. 2001; Snow et al. 2002; Galazutdinov et al. 2002, 2008).

Several methods can be used to search for interstellar features. Observations of spectroscopic binaries at different orbital phases provide a clear way to separate stellar from interstellar lines owing to the stationary nature of the latter lines (see e.g. Hobbs et al. 2008, for a recent example). While powerful, this method can only be used for lines of sight where a suitable binary is available. DIB surveys have therefore often reverted to using a pair-wise comparison between reddened targets and unreddened standards of the same spectral type to distinguish stellar from interstellar lines (see e.g. Herbig 1975; Jenniskens & Desert 1994; Tuairisg et al. 2000; Hobbs et al. 2009). However, even with a good spectral match, some ambiguities often remain in recognizing (especially broad) interstellar lines (see e.g. Hobbs et al. 2009).

⁵ <http://hitran.iao.ru/xsections>

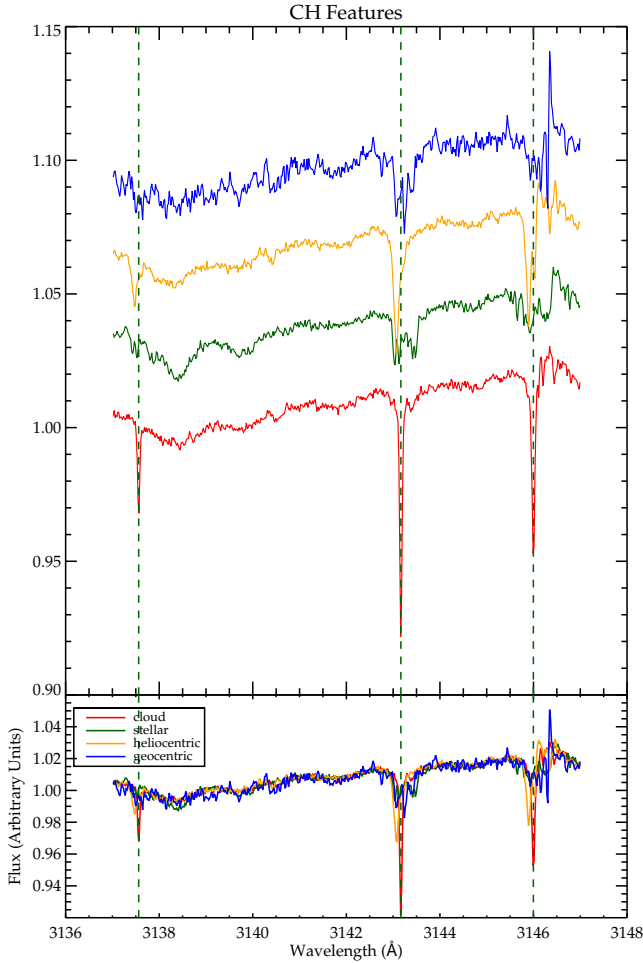


FIG. 4.— The geocentric (top; blue), heliocentric (yellow), stellar (green) and interstellar (bottom; red) superspectra between 3137Å and 3148Å. A triplet of CH features shows up prominently in our interstellar superspectrum. These lines appeared moderately strong in about half of the reddened sightlines.

Here, we tried out a different approach that is based on having a large sample of reddened targets. The basic premise is that stellar and interstellar radial velocities are generally quite different for each of our targets, and are either known and/or easy to determine. By shifting all of our target spectra to their respective interstellar cloud rest frame, interstellar features line up, while stellar lines are spread out; co-adding will thus result in stellar lines that are broadened and weakened, but the interstellar lines should be fairly prominent (and relatively narrow). Similarly, when shifting to the stellar rest frame and co-adding, stellar lines are emphasized while interstellar lines are smeared out. A comparison between these two co-added “*superspectra*” should thus – in principle – readily reveal all interstellar features. Additionally, the co-added superspectrum has a much higher signal-to-noise ratio which allows to detect even weak features (provided that they are weakly present in a majority of the targets). An important caveat though is that most of our reddened targets are not single cloud lines of sight, i.e. their interstellar lines show more than one component at different radial velocities. Some interstellar features may not be present in all components.

In practice, we first determined stellar radial velocities

for all of our targets from cross-correlating the observed spectrum with a simple synthetic spectrum comprised of only hydrogen and helium lines. To determine the interstellar cloud velocities, we first note that all (reddened) targets clearly show the narrow absorption lines in the Na I doublet at 3302Å. In all cases, we have measured the radial velocity corresponding to the deepest absorption in this Na I doublet. Table 3 lists all radial velocities we measured in this way. Where available, we have compared our results to literature values and found good agreement.

We then created four different superspectra (see e.g. Fig. 3), and refer to them by the radial velocity rest frame to which the individual spectra were shifted before co-adding. The geocentric superspectrum corresponds to no shifts at all, and is useful to recognize telluric features. The heliocentric superspectrum is the co-add after applying just a heliocentric correction to the spectra. We then shifted all spectra to their stellar rest frame, and the resulting co-add is the stellar superspectrum. Finally, the interstellar superspectrum results from co-adding the spectra shifted to the interstellar rest frame. Note that each of the superspectra is a weighted mean, where the weights are again inversely proportional to the variance of the individual optimal spectra.

To illustrate our method, we first present in Fig. 3 the four superspectra around the Na I doublet near 3302Å. As expected, the Na I lines are sharp and well-defined in the interstellar superspectrum. Note that the superspectrum even records a smaller secondary peak originating from the fact that most lines of sight have multiple clouds in the line of sight. Fig. 4 shows the same superspectra around a triplet of known interstellar CH features at 3137.530Å, 3143.150Å and 3146.010Å. Also these lines are much better defined in the interstellar superspectrum, thus establishing their interstellar nature. This forms the basis of our search for interstellar features in the near-UV.

3.2. Sensitivity & Limitations

Throughout our entire wavelength range, the S/N of the interstellar superspectrum is typically ≥ 1500 . Thus, the 3σ detection limit for an unresolved line (FWHM $\sim 45\text{m}\text{\AA}$) is technically $W \approx 0.1\text{m}\text{\AA}$. However, we found that this is an optimistic estimate of our sensitivity, since a detection stems from a comparison to the other superspectra, and those have different noise characteristics (see below). As a test, we introduced a synthetic feature in the optimal spectra of each of our targets and tried to detect it in the superspectrum. We found that a more realistic estimate of our detection limit is $W \gtrsim 0.3\text{m}\text{\AA}$ (as illustrated in Fig. 5).

It is clear that the apparent S/N in the various superspectra (as measured from the variance in the flux in a region without clear spectral lines) is quite different, even though they result from co-adding the same optimal target spectra (see Fig. 5). The S/N is systematically lowest (by a large margin) for the geocentric superspectrum. This is not indicative of the quality of the spectra, but must be the consequence of having a large number of weak and narrow telluric features in our spectra that get smeared out in the other superspectra. While it is reassuring to see that very little is left of these features in

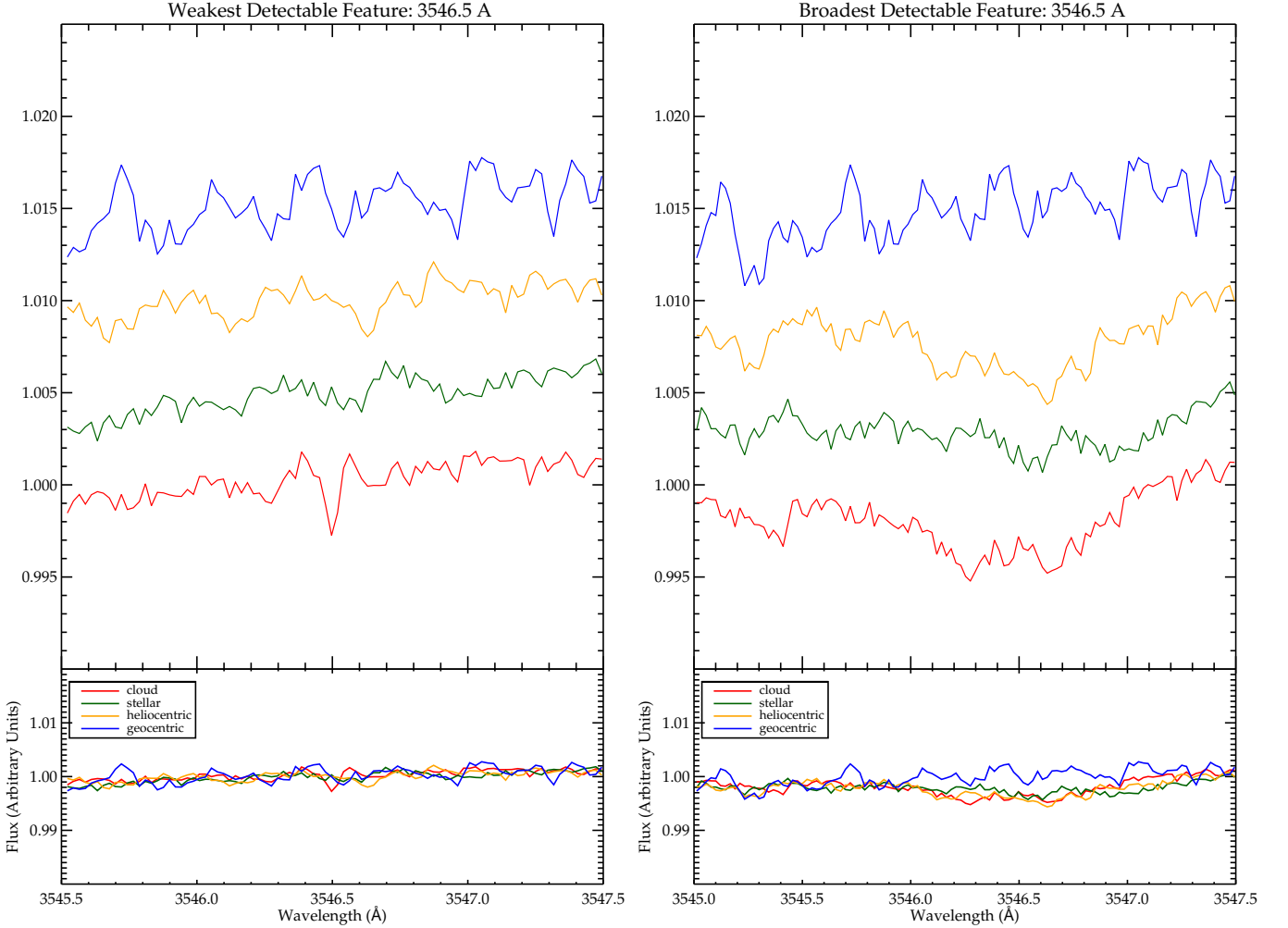


FIG. 5.— The superspectra after introducing an artificial interstellar feature in each of the target optimal spectra (at an interstellar rest wavelength of $\lambda=3546.500\text{\AA}$). Both panels show the geocentric (top; blue), heliocentric (yellow), stellar (green) and interstellar (bottom; red) superspectra. Note that the geocentric superspectrum does not contain the artificially introduced features and is shown only for comparison. (*Left:*) the artificial feature is an unresolved line with an equivalent width of $W = 0.3\text{m\AA}$. This is about the weakest unresolved feature we can detect. (*Right:*) the artificial feature now has a FWHM of 0.8\AA and a depth of about 0.5% (corresponding to an equivalent width of $W \approx 6\text{m\AA}$). This is about the broadest weak feature that we can reliably detect as an interstellar feature.

the interstellar superspectrum, it turns out that chance superpositions sometimes result in weak features in the other superspectra. This is further discussed in Sect. 3.3.

A clear limitation of our method is that we are not sensitive to broad (and shallow) interstellar features. Indeed, for broad lines, there is not enough contrast between the interstellar and stellar superspectra to reliably detect such features or to tell them apart from what could be stellar lines. To get a sense of this limit, we once more introduced a feature in each of the optimal spectra, with a depth of 0.5% and changing the FWHM of the feature until we could not reliably identify it as an interstellar feature anymore. We found that this limit is at a FWHM of about 0.8\AA , corresponding to an equivalent width of $W \approx 6\text{m\AA}$. This is thus the broadest weak interstellar feature we could hope to detect with our method (see Fig. 5).

In the process of searching for interstellar lines described below, we also considered some variations on our strategy to improve the detection probability. Sometimes, it is advantageous to not include all lines of sight

in the superspectrum. Indeed, if a feature only appears in a small number of sightlines, the feature would be damped in the superspectrum by the larger number of spectra where the feature is absent. Thus, such a feature may be more easily detected by excluding these latter targets and making a superspectrum of a smaller subset of spectra. This then results in a larger contrast in the feature, which can sometimes more than compensate for the lower S/N of the resulting co-add. However, in practice we detected all features in the superspectra comprised of all 51 reddened targets although we found it helpful to consider well-defined subsets of targets (e.g. the most or least reddened) for distinguishing between artefacts and potential interstellar features.

Finally, we also compared the reddened superspectrum to the corresponding unreddened superspectrum (see e.g. Fig. 15). Note that stellar lines between the two do not match, since the spectral types of the contributing targets in both cases is different. However, it is often an insightful comparison that can give more confidence that weak features are truly interstellar lines.

TABLE 1
INTERSTELLAR ATOMIC, MOLECULAR AND UNIDENTIFIED FEATURES IN THE NEAR-UV.

Species	Wavelength(Å, air)
Cr I	3578.683 ^a , 3593.482 ^a
Fe I	3440.606 ^a , 3679.913 ^a
Na I	3302.368 ^a , 3302.987 ^a
Ti II	3066.354 ^a , 3072.984 ^a , 3229.199 ^a , 3241.994 ^a , 3383.768 ^a
CH	3137.530 ^e , 3143.150 ^e , 3146.010 ^e , 3627.403 ^d , 3633.289 ^d , 3636.222 ^d
CH ⁺	3447.075 ^g , 3579.020 ^b
CN	3579.453 ^f , 3579.963 ^f , 3580.937 ^f
NH	3353.924 ^b , 3358.053 ^b
OH	3072.010 ^c , 3072.064 ^c , 3078.440 ^c , 3078.472 ^c , 3081.664 ^c
OH ⁺	3583.769 ^b
Unident	3147.985 [*] , 3247.578 [*] , 3346.968 [*] , 3362.942 [*] , 3572.656 [*]

REFERENCES. — (a) Peter van Hoof line list; (b) Gredel et al. (2011); (c) Felenbok & Roueff (1996); (d) Weselak et al. (2011); (e) Chaffee & Lutz (1977); (f) Meyer et al. (1989); (g) Douglas & Morton (1960); (*) this work.

3.3. Detections

To search for interstellar features, we started by comparing the interstellar to the stellar superspectrum. We stepped through the entire wavelength range in steps of 5Å (see Figs. 14). We visually inspected apparent absorption features, and marked them as interstellar line candidates if they were detectable above the noise, and if they appeared better defined in the interstellar superspectrum compared to the stellar one. This resulted in 106 features (many of them weak) that we further investigated.

We then compared the wavelengths of our features to those of known atomic (ionic) transitions for various elements. For each of the detected features, we searched for all possible transitions (originating from the electronic ground state) that fall within 0.1Å of the observed wavelength, using Peter van Hoof’s database⁶. This way, we found 11 matching transitions due to 4 ions: Cr I, Fe I, Na I, and Ti II (see Table 1).

We also searched for correspondences with known molecular features in this wavelength range. To the best of our knowledge, no database with molecular transitions in this wavelength range exists, and thus we relied this time on various literature sources. We identified 19 of our features with transitions due to 6 molecular species: CH, CH⁺, CN, NH, OH, and OH⁺ (see Table 1).

We investigated the nature of the remaining 76 features in more detail by comparing all of the superspectra, but also by studying the optimal spectra of individual targets. We conclude that the majority of these features are artefacts that are due to atmospheric and/or instrumental issues. An example is shown in Fig. 6 where a telluric feature is clearly present, but is not entirely washed out in the interstellar superspectrum. In other cases, the ori-

gins of the features are less clear, and sometimes several neighbouring weak atmospheric features conspire to create features in the interstellar superspectrum, making it even harder to establish the nature of resulting absorption features.

Of the 76 remaining tentative features, we established that 71 are certainly *not* interstellar features. The 5 remaining features could possibly be very weak interstellar lines – they all are near our sensitivity limit. In investigating these features, we found 2 more very weak possible interstellar lines.

Thus, our careful search for interstellar features in the near-UV results in 11 known atomic lines, 19 known molecular lines, and in the best possible case 7 weak unidentified lines (see Table 1). The resulting superspectra for each of the features with identifications is shown in Fig. 7, and over the entire spectral range in Figs. 14; we discuss these features in some more detail below.

As an independent check, we have also created an additional superspectrum in the interstellar rest frame and a corresponding superspectrum using unreddened comparison stars using only those reddened stars for which we have good matching unreddened comparison stars. This subset is comprised of 26 pairs of reddened and unreddened targets; however, only 13 of the unreddened targets are unique. The resulting superspectra are shown in Fig 15. A comparison between these two superspectra should also reveal the interstellar lines quite readily, and could potentially also turn up broader features. We visually compared the reddened and unreddened superspectra on a few different scales. Searching on 50Å wide segments, we did not detect any moderate strength, broad features (i.e. comparable to stellar lines). More detailed searches on finer scales (20Å, 5Å segments) turned up all the features we flagged before, and some more atmospheric features. These searches suggest that there are no obvious broad interstellar lines (i.e. that not blended with stellar lines; see Figs. 15).

It is reassuring that the detections found by comparing superspectra in various rest frames is in agreement with the more commonly used method of comparing reddened targets to unreddened standards. This suggests that comparing rest frames may be a viable alternative to the standard method when searching for interstellar lines. Our method has two clear advantages: it does not require unreddened standards, and it results in a higher sensitivity than a pairwise comparison from the gain in S/N when co-adding the optimal spectra. However, it requires a large number of observations to work properly, and is not sensitive to broad features. At the same time, it takes a significant amount of work to establish the true nature of detected features. Thus, a pairwise comparison of matching target/standard pairs may still be the best method to use if high quality observations of good spectral matches are available; in other cases, the rest frame comparison method may be an appealing alternative.

3.4. Detected atomic lines

Na I – Na is a well-known interstellar gas component that is commonly detected in the well-known Na D lines at optical wavelengths. For many lines of sight, these D lines are very saturated. The Na U doublet lines near 3302Å are generally less saturated due to weaker tran-

⁶ <http://www.pa.uky.edu/~peter/atomic/>

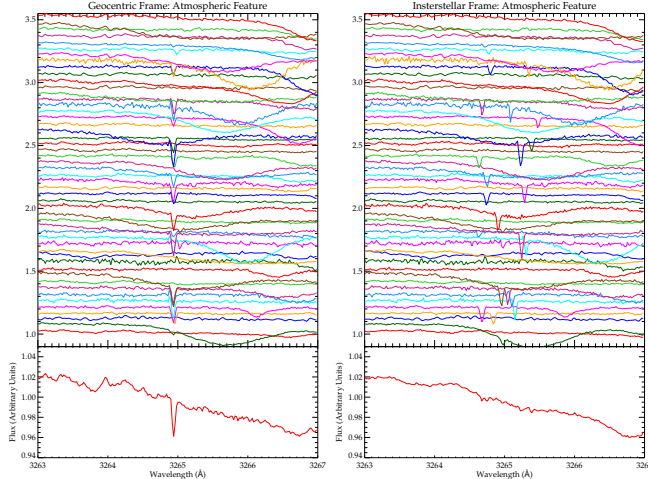


FIG. 6.— (Left:) A feature clearly aligns around 3265Å in the optimal, geocentric spectra for all targets. Note that the varying relative strength suggests an atmospheric rather than an instrumental origin in this case. (Right:) In the interstellar rest frame, the feature appears at different wavelengths, and thus is greatly washed out in the interstellar superspectrum. However, chance alignments of interstellar clouds still result in very weak features.

sition probabilities (de Boer & Pottasch 1974) – they have 1.4% the oscillator strength of the Na D lines (Kemp et al. 2002). In conjunction with the Na D doublet, these sodium lines can therefore be used to yield more reliable Na column densities (Blades et al. 1980).

The Na U doublet is seen in all of our reddened targets, and even weakly in several of our unreddened standards. In many cases, Doppler splitting reveals 2 or more components. These lines are thus certainly useful to determine Na column densities in all our lines of sight.

Ti II – We detect several lines of interstellar Ti II in most of our targets. In our wavelength range, there are six possible transitions for interstellar Ti II (3057.403, 3066.354, 3072.984, 3229.199, 3241.994 and 3383.768Å). All but the first line have been previously described (see e.g. Chaffee & Lutz 1977; Federman et al. 1996; Felenbok & Roueff 1996; Welty & Crowther 2010). In the UVES spectra, the region around 3050Å is furthermore very noisy, and thus we cannot detect the first transition in our data set either. In our spectra, the 3384Å resonance line is the most notable. It is commonly found in the ISM, and is useful for estimating electron densities (Stokes 1978).

Cr I – In our wavelength range, there are three neutral chromium transitions ($\lambda\lambda$ 3578.683, 3593.482, 3605.322). Meyer & Roth (1990) detected the first of these weak features in ζ Oph with S/N=1250; all three lines are detected toward HD 72127B (Welty et al. 2008). In our interstellar superspectrum, we detect the first two lines. We also detect these Cr I lines in several targets. The Cr I is certainly a trace species; we find that our measured equivalent widths for the strongest of the bands, 3578.683Å, is about 1mÅ in our superspectrum – this is within the range determined by Welty et al. (2008) and Meyer & Roth (1990). It is reasonable that we do not detect the 3605.322Å line since, of the three features, it has the lowest oscillator strength (Morton 2003).

Fe I – There are three possible Fe I transitions in our wavelength range: $\lambda\lambda$ 3440.606, 3649.302, 3679.913; of these, we detect the first and the third. These transitions occur in a handful of sightlines. The 3440.606Å feature has been detected in HD 72127B, and QSO HE0001-2340 (Welty et al. 2008; D’Odorico 2007). The non-detection of the 3649.302Å line is consistent with its low absorption oscillator strength – it is a few orders of magnitude smaller than the detected lines (Fuhr & Wiese 2006).

In addition to these detected lines, we also detected a very weak feature at 3217.154Å. This is right at the rest wavelength for the $4s_{1/2} - 7p_{3/2}$ transition of K I, and we considered the possibility that indeed this feature could be identified with K I. However, there are several more K I transitions in this wavelength range that should be stronger, but that we do not detect. Moreover, the oscillator strength for this transition is far too low ($\sim 10^{-4}$; Nandy et al. 2012) to cause measurable absorption. We thus conclude that this is not a real K I feature.

Finally, we also searched for the 3130.42Å and 3131.06Å features of interstellar Be I (see e.g. Chaffee & Lutz 1977; Morton 1978; Bosegaard 1985); we do not detect either of these transitions in our interstellar superspectrum nor in any individual line of sight. Similarly, we could not detect the Ni I feature at 3369.565Å (see e.g. Magnani & Salzer 1991; Welty et al. 2008). Additionally, like Welty et al. (2008), we did not detect Al I or Ti I lines which could appear in our wavelength range.

3.5. Detected molecular lines

CH – Our spectra show strong interstellar CH lines; all 6 known transitions in this spectral range are detected. A striking example of the *C-X* system of CH is displayed in Fig. 4. Weselak et al. (2011) report detections of the *B-X* system around 3627Å in 13 targets. For the targets we have in common, we generally confirm these detections. Note that in many cases, two of these features are often found superimposed atop a stellar He I line.

CH⁺ – About 10 of our sightlines also show absorption due to CH⁺. This species is detected at 3447.076Å and/or 3579.020Å. These correspond to the *R(0)* line from the 4 – 1 band, and the *R(0)* line of the 3 – 0 band (Douglas & Morton 1960). While CH⁺ was originally thought to trace shocks, it is now thought to trace turbulent dissipation regions (see e.g. Tielens 2013).

CN – CN is well known as an interstellar molecule for its potential to measure the temperature of the cosmic microwave background radiation by using the $B^2\Sigma - X^2\Sigma$ optical lines (Meyer & Jura 1985). In our spectral range, three transitions in the (1,0) vibrational band – the R(1), R(0), and P(1) lines – are detected at $\lambda\lambda$ 3579.453, 3579.963, 3580.937 towards a handful of targets. Typically the P(1) line is not seen, likely because it is too weak – it has the lowest oscillator strength of the three transitions (Meyer et al. 1989).

NH – NH was first detected in the near-UV by

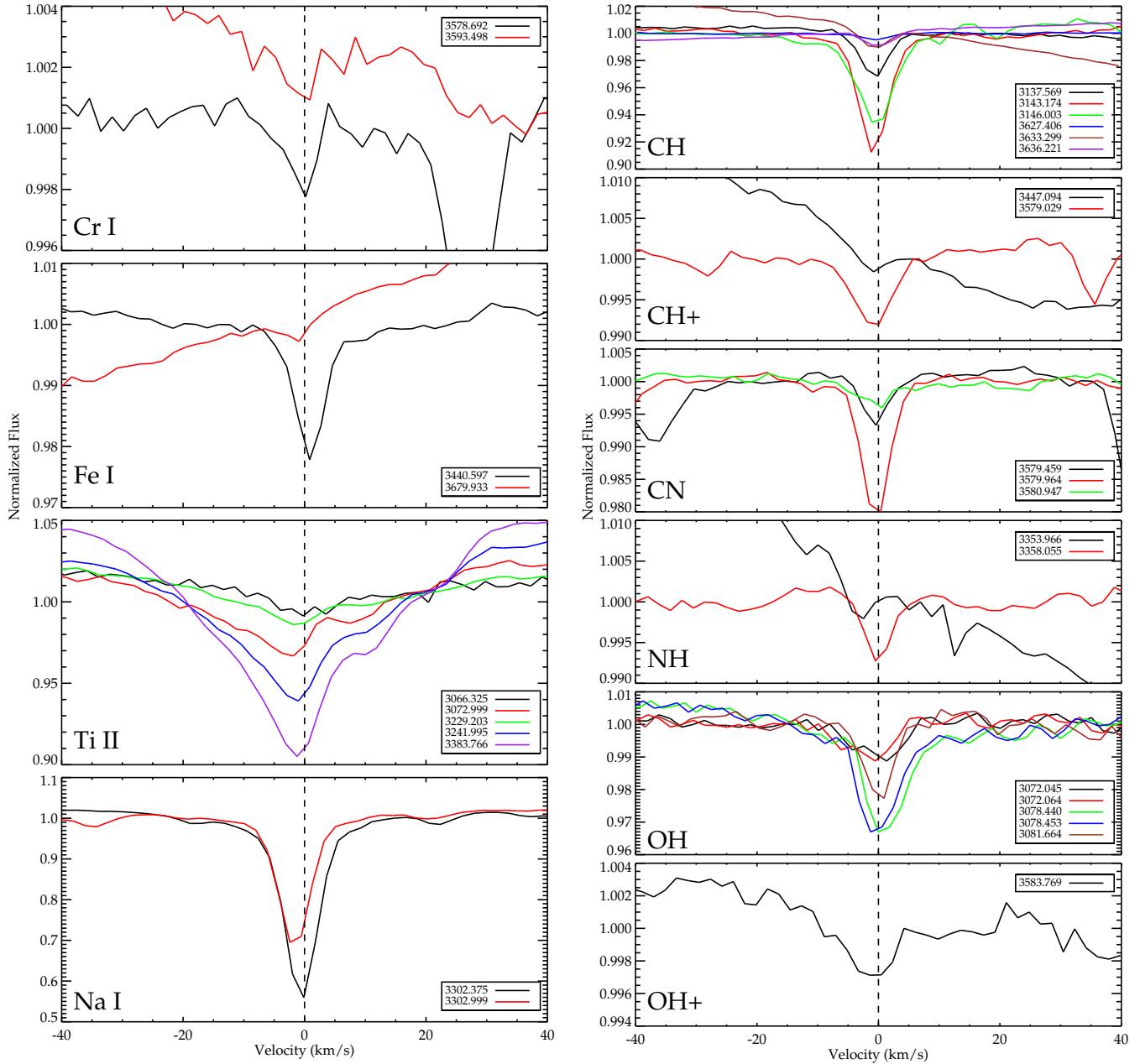


FIG. 7.— An overview of each identified interstellar feature in our superspectra: atomic (*left*) and molecular (*right*). The velocity scale is based on the interstellar superspectrum, that is, it is relative to the deepest component of the 3302 Na I doublet. Note that the OH lines are blends of several transitions.

Meyer & Roth (1991) who detected both the R₁(0) and the ^RQ₂₁(0) transitions of the A³Π-X³Σ system at respectively 3358.0525Å and 3353.9235Å. We detect these transitions in \sim 5 sightlines.

OH – The spectra of \sim 10 targets also show absorption due to OH. There are 5 A-X lines associated with this species in our wavelength range. However, we can only really observe three features: a blend of the 3072.01Å and 3072.0637Å lines; a blend of the 3078.4399Å and 3078.472Å features; and the 3081.664Å feature. Of

these, the 3072Å transitions R₁ (3/2) and R_{Q₂₁} (3/2) are the most recent to be discovered; all features are described by Felenbok & Roueff (1996). The blends pose difficulties in providing accurate measurements for the individual lines.

OH⁺ – OH⁺ is one of the more recently detected interstellar species (Wyrowski et al. 2010). The near-UV line near 3584Å was previously described by various authors (Krelowski et al. 2010; Gredel et al. 2011; Porras et al. 2014). The lack of velocity shifts between the neutral and ionized species rules out a shock for-

mation mechanism; Porras et al. (2014) conclude that cosmic ray ionization is the most likely route for this species. We report the detections of the OH⁺ feature in BD -14° 5037.

We could furthermore not detect the 3360Å line of SH⁺ in our interstellar superspectrum, nor in any individual line of sight.

3.6. Tentative Interstellar Features

3147.985Å – When comparing the interstellar superspectrum of reddened targets to its unreddened counterpart, a weak and relatively broad feature is apparent near 3148Å (see Fig. 15). This feature is not detected when comparing the reddened targets in the various rest frames. When measured in the interstellar superspectrum, this feature has $W_{\lambda}=1.0 \pm 0.3$ mÅ, corresponding to a 3σ detection. This may thus be a weak interstellar feature.

3246.711, 3247.578, 3248.313 Å – A weak feature aligns in the spectra of HD 161056, HD 170740 and HD 172028 at 3247.578Å (see Fig. 8). Coincidentally, this is close to the wavelength of one of two ground state electronic transitions of Cu I in our wavelength range. If this line were indeed a Cu I line, we should also see the line at 3273.954Å whose oscillator strength is only a factor of two lower (Moise 1966). However, we do not see any hint of an absorption line at that wavelength; thus, this line is not likely to be the Cu I line. On either side of this possible interstellar lines are two even weaker lines that appear to line up at 3246.711Å, 3248.313Å. All these are marginal though – they may or may not be true interstellar lines.

3346.968Å – A weak, but conspicuous feature is apparent in the interstellar superspectrum at 3346.968Å (see Fig. 9). The feature is better defined still when considering a limited sample of targets: HD 115363, HD 142758, HD 188220, HD 210121, HD 143448 where we also tentatively see the feature in the optimal target spectra. This feature also shows up prominently in a comparison between reddened and unreddened superspectra (see Fig. 15). Therefore, this does appear to be a true interstellar absorption feature. We have not been able to find an identification for this feature. When measured in the interstellar superspectrum, this feature has $W_{\lambda}=0.5 \pm 0.1$ mÅ, corresponding to a 5σ detection.

3362.942Å – A weak and shallow feature may be present in the interstellar superspectrum at 3362.942Å. However, we do not detect this feature in any individual object. Moreover, the geocentric superspectrum exhibits two absorption features bracketing the possible interstellar feature. Since interstellar velocities are fairly low, it is possible that the apparent interstellar feature results from a chance superposition of these telluric lines when shifting to the interstellar rest frames. On the other hand, the feature shows up quite clearly when comparing the reddened to the unreddened superspectrum (see Fig. 15) thus strengthening the case for an interstellar band. When measured in the interstellar superspectrum,

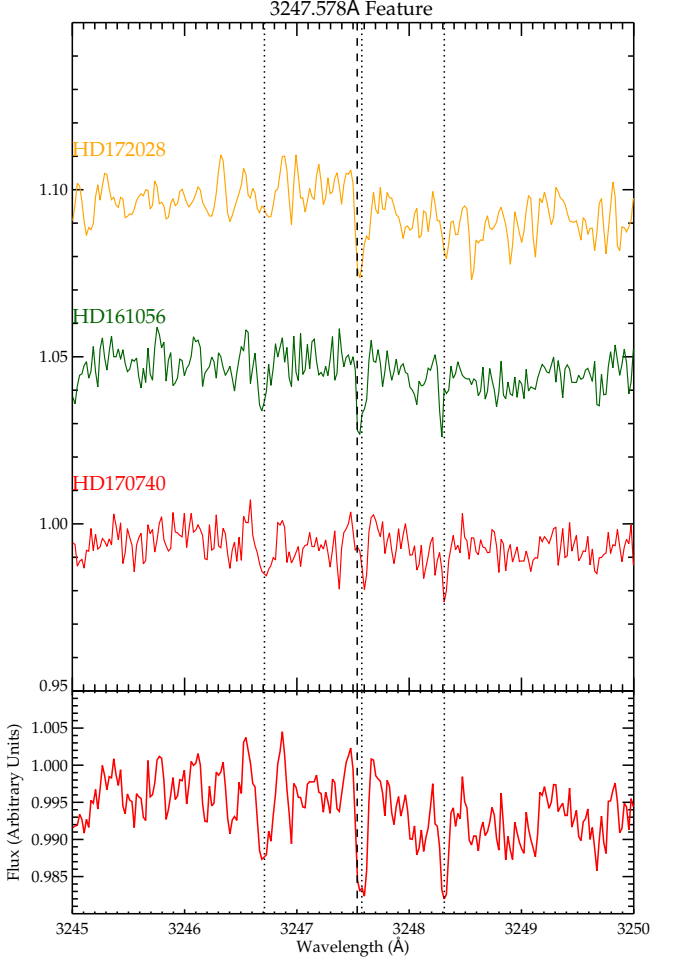


FIG. 8.— The optimal spectra of HD 172028, HD 161056 and HD 170740 in the interstellar rest frame near the rest wavelength of a Cu I line at 3247.537Å (marked with a broken dashed line) show a feature at 3247.578Å. In the same range, two more features are seen to line up in these targets at $\lambda\lambda$ 3246.711, 3248.313, marked with a dotted line. Each of these features is seen more clearly in the co-add of these three targets (bottom panel).

this feature has $W_{\lambda}=0.6 \pm 0.1$ mÅ, corresponding to a 6σ detection.

3572.656Å – A slightly broader feature shows up in the interstellar superspectrum at 3572.656. We suspect that the strong telluric residuals in this range will have at least some contribution from this geocentric feature. However, the feature also shows up when comparing the reddened to the unreddened superspectrum (see Fig. 15). When measured in the interstellar superspectrum, its strength is comparable to the atomic, and molecular features which appear around 3578Å(Cr I, CN, CH⁺): $W_{\lambda}=1.1 \pm 0.1$ mÅ, corresponding to a 10σ detection.

3.7. Line of sight measurements

We have measured basic line properties (central wavelengths, widths⁷ and equivalent widths) for each identified line that we could detect in the optimal spectrum of each of our targets. This was done by fitting (a) Gaussian profile(s) to the features in the interstellar rest frame. In

⁷ Full Width at Half Maximum, FWHM

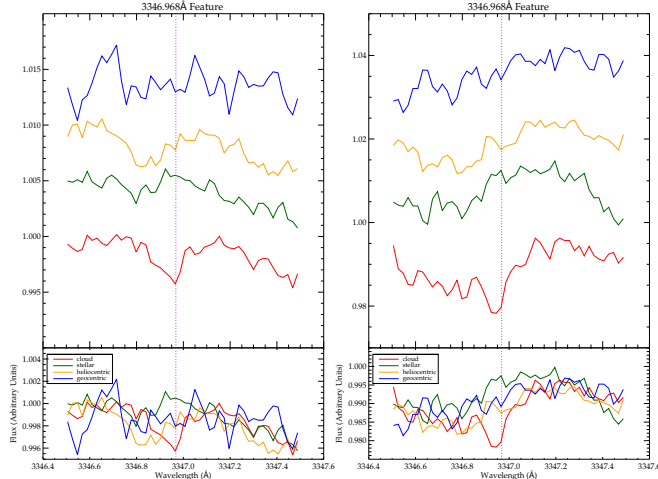


FIG. 9.— The top panel shows the geocentric (blue), heliocentric (yellow), stellar (green) and interstellar (red) rest frame. (*Left:*) A broad, asymmetric feature appears in the interstellar superspectrum (red) of all targets. There is no corresponding atmospheric feature at this position. (*Right:*) Focusing on the targets which clearly show this feature (i.e. HD 115363, HD 142758, HD 188220, HD 210121 and HD 143448, the asymmetric feature becomes much more regular in the interstellar frame.

many cases, this involved fitting several components originating from different clouds at the same time. We only aimed at reproducing the strongest components; thus, in some cases, weak residual shoulders are still visible in e.g. the Na I lines. The Ti II lines typically exhibit more components (often blended) over a wider velocity range than the Na I or molecular lines; since many lines are also weak, this required a slightly different approach. For these lines, we first determined the number of cloud components by fitting the strongest line (at 3383.768 Å). Once a satisfactory fit was obtained, we used the same components to fit the other lines while keeping the number of components as well as their central wavelengths and widths fixed (thus only allowing the strength of the lines to vary). Note that we do not account for any potential stellar absorption since this should not be a major contribution for early-type stars (Welty & Crowther 2010).

The resulting line fits can be inspected in Fig. 16; the measured values are listed in Table 4. Features that are not reported represent non-detections. The equivalent widths listed in Table 4 are derived from the Gaussian fit parameters and uncertainties are the formal 1σ uncertainties derived from the fit. For many of the Ti II lines, we only list an uncertainty for the equivalent width since all other parameters were fixed as described above. For multi-component features, we also present the measured equivalent width obtained by integrating across the entire profile; these values are listed in square brackets in Table 4. The largest source of uncertainty on this measurement is the exact positioning of the local continuum. To get a good sense of this uncertainty and its effect on the measurement, we carried out a Monte Carlo experiment in which we reposition the continuum many times, commensurate with the local S/N, and integrate again. The average over all trials is what we used as the measured equivalent width in Table 4; the standard deviation over all runs is what is used as its uncertainty.

We compared our equivalent widths of the CH $B -$

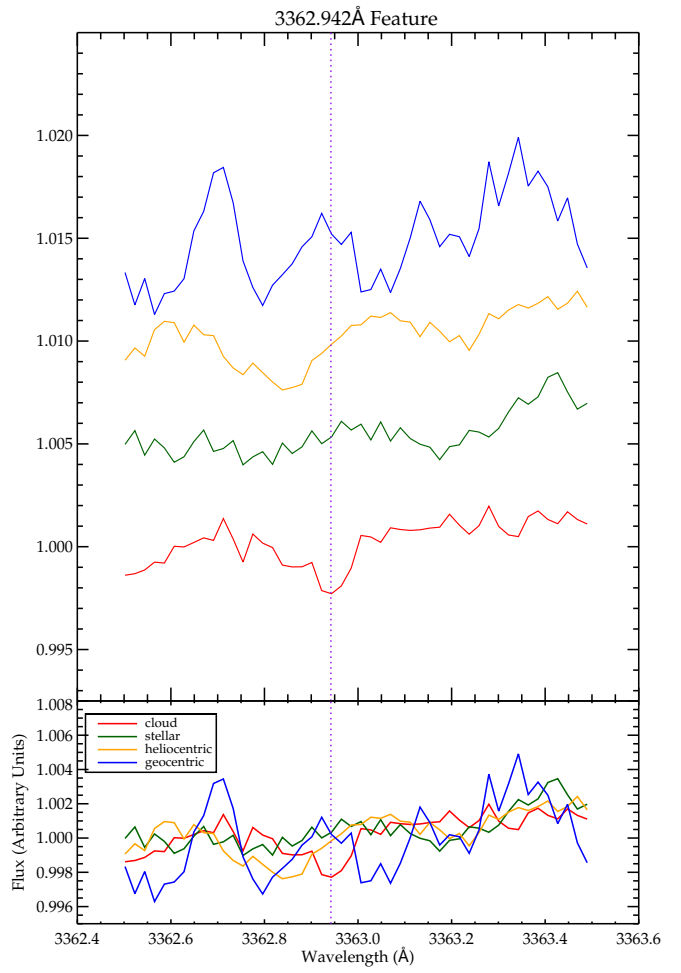


FIG. 10.— The top panel shows the geocentric (top; blue), heliocentric (yellow), stellar (green) and interstellar (bottom; red) rest frame. A weak, diffuse band appears in the interstellar superspectrum (red; bottom spectrum of the top panel). Note the prominent atmospheric features are bracketing this possible interstellar line.

X system measurements to Weselak et al. (2011), and found that our values were generally in excellent agreement. We noted that Weselak et al. (2011) reported some measurements for borderline detections ($W_\lambda < 3\sigma$) in sightlines where optical CH lines were quite strong. For the sake of consistency, we have included these CH features as well. We also compared our results for the $\lambda\lambda$ 3072, 3241, 3383 Ti II features to Welty & Crowther (2010) and again found excellent agreement. Note that these authors also include plots of Ti II features in the heliocentric frame that are entirely consistent with our results.

It is interesting to note that only the Na I doublet and the 3241.994 Å and 3383.768 Å Ti II features are observed in each target. On the other hand, only a handful of targets show Cr I, NH, CH, or OH⁺. We also note that some targets show a feature coincident with the 3066.354 Å line of Ti II; however, this region of our spectra is very noisy. Similarly, we noticed systematic problems (artefacts) in many spectra around the CH feature at 3146.010 Å. This probably points to issues with the data reduction or CCD itself; therefore, measurements of this feature should be used with caution.

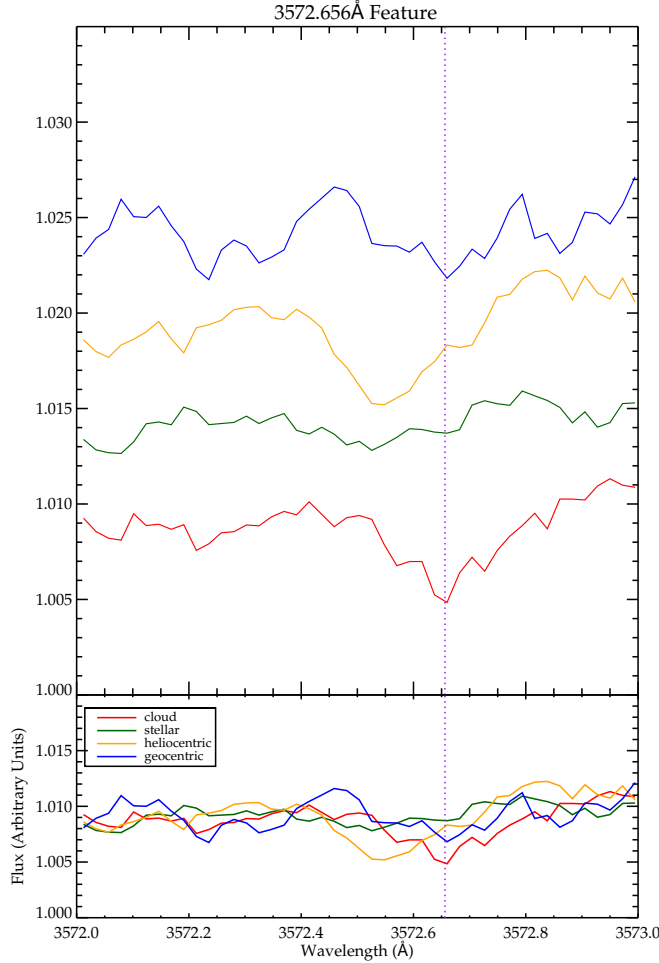


FIG. 11.— The top panel shows the geocentric (top; blue), heliocentric (yellow), stellar (green) and interstellar (bottom; red) rest frame. A broad interstellar feature appears around 3572.656 Å. It may have some geocentric contribution.

On first sight, one may expect to find that the presence (and strength) of these features should roughly increase with $E(B - V)$. This, however, is clearly not the case. For instance, the line of sight toward HD 183143 has $E(B - V) = 1.21$ but shows only 12 features, and many of those are weak. HD 154368 on the other hand has a much lower reddening ($E(B - V) = 0.47$), but has many more features that are much stronger. While differences in abundances may play a role, such differences are primarily attributable to very different physical conditions that lead to different chemistry (see e.g. Snow et al. 1996). This is reminiscent of the very clear differences in terms of molecular lines and DIBs observed in the lines of sight toward ζ Oph (HD 149757) and σ Sco (HD 147165) and attributable to differences in the physical conditions of the intervening clouds (see e.g. Cami et al. 1997).

4. DISCUSSION

It is reassuring that we detect tens of known interstellar atomic and molecular lines in this wavelength range, even if they do not appear in the majority of the individual targets. For instance, while we detect Na I in all 51 sightlines, the Cr I lines are only found in a handful (< 10) of sightlines, yet they do show up in our interstellar superspectrum. This confirms that our method is

TABLE 2
UPPER LIMITS FOR THE COLUMN DENSITIES OF SMALL NEUTRAL PAHS
IN THE NEAR-UV.

Species	λ [Å]	f [10^{-3}]	$W_{\lambda,\max}$ [mÅ]	N_{\max} [10^{12} cm $^{-2}$] (Here)	N_{\max} (Lit.)
Anthracene	3610.74	16 ^a	0.47	0.25	0.53 ^a
Phenanthrene	3409.21	.16 ^a	0.40	24.90	62.0 ^a
Pyrene	3208.22	97 ^a	2.38	0.27	0.11 ^a
	3166.26	33 ^a	2.75	0.92	0.34 ^a
2,3-benzofluorene	3344.16	8.5 ^a	0.44	0.52	1.20 ^a
	3266.63	2.5 ^a	0.42	1.77	4.20 ^a
Benzo[ghi]perylene	3512.15	9 ^a	2.18	2.20	1.00 ^a
	3501.76	5 ^a	1.75	3.08	1.80 ^a
Acenaphthene	3175	2.2 ^b	0.78	3.99	3.00 ^b
Benzo[ghi]perylene	3689.4	150 ^c	0.71	0.04	0.12 ^b
2-methylnaphthalene	3152.7	2.3 ^b	0.80	3.93	4.90 ^b
Phenanthrene	3408.4	23 ^b	0.66	0.28	0.21 ^b
Pyrene	3205.8	160 ^b	2.56	0.18	0.97 ^b
Benzofluorene	3345.1	24 ^d	0.29	0.12	0.69 ^b
Anthracene	3611.8	10 ^e	0.32	0.28	2.60 ^b
Triphenylene	3293.52	0.7 ^f	0.43	6.56	

REFERENCES. — (a) Gredel et al. (2011); (b) Salama et al. (2011); (c) Tan & Salama (2005); (d) Staicu et al. (2006); (e) Hermine (1994);(f) Kokkin et al. (2007)

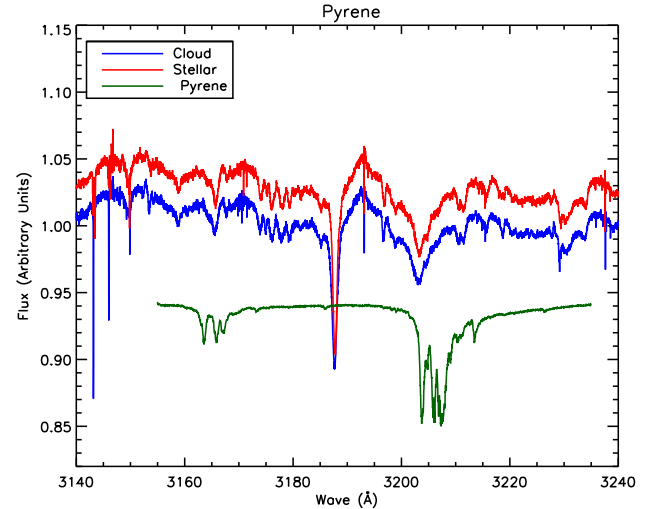


FIG. 12.— A laboratory spectrum of pyrene (bottom; green) is compared to both the stellar (top; red), and interstellar superspectra (middle; blue). Around 3160 Å, all spectra have a series of features. However, there is no similarity between the features in pyrene and the others.

indeed sensitive to most narrow interstellar lines. We are thus confident that if a (narrow) feature was somewhat common in the ISM, we should have detected it. However, our method does not work well for broad features, and thus we may not be sensitive to see broad, DIB-like absorption features. This is an important caveat to bear in mind for the discussion that follows.

Apart from known interstellar species, our survey results in only 7 possible new features that could be atomic or molecular lines, or narrow DIBs. If the latter is the case, such a low number is in line with the decreasing density of DIBs toward the blue at optical wavelengths (see e.g. Witt 2014, and references therein). Thus, there

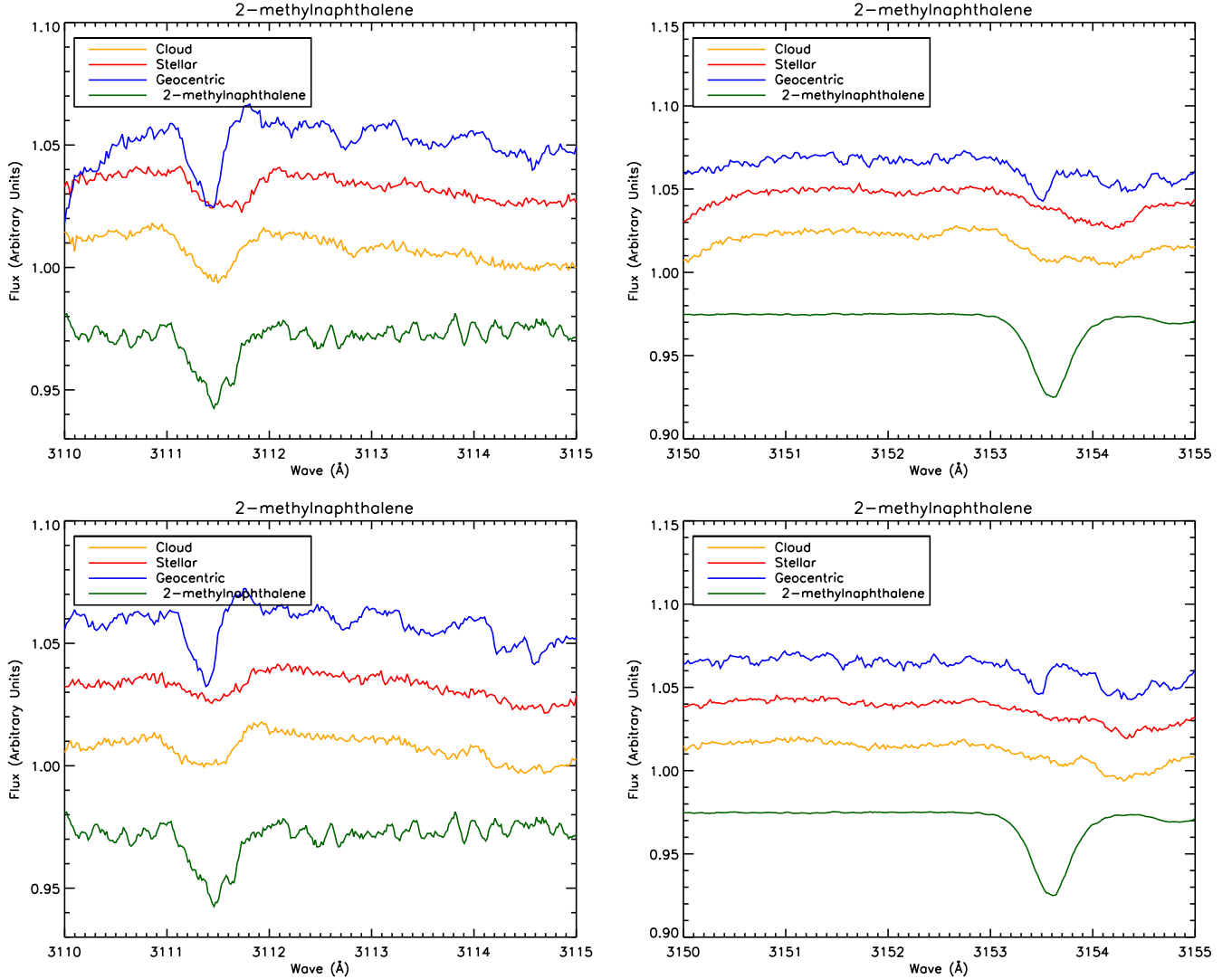


FIG. 13.— A laboratory spectrum of 2-methylnaphthalene in the region of two of its strongest transitions near 3111.5\AA (left panels) and 3152.7\AA (right panels) is compared to the superspectra of the reddened targets (top panels), and unreddened targets (bottom panels). Each figure shows the geocentric (top; blue), stellar (red), and interstellar (orange) superspectra compared to the (scaled) laboratory spectrum (bottom; green). At both wavelengths, a feature appears in the interstellar spectrum with approximately the same characteristics (wavelength, width) as the laboratory spectrum. However, this feature is much better defined (narrower) in the geocentric superspectrum, suggesting that this feature is telluric in nature – possibly 2-methylnaphthalene in the earth’s atmosphere.

are at most very few unknown interstellar lines left in the near-UV range.

The absence of features in a sensitive survey can be used to determine upper limits to the column densities of molecular species whose gas-phase spectra are known, and that could possibly be present in the interstellar medium. Following the approach of Salama et al. (2011) and Gredel et al. (2011), we determined upper limits to the average ISM column densities of several PAHs from the aforementioned works, as well as from Kokkin et al. (2007); the results are listed in Table 2. Note that this is the first time that triphenylene has been compared to observations. These upper limits are of the same order of magnitude as those listed by the previous authors. Note though that the peak positions and oscillator strengths of phenanthrene, pyrene, benzofluorene and anthracene used by Salama et al. (2011) and Gredel et al. (2011) differ noticeably from one another.

Since we have used many more targets than both Salama et al. (2011) and Gredel et al. (2011), we would expect our upper limits to be more significant. Gredel et al. (2011) use a detection limit of $1\text{m}\text{\AA}$ for all bands. This strategy is a reasonable to first-order. However, we find that the S/N decreases towards the blue (see Figures 14). Therefore, a more realistic upper limit is obtained by measuring the S/N in the region of the feature – this is the method we followed. Salama et al. (2011) also followed this procedure. However, we noticed that their quoted S/N of their co-adds are comparable, and in some cases, significantly higher than those from our interstellar superspectrum, notwithstanding the fact that we use many more reddened targets than their 17 lines of sight.

For comparison, we have created a co-add that includes 12 of their 17 targets (the other 5 are not in our target list) and show a part of the spectrum in Fig. 12; this

should be compared with their Fig. 11. It is clear that the two are rather different; where our co-adds show many stellar lines, there is no trace of stellar lines in the Figures by Salama et al. (2011), and it is not clear how the authors removed these. We attempted to fit the stellar lines ourselves, and inevitably found that this procedure resulted in clear residuals near the line cores; these residuals did bear some resemblance to the pyrene laboratory spectra. From our superspectra, we find no evidence for interstellar lines in this range though. Note also that Salama et al. (2011) state that their stellar spectra are free of telluric features, which would otherwise interfere with detecting weak features; as we have shown, there are many weak telluric residuals left in our spectra.

Finally, we point out an intriguing case which exemplifies the need to carefully consider features in the geocentric frame. When comparing our superspectra to the laboratory spectrum of 2-methylnaphthalene, we noticed that there was a fairly good correspondence between the astronomical and the laboratory spectra (see Fig. 13). Indeed, both near 3111.5 Å and 3153.5 Å, we found absorption bands at about the location of the strongest transitions of 2-methylnaphthalene. However, when considering the geocentric superspectrum, those bands appear much narrower and much more defined. This then suggests that the feature is telluric in origin – possibly, we are seeing 2-methylnaphthalene in the earth’s atmosphere. It is worth noting that small PAHs, including alkylated naphthalenes are detectable in ambient air (Zielinska et al. 1989).

While Gredel et al. (2011) and Salama et al. (2011)

obtained upper limits for specific wavelengths and for a few neutral PAHs, our survey shows that similar upper limits hold for the entire wavelength range studied here (with of course the exception of the 7 unidentified features). Thus, there is not much room for molecular species that have narrow absorption bands. Only very broad (tens of Å) and shallow bands could possibly still be present in this part of the spectrum.

5. CONCLUSIONS

We have carried out a sensitive survey for interstellar features in the near-UV (from 3050–3700 Å) using archival UVES data and a method that compares various co-adds corresponding to different rest frames. Our survey has revealed 30 known interstellar atomic and molecular features, and 7 weak features that appear interstellar in nature, but are unidentified. The high sensitivity of our survey allows us to determine significant upper limits to the column densities of various molecular carriers, and over the entire wavelength range studied. Thus, there are only very few narrow and unidentified interstellar features in the 3050–3700 Å range.

We would like to thank Steve Federman and Dan Welty for assisting us with the identification of some transitions. We are grateful to the referee for the constructive comments that have improved this paper. We acknowledge support from the Natural Sciences and Engineering Research Council of Canada (NSERC) through a Discovery grant and an Undergraduate Student Research Award (USRA).

REFERENCES

- Berghofer T.W., Schmitt J.H.M.M., Cassinelli J.P., 1996, A&AS, 118, 481
- Blades J.C., Wynne-Jones I., Wayte R.C., 1980, MNRAS, 193, 849
- Bosegaard A.M., 1985, PASP, 97, 37
- Burrows J.P., Richter A., Dehn A., et al., 1999, JQRST, 61, 509
- Cami J., Sonnentrucker P., Ehrenfreund P., Foing B.H., 1997, A&A, 326, 822
- Chaffee, Jr. F.H., Lutz B.L., 1977, ApJ, 213, 394
- Crawford I.A., 1989, Obs, 109, 232
- de Boer K.S., Pottasch S.R., 1974, A&A, 32, 1
- Dekker H., D’Odorico S., Kaufer A., Delabre B., Kotzlowski H., 2000, In: Iye M., Moorwood A.F. (eds.), Optical and IR Telescope Instrumentation and Detectors, vol. 4008 of SPIE Conference Series, pp. 534–545
- D’Odorico V., 2007, A&A, 470, 523
- Douglas A.E., Morton J.R., 1960, ApJ, 131, 1
- Ehrenfreund P., Foing B.H., 1996, A&A, 307, L25
- Federman S.R., Weber J., Lambert D.L., 1996, ApJ, 463, 181
- Felenbok P., Roueff E., 1996, ApJ, 465, L57
- Fitzgerald M.P., 1970, A&A, 4, 234
- Fitzpatrick E.L., Massa D., 2007, ApJ, 663, 320
- Friedemann C., 1992, Bull. Inf. Cent. Donnees Stellaires, 40, 31
- Fehr J.R., Wiese W.L., 2006, JPCRD, 35, 1669
- Galazutdinov G., Stachowska W., Musaev F., et al., 2002, A&A, 396, 987
- Galazutdinov G.A., LoCurto G., Krełowski J., 2008, ApJ, 682, 1076
- Galazutdinov G.A., Musaev F.A., Schmidt M.R., Krełowski J., 2001, MNRAS, 323, 293
- Gredel R., Carpentier Y., Rouillé G., et al., 2011, A&A, 530, A26
- Guarinos J., 1988, Bull. Inf. Cent. Donnees Stellaires, 34, 141
- Gudennavar S.B., Bubbly S.G., Preethi K., Murthy J., 2012, ApJS, 199, 8
- Herbig G.H., 1975, ApJ, 196, 129
- Herbig G.H., 1995, ARA&A, 33, 19
- Herbig G.H., 2000, ApJ, 542, 334
- Hermine P., 1994, Univ. Paris Sud, Orsay
- Hobbs L.M., York D.G., Snow T.P., et al., 2008, ApJ, 680, 1256
- Hobbs L.M., York D.G., Thorburn J.A., et al., 2009, ApJ, 705, 32
- Hunter I., Smoker J.V., Keenan F.P., et al., 2006, MNRAS, 367, 1478
- Jamar C., Macau-Hercot D., Monfils A., et al., 1995, VizieR Online Data Catalog, 3039, 0
- Jenniskens P., Desert F.X., 1994, A&AS, 106, 39
- Kemp S.N., Bates B., Beckman J.E., et al., 2002, MNRAS, 333, 561
- Kerr T.H., Hibbins R.E., Miles J.R., et al., 1996, MNRAS, 283, L105
- Kokkin D.L., Reilly N.J., Troy T.P., Nauta K., Schmidt T.W., 2007, JChPh, 126, 084304
- Krełowski J., Beletsky Y., Galazutdinov G.A., 2010, ApJ, 719, L20
- Krełowski J., Schmidt M., 1997, ApJ, 477, 209
- Magnani L., Salzer J.J., 1991, AJ, 101, 1429
- Meyer D.M., Jura M., 1985, ApJ, 297, 119
- Meyer D.M., Roth K.C., 1990, ApJ, 349, 91
- Meyer D.M., Roth K.C., 1991, ApJ, 376, L49
- Meyer D.M., Roth K.C., Hawkins I., 1989, ApJ, 343, L1
- Moise N.L., 1966, ApJ, 144, 774
- Morton D.C., 1978, ApJ, 222, 863
- Morton D.C., 2003, ApJS, 149, 205
- Müller H.S.P., Schlöder F., Stutzki J., Winnewisser G., 2005, JMoST, 742, 215
- Müller H.S.P., Thorwirth S., Roth D.A., Winnewisser G., 2001, A&A, 370, L49
- Nandy D.K., Singh Y., Shah B.P., Sahoo B.K., 2012, PhRvA, 86, 052517

- Porras A.J., Federman S.R., Welty D.E., Ritchey A.M., 2014, ApJ, 781, L8
- Raimond S., Lallement R., Vergely J.L., Babusiaux C., Eyer L., 2012, A&A, 544, A136
- Salama F., Galazutdinov G.A., Krełowski J., et al., 2011, ApJ, 728, 154
- Sarre P.J., 2006, JMSP, 238, 1
- Savage B.D., Massa D., Meade M., Wesselius P.R., 1985, ApJS, 59, 397
- Slyk K., Bondar A.V., Galazutdinov G.A., Krełowski J., 2008, MNRAS, 390, 1733
- Snow T.P., Black J.H., van Dishoeck E.F., et al., 1996, ApJ, 465, 245
- Snow T.P., Zukowski D., Massey P., 2002, ApJ, 578, 877
- Snow, Jr. T.P., York D.G., Welty D.E., 1977, AJ, 82, 113
- Staicu A., Krasnokutski S., Rouillé G., Henning T., Huisken F., 2006, JMSt, 786, 105
- Stokes G.M., 1978, ApJS, 36, 115
- Tan X., Salama F., 2005, JChPh, 123, 014312
- Tielens A.G.G.M., 2013, RvMP, 85, 1021
- Tuairisg S.Ó., Cami J., Foing B.H., Sonnentrucker P., Ehrenfreund P., 2000, A&AS, 142, 225
- Vos D.A.I., Cox N.L.J., Kaper L., Spaans M., Ehrenfreund P., 2011, A&A, 533, A129
- Walborn N.R., Vreux J.M., Conti P.S., 1980, PASP, 92, 284
- Wegner W., 2002, BaltA, 11, 1
- Welty D.E., Crowther P.A., 2010, MNRAS, 404, 1321
- Welty D.E., Hobbs L.M., 2001, ApJS, 133, 345
- Welty D.E., Hobbs L.M., Morton D.C., 2003, ApJS, 147, 61
- Welty D.E., Simon T., Hobbs L.M., 2008, MNRAS, 388, 323
- Weselak T., Galazutdinov G., Beletsky Y., Krełowski J., 2011, AN, 332, 167
- Westerlund B.E., Krełowski J., 1988, A&A, 203, 134
- Witt A.N., 2014, In: Cami J., Cox N.L.J. (eds.), IAU Symposium, vol. 297 of IAU Symposium, pp. 173–179
- Wyrowski F., Menten K.M., Güsten R., Belloche A., 2010, A&A, 518, A26
- Zielinska B., Arey J., Atkinson R., McElroy P.A., 1989, EnST, 23, 723
- Zorec J., Cidale L., Arias M.L., et al., 2009, A&A, 501, 297

APPENDIX

TABLE 3
BASIC DATA OF OUR TARGETS AND OBSERVATIONS.

Object	Sp.Type ¹	RA [J2000]	DEC [J2000]	E_{B-V} [mag]	v_* ¹ [km·s ⁻¹]	v_{ISM} ² [km·s ⁻¹]	# Obs ³	Prog. IDs	S/N ⁴	Type ⁵
HD 36861	O8III	05 35 08.27	+09 56 02.96	0.09 ⁱ	33	25.2 (26.8 ^{aa})	6	266.D-5655	141	R
HD 67536	B2.5V	08 04 42.93	-62 50 10.84	0.12 ^c	0	14.3	3	266.D-5655	337	R
HD 68761	B0.5III	08 12 27.36	-36 59 21.23	0.13 ^c	43	18.3	2	266.D-5655	245	R
HD 94963	O6.5III	10 56 35.79	-61 42 32.22	0.24 ^h	-3	10.1	2	266.D-5655	159	R
HD 96917	O8.5Ib	11 08 42.61	-57 03 56.91	0.32 ⁱ	9	-15.8	2	266.D-5655	231	R
HD 105056	O9.5Ia	12 05 49.87	-69 34 22.98	0.36 ^b	1	17.5	2	266.D-5655	188	R
HD 105071	B6Ia/Ib	12 05 53.61	-65 32 48.75	0.19 ^c	-12	0.5	2	266.D-5655	136	R
HD 106068	B8Ia/Ib	12 12 21.98	-62 57 02.78	0.26 ^c	-2	7.3	2	266.D-5655	111	R
HD 109867	B1Ia	12 38 52.35	-67 11 34.97	0.19 ^c	-16	6.1	2	266.D-5655	224	R
HD 110432	B2pe	12 42 50.26	-63 03 31.05	0.40 ^d	35	6.8	2	65.I-0526	291	R
HD 112244	O9Ibe	12 55 57.13	-56 50 08.90	0.29 ^e	18	-17.1	4	65.I-0526	257	R
HD 112842	B4IV	13 00 31.52	-60 22 31.31	0.25 ^c	-22	7.4	3	266.D-5655	254	R
HD 114213	B1Ib	13 10 21.37	-61 28 20.88	1.13 ^a	-31	-17.9	4	65.I-0526	263	R
HD 115363	B1Ia	13 18 06.86	-63 41 13.62	0.63 ^c	-71	4.9	2	266.D-5655	147	R
HD 115842	B0.5Ia	13 18 13.44	-48 31 17.16	0.41 ^c	-3	-12.0	2	266.D-5655	181	R
HD 136239	B2Iae	15 22 20.07	-59 08 49.93	0.94 ^c	-61	-14.3	2	266.D-5655	133	R
HD 142758	B1.5Ia	15 59 23.73	-58 43 34.40	0.31 ^c	12	-10.3	2	266.D-5655	220	R
HD 143448	B3IV	16 03 44.46	-60 29 54.47	0.16 ^c	-3	4.0	2	266.D-5655	196	R
HD 147701	B5III	16 24 21.31	-25 01 31.44	0.69 ^f	12	-6.2	1	65.I-0526	205	R
HD 147889	B2III/IV	16 25 24.31	-24 27 56.57	1.08 ^e	-4	-7.7 (-9.0 ^{bb})	5	65.I-0526	313	R
								67.C-0281		
HD 147933	B2/B3V	16 25 35.10	-23 26 48.70	0.48 ^e	-10	-8.0 (-8.0 ^{aa})	2	65.I-0526	238	R
HD 148184	B2Vne	16 27 01.43	-18 27 22.49	0.52 ^c	-3	-11.1 (-11.2 ^{aa})	3	266.D-5655	335	R
								65.I-0526		
HD 148379	B2Iap	16 29 42.32	-46 14 35.60	0.61 ^c	-11	-22.4	3	266.D-5655	298	R
								65.I-0526		
HD 149404	O9Ia	16 36 22.56	-42 51 31.89	0.68 ^g	-36	0.6	1	65.I-0526	256	R
HD 149757	O9V	16 37 09.53	-10 34 01.52	0.33 ^g	-15	-14.5 (-16.3 ^{aa})	6	65.I-0526	302	R
HD 150136	03.5If	16 41 20.42	-48 45 46.74	0.48 ^h	23	0.5	1	65.I-0526	237	R
HD 152003	O9.7Iab	16 52 47.36	-41 47 08.98	0.53 ^h	-28	1.2	2	266.D-5655	164	R
HD 152235	B1Ia	16 53 58.85	-41 59 39.58	0.66 ^h	36	-1.1	4	266.D-5655	289	R
HD 152236	B0.5Ia	16 53 59.72	-42 21 43.30	0.73 ^a	-26	0.8	2	65.I-0526	223	R
HD 154368	O9.5Iab	17 06 28.36	-35 27 03.76	0.47 ^c	1	-3.0 (-5.0 ^{aa})	3	65.I-0526	221	R
								67.C-0281		
HD 154811	OC9.7Ib	17 09 53.08	-47 01 53.18	0.46 ^c	-14	-9.1	2	266.D-5655	213	R
HD 154873	B1Ib	17 10 20.83	-46 44 18.27	0.47 ^c	-21	3.7	4	266.D-5655	247	R
HD 156575	B1.5III	17 20 37.62	-46 02 46.43	0.31 ^c	-18	0.7	3	266.D-5655	202	R
HD 157038	B1/B2Ia	17 22 39.21	-37 48 16.69	0.81 ^c	-14	-15.9	4	266.D-5655	228	R
HD 161056	B1.5V	17 43 47.02	-07 04 46.58	0.59 ⁱ	-26	-13.3	1	65.I-0526	238	R
HD 163800	O+...	17 58 57.25	-22 31 03.16	0.61 ^e	5	-11.6	4	266.D-5655	126	R
HD 163758	O6.5Ia	17 59 28.36	-36 01 15.58	0.34 ^c	-48	-5.8	3	266.D-5655	224	R
HD 166734	08e	18 12 24.65	-10 43 53.04	1.35 ⁱ	-11	-12.4	2	65.I-0526	279	R
HD 167971	O8Ib	18 18 05.89	-12 14 33.29	1.07 ^a	1	-12.0	1	65.I-0526	215	R
BD-145037	B1.5a	18 25 06.18	-14 38 57.70	1.59 ^a	4	4.6	3	65.I-0526	223	R
HD 169454	O+...	18 25 15.19	-13 58 42.30	1.10 ⁱ	25	-9.0	18	079.C-0597	403	R
								266.D-5655		
								65.I-0526		
								67.C-0281		
								71.C-0513		
HD 170235	B2V	18 29 21.98	-25 15 23.77	0.30 ⁱ	-4	-1.5	2	266.D-5655	190	R
HD 170740	B2V	18 31 25.69	-10 47 45.01	0.45 ⁱ	-15	-10.1	1	65.I-0526	325	R
HD 171432	B1/B2Iab	18 35 36.75	-18 33 02.24	0.40 ^j	12	-6.2	3	266.D-5655	310	R
HD 172028	B2V	18 37 56.62	-00 23 09.05	0.79 ^k	-7	-10.3	1	65.I-0526	251	R
HD 182985	A0V	19 28 46.86	-36 00 00.92	0.12 ^k	12	-2.4	2	65.I-0526	286	R
HD 183143	B7Ia	19 27 26.56	+18 17 45.19	1.21 ⁱ	12	6.7	4	65.I-0526	211	R
								67.C-0281		
HD 188220	A0V	19 54 40.95	-15 54 49.07	0.27 ^k	12	-8.7	5	65.I-0526	224	R
HD 205637	B3V:p	21 37 04.83	-19 27 57.64	0.02 ^k	-23	-19.9	7	65.I-0526	358	R
HD 210121	B3V	22 08 11.90	-03 31 52.76	0.40 ^k	2	-14.2	12	65.I-0526	310	R
HD 212571	B1Ve	22 25 16.62	+01 22 38.63	0.23 ^l	4	-3.9 (-5 ^{cc})	10	65.I-0526	288	R
HD 358	B9II	00 08 23.25	+29 05 25.55	0.03 ^a	-10	...	7	076.B-0055	302	ST
								268.D-5738		
HD 10144	B6Vep	01 37 42.84	-57 14 12.31	0.05 ^a	18	...	2	266.D-5655	402	ST
HD 19698	B8V	03 10 38.79	+11 52 21.44	0.05 ^u	0	...	1	69.A-0204	156	ST
HD 24587	B5V	03 53 42.70	-24 36 44.03	0.02 ^a	20	...	6	074.B-0639	85	ST
								076.B-0055		

TABLE 3 — *Continued*

Object	Sp. Type ¹	RA [J2000]	DEC [J2000]	E_{B-V} [mag]	v_{\star}^1 [km·s $^{-1}$]	v_{ISM}^2 [km·s $^{-1}$]	# Obs ³	Prog. IDs	S/N ⁴	Type ⁵
HD 33949	B7V	05 13 13.87	-12 56 28.64	0.01 ⁿ	20	...	16	68.D-0546	363	ST
HD 35468	B2III	05 25 07.86	+06 20 58.93	0.02 ^a	18	...	8	266.D-5655	402	ST
HD 35777	B2V	05 26 59.16	-02 21 38.34	0.06 ^a	18	...	1	68.D-0237	108	ST
HD 36430	B2V	05 31 20.89	-06 42 30.16	0.06 ^a	23	...	4	68.D-0237	33	ST
HD 36916	B8IIIp	05 34 53.96	-04 06 37.50	0.04 ^u	13	...	2	072.D-0410	184	ST
HD 36960	B0.5V	05 35 02.68	-06 00 07.30	0.03 ^a	27	...	1	076.B-0055	52	ST
HD 37058	B3Vp	05 35 33.35	-04 50 15.17	0.08 ^u	22	...	1	072.D-0410	52	ST
HD 37490	B3IIIe	05 39 11.14	+04 07 17.27	0.12 ^a	21	...	6	266.D-5655	52	ST
HD 43285	B6Ve	06 15 40.17	+06 03 58.19	0.00 ⁿ	28	...	1	266.D-5655	113	ST
HD 49131	B2III	06 45 31.18	-30 56 56.33	0.04 ^a	7	...	8	266.D-5655	159	ST
HD 51876	B9Iw	06 58 24.24	-16 03 16.57	0.06 ^o	2*	...	3	266.D-5655	82	ST
HD 52918	B1V	07 02 54.77	-04 14 21.23	0.05 ^a	24	...	1	266.D-5655	389	ST
HD 60498	B4III	07 33 25.18	-33 23 59.63	0.05 ^a	29	...	4	266.D-5655	499	ST
HD 64972	B6II	07 55 21.75	-28 17 02.28	0.05 ^c	11*	...	3	266.D-5655	43	ST
HD 72067	B2Vne	08 29 07.56	-44 09 37.49	0.08 ^a	3	...	2	266.D-5655	223	ST
HD 76131	B6III	08 51 45.55	-55 48 31.87	0.09 ^u	3*	...	4	266.D-5655	165	ST
HD 89587	B3III	10 19 02.56	-50 42 57.96	0.01 ⁿ	7	...	2	266.D-5655	323	ST
HD 98718	B5Vn	11 21 00.40	-54 29 27.66	0.01 ^m	9	...	2	074.C-0134	301	ST
HD 100841	B9III	11 35 46.88	-63 01 11.43	0.02 ⁿ	-1	...	2	266.D-5655	261	ST
HD 106625	B8III	12 15 48.37	-17 32 30.94	0.00 ^k	-4	...	2	65.I-0526	93	ST
HD 109026	B5V	12 32 28.01	-72 07 58.75	0.02 ^a	2	...	1	266.D-5655	148	ST
HD 122451	B1III	14 03 49.40	-60 22 22.92	0.02 ^k	5	...	5	266.D-5655	426	ST
HD 125823	B7IIIpv	14 23 02.23	-39 30 42.54	0.06 ⁿ	7	...	15	073.D-0504	102	ST
HD 129116	B3V	14 41 57.59	-37 47 36.59	0.03 ^u	2	...	10	68.D-0546	176	ST
HD 130274	B9V	14 47 57.55	-26 38 46.15	0.06 ^u	6	...	3	67.D-0439	291	ST
HD 145482	B2V	16 12 18.20	-27 55 34.94	0.08 ^a	0	...	2	266.D-5655	358	ST
HD 158148	B5V	17 26 49.12	+20 04 51.51	0.04 ^a	-29	...	4	087.B-0308	37	ST
HD 162374	B6V	17 52 13.66	-34 47 57.11	0.01 ⁿ	-11	...	2	266.D-5655	122	ST
HD 163745	B5II	17 59 40.84	-41 29 13.39	0.01 ^c	0*	...	12	073.B-0607	136	ST
				.	.	266.D-5655				
				.	.	71.B-0529				
HD 163955	B9V	17 59 47.55	-23 48 58.08	0.05 ^a	-18	...	5	087.B-0308	285	ST
HD 165470	B2III	18 07 54.37	-38 33 55.52	0.03 ^u	0*	...	4	079.C-0597	447	ST
				.	.	67.C-0281				
HD 166197	B1V	18 10 55.34	-33 48 00.24	0.10 ^a	-25	...	4	71.D-0155	343	ST
HD 176437	B9III	18 58 56.62	+32 41 22.40	0.02 ^a	-20	...	4	67.D-0384	447	ST
				.	.	079.D-0567				
HD 222661	B9V	23 42 43.34	-14 32 41.65	0.02 ^m	3	...	3	68.D-0094	423	ST
				.	.	68.D-0546				
HD 223145	B3V	23 47 15.99	-50 13 35.25	0.01 ^k	11	...	3	076.D-0546	147	ST
				.	.	267.B-5698				

REFERENCES. — (a) Snow et al. (1977); (b) Walborn et al. (1980); (c) Hunter et al. (2006); (d) Crawford (1989); (e) Savage et al. (1985); (f) Fitzpatrick & Massa (2007); (g) Guarinos (1988); (h) Friedemann (1992); (i) Wegner (2002); (j) Slyk et al. (2008); (k) Gudennavar et al. (2012); (l) Berghoefer et al. (1996); (m) Zorec et al. (2009); (n) Jamar et al. (1995); (o) Raimond et al. (2012); (u) estimated using Fitzgerald (1970) and SIMBAD Database; (aa) Welty et al. (2003); (bb) Vos et al. (2011); (cc) Welty & Hobbs (2001).

The observations came from 27 different observing programmes: 65.I-0526 (PI: E. Roueff); 67.C-0281 (PI: P. Ehrenfreund); 67.D-0384 (PI: J. Orosz); 67.D-0439 (PI: F. Primas); 68.D-0094 (PI: F. Primas); 68.D-0237 (PI: F. Primas); 68.D-0323 (PI: L. Dessart); 68.D-0546 (PI: M. Asplund); 69.A-0204 (PI: V. D'Odorico); 71.B-0529 (PI: D. Silva); 71.C-0513 (PI: M. André); 71.D-0155 (PI: L. Pasquini); 072.D-0410 (PI: S. Bagnulo); 073.B-0607 (PI: D. Silva); 073.D-0504 (PI: S. Hubrig); 074.B-0639 (PI: D. Silva); 074.C-0134 (PI: N.C. Santos); 076.B-0055 (PI: D. Silva); 076.D-0169 (PI: C.R. Cowley); 076.D-0546 (PI: N. Christlieb); 079.C-0597 (PI: R. Gredel); 079.D-0567 (PI: D. Silva); 082.C-0566 (PI: Beletsky); 087.B-0308 (PI: P. Coelho); 266.D-5655 (PI: Paranal Observatory); 267.B-5698 (PI: D. Hutsmekers); 268.D-5738 (PI: G.M. Wahlgren).

¹ Taken from SIMBAD Database (<http://simbad.u-strasbg.fr/simbad/>)

² Measured using strongest component of Na I line at 3302.368 Å. Compared to literature values where possible.

³ The number of distinct observations co-added to create the optimal spectrum of the target.

⁴ Estimated from the co-added spectra between 3450Å–3452Å.

⁵ Designates whether target is classified as reddened (R), or an unreddened standard (S).

* Estimated by cross-correlating target against synthetic spectrum of hydrogen and helium lines.

TABLE 4
 LINES OF SIGHT MEASUREMENTS

Target	Species	λ_{helio} [Å]	v_{helio} [km s $^{-1}$]	W_λ [mÅ]	FWHM	
					[mÅ]	[km s $^{-1}$]
BD-14° 5037	Cr I	3578.720 ± 0.004	3.1 ± 0.3	1.39 ± 0.07	115.0 ± 8.4	9.64 ± 0.70
	Fe I	3440.522 ± 0.004	-7.3 ± 0.4	1.14 ± 0.07	60.0 ± 10.5	5.23 ± 0.92
		3440.665 ± 0.004	5.2 ± 0.4	4.03 ± 0.28	139.1 ± 11.7	12.12 ± 1.02
				[5.11 ± 0.75]		
	Na I	3302.289 ± 0.002	-7.2 ± 0.2	46.86 ± 0.22	74.3 ± 0.6	6.75 ± 0.06
		3302.424 ± 0.002	5.1 ± 0.2	106.05 ± 0.36	120.5 ± 0.7	10.94 ± 0.06
				[156.68 ± 1.08]		
	Na I	3302.904 ± 0.002	-6.7 ± 0.2	33.94 ± 0.14	61.5 ± 0.6	5.58 ± 0.05
		3303.031 ± 0.002	4.9 ± 0.2	72.93 ± 0.31	109.0 ± 0.7	9.89 ± 0.06
				[109.52 ± 0.70]		
Ti II	3066.224	-12.7		3.22 ± 0.56	76.3	7.46
	3066.313	-4.0		7.69 ± 0.54	116.0	11.34
	3066.420	6.5		7.84 ± 0.92	123.1	12.03
				[22.92 ± 4.38]		
	3072.854	-12.7		7.13 ± 0.48	76.5	7.46
	3072.943	-4.0		15.53 ± 0.46	116.2	11.34
	3073.051	6.5		12.38 ± 0.77	123.3	12.03
				[36.09 ± 3.12]		
	3229.062	-12.7		4.43 ± 0.39	80.4	7.46
	3229.156	-4.0		9.64 ± 0.36	122.2	11.34
Ti II	3229.269	6.5		8.09 ± 0.59	129.6	12.03
				[23.10 ± 2.51]		
	3241.857	-12.7		16.49 ± 0.17	80.7	7.46
	3241.951	-4.0		31.01 ± 0.16	122.6	11.34
	3242.064	6.5		28.47 ± 0.29	130.1	12.03
				[96.82 ± 2.04]		
	3383.624 ± 0.002	-12.7 ± 0.2		19.08 ± 1.79	83.8 ± 3.7	7.42 ± 0.33
	3383.723 ± 0.003	-4.0 ± 0.3		42.43 ± 4.66	129.8 ± 13.4	11.50 ± 1.19
	3383.842 ± 0.006	6.5 ± 0.5		37.45 ± 3.50	135.2 ± 6.2	11.98 ± 0.55
				[101.18 ± 1.05]		
CH	3137.497 ± 0.003	-3.2 ± 0.3		3.20 ± 0.21	43.1 ± 6.6	4.12 ± 0.63
	3137.604 ± 0.006	7.0 ± 0.6		6.86 ± 1.04	109.8 ± 10.9	10.49 ± 1.04
				[10.30 ± 2.37]		
	3143.100 ± 0.001	-4.7 ± 0.1		10.64 ± 0.33	61.5 ± 3.2	5.87 ± 0.30
	3143.219 ± 0.001	6.6 ± 0.1		14.94 ± 0.49	79.8 ± 3.4	7.61 ± 0.32
				[27.47 ± 1.72]		
	3145.930 ± 0.006	-7.6 ± 0.6		6.59 ± 0.85	60.9 ± 12.9	5.80 ± 1.23
	3146.046 ± 0.005	3.4 ± 0.5		10.11 ± 1.25	75.9 ± 13.0	7.23 ± 1.24
				[18.14 ± 4.97]		
	3633.215 ± 0.006	-6.1 ± 0.5		1.52 ± 0.25	48.5 ± 13.6	4.00 ± 1.12
CH	3633.348 ± 0.007	4.9 ± 0.6		2.52 ± 0.35	76.9 ± 9.2	6.34 ± 0.76
				[3.91 ± 1.36]		
	3636.146 ± 0.003	-6.3 ± 0.2		1.63 ± 0.10	60.6 ± 6.0	4.99 ± 0.50
	3636.279 ± 0.003	4.7 ± 0.2		2.31 ± 0.12	82.4 ± 0.2	6.79 ± 0.02
				[3.70 ± 0.34]		
	CH ⁺	3446.976 ± 0.004	-8.6 ± 0.4	0.39 ± 0.11	29.1 ± 9.3	2.53 ± 0.81
		3447.132 ± 0.004	5.0 ± 0.4	1.16 ± 0.28	54.7 ± 8.4	4.76 ± 0.73
				[1.53 ± 0.53]		
	CH ⁺	3578.918 ± 0.010	-8.6 ± 0.8	0.45 ± 0.20	42.2 ± 9.9	3.53 ± 0.83
		3579.086 ± 0.004	5.5 ± 0.4	3.15 ± 0.29	82.4 ± 0.2	6.90 ± 0.02
CN				[3.66 ± 1.07]		
	CN	3579.376 ± 0.004	-6.5 ± 0.3	1.72 ± 0.23	64.1 ± 8.8	5.37 ± 0.73
		3579.529 ± 0.012	6.4 ± 1.0	0.68 ± 0.20	56.9 ± 23.6	4.76 ± 1.97
				[2.38 ± 0.97]		
	CN	3579.885 ± 0.003	-6.5 ± 0.2	4.88 ± 0.36	54.4 ± 6.0	4.56 ± 0.50
		3580.009 ± 0.007	3.9 ± 0.6	2.32 ± 0.39	67.1 ± 4.2	5.62 ± 0.35
				[7.19 ± 2.04]		
	CN	3580.858 ± 0.005	-6.6 ± 0.5	1.06 ± 0.20	60.8 ± 12.8	5.09 ± 1.07
	OH	3078.385 ± 0.003	-5.4 ± 0.3	5.74 ± 0.43	63.6 ± 7.2	6.19 ± 0.70
		3078.507 ± 0.007	6.6 ± 0.6	2.91 ± 0.68	69.1 ± 16.2	6.73 ± 1.57
HD105056	OH	3081.607 ± 0.005	-5.6 ± 0.5	5.71 ± 0.60	110.5 ± 11.9	10.75 ± 1.15
	OH ⁺	3583.654 ± 0.004	-9.7 ± 0.3	0.36 ± 0.03	35.1 ± 1.7	2.93 ± 0.14
		3583.813 ± 0.004	3.7 ± 0.3	2.28 ± 0.15	120.7 ± 9.0	10.10 ± 0.75
				[2.32 ± 0.39]		
	Na I	3302.511 ± 0.004	13.0 ± 0.3	11.67 ± 0.72	171.0 ± 8.7	15.53 ± 0.79
	Na I	3303.120 ± 0.010	12.9 ± 0.9	4.17 ± 0.69	139.2 ± 23.2	12.63 ± 2.11
	Ti II	3066.414	5.9	5.01 ± 2.02	128.3	12.54
		3066.269	-8.3	3.07 ± 1.03	96.3	9.41
		3066.150	-19.9	2.98 ± 1.54	141.7	13.85
				[16.98 ± 12.26]		
Ti II	3073.044	5.9		10.48 ± 1.07	128.5	12.54
	3072.899	-8.3		6.21 ± 0.55	96.5	9.41
	3072.780	-19.9		9.13 ± 1.26	142.0	13.85

TABLE 4 — *Continued*

Target	Species	λ_{helio} [Å]	v_{helio} [km s $^{-1}$]	W_λ [mÅ]	FWHM [mÅ]	FWHM [km s $^{-1}$]	
Ti II	3229.262	5.9	[33.03 ± 7.17]	6.60 ± 0.53	135.1	12.54	
	3229.110	-8.3		2.71 ± 0.25	101.4	9.41	
	3228.985	-19.9		4.41 ± 0.59	149.2	13.85	
Ti II	3242.057	5.9	[14.20 ± 1.62]	21.29 ± 0.43	135.6	12.54	
	3241.904	-8.3		9.10 ± 0.21	101.8	9.41	
	3241.779	-19.9		12.06 ± 0.50	149.8	13.85	
Ti II	3383.831 ± 0.001	5.6 ± 0.1	[42.94 ± 1.97]	31.20 ± 0.43	141.7 ± 2.7	12.55 ± 0.24	
	3383.675 ± 0.002	-8.3 ± 0.2		14.08 ± 0.37	106.3 ± 6.0	9.42 ± 0.53	
	3383.543 ± 0.004	-19.9 ± 0.4		20.71 ± 0.65	156.2 ± 7.0	13.84 ± 0.62	
HD105071	Na I	3302.363 ± 0.002	-0.5 ± 0.2	[65.55 ± 1.39]	16.31 ± 0.28	61.0 ± 1.8	5.54 ± 0.17
		3302.454 ± 0.003	7.8 ± 0.3		3.10 ± 0.19	50.5 ± 7.1	4.59 ± 0.64
	Na I	3302.973 ± 0.001	-0.4 ± 0.1	[20.20 ± 1.20]	9.96 ± 0.33	69.6 ± 3.2	6.32 ± 0.29
		3303.068 ± 0.004	8.2 ± 0.4		1.89 ± 0.13	49.3 ± 9.8	4.48 ± 0.89
Ti II	3072.721	-25.6	[11.51 ± 0.92]	8.66 ± 1.88	161.0	15.71	
	3072.923	-5.9		11.96 ± 1.21	128.0	12.49	
	3073.040	5.5		4.65 ± 0.94	91.2	8.90	
Ti II	3228.923	-25.6	[35.84 ± 9.44]	2.83 ± 0.74	169.2	15.71	
	3229.135	-5.9		5.96 ± 0.48	134.5	12.49	
	3229.258	5.5		3.82 ± 0.36	95.9	8.90	
Ti II	3241.717	-25.6	[13.36 ± 2.82]	16.98 ± 0.86	169.9	15.71	
	3241.930	-5.9		20.65 ± 0.54	135.1	12.49	
	3242.054	5.5		11.60 ± 0.41	96.3	8.90	
Ti II	3383.479 ± 0.003	-25.6 ± 0.3	[54.52 ± 3.22]	24.78 ± 1.60	180.1 ± 7.6	15.95 ± 0.67	
	3383.701 ± 0.003	-5.9 ± 0.3		30.38 ± 1.43	139.7 ± 8.6	12.38 ± 0.76	
	3383.830 ± 0.003	5.5 ± 0.3		18.43 ± 1.16	101.0 ± 5.2	8.95 ± 0.46	
HD106068	Na I	3302.449 ± 0.002	7.3 ± 0.2	[79.51 ± 2.59]	17.41 ± 0.21	50.7 ± 1.0	4.60 ± 0.09
	Na I	3303.061 ± 0.002	7.5 ± 0.2		9.15 ± 0.25	47.8 ± 2.0	4.34 ± 0.18
	Ti II	3072.779	-20.0	[12.01]	13.51 ± 1.47	123.1	
Ti II	3072.879	-10.2		0.40 ± 0.01	22.0	2.15	
	3072.915	-6.7		13.08 ± 1.31	137.7	13.43	
	3073.030	4.5		6.79 ± 1.09	89.4	8.72	
Ti II	3228.983	-20.0	[42.92 ± 10.05]	9.21 ± 1.33	129.4	12.01	
	3229.089	-10.2		0.24 ± 0.00	23.2	2.15	
	3229.127	-6.7		7.65 ± 1.06	144.7	13.43	
Ti II	3229.247	4.5		7.20 ± 0.84	93.9	8.72	
	3241.777	-20.0	[29.09 ± 6.33]	28.75 ± 0.67	129.9	12.01	
	3241.884	-10.2		0.65 ± 0.00	23.3	2.15	
Ti II	3241.921	-6.7		21.08 ± 0.60	145.2	13.43	
	3242.043	4.5		17.24 ± 0.50	94.3	8.72	
			[77.00 ± 4.18]				
Ti II	3383.542 ± 0.002	-20.0 ± 0.2	[38.65 ± 0.65]	135.6 ± 2.0	12.01 ± 0.18		
	3383.654 ± 0.001	-10.1 ± 0.1		1.27 ± 0.02	24.0 ± 2.8	2.13 ± 0.25	
	3383.692 ± 0.002	-6.7 ± 0.2		29.53 ± 0.37	150.7 ± 5.3	13.36 ± 0.47	
HD109867	CH ⁺	3383.820 ± 0.002	4.6 ± 0.2	[23.35 ± 0.45]	98.9 ± 2.0	8.76 ± 0.18	
	Na I	3579.106 ± 0.004	7.2 ± 0.4	[97.16 ± 1.70]	3.37 ± 0.35	72.0 ± 10.1	6.03 ± 0.85
	Na I	3302.440 ± 0.002	6.5 ± 0.2		20.77 ± 0.28	92.7 ± 1.4	8.41 ± 0.12
Ti II	Na I	3303.051 ± 0.001	6.6 ± 0.1		14.15 ± 0.40	109.9 ± 2.6	9.97 ± 0.23
	3072.505	-46.7	[4.66]	1.47 ± 0.47	47.8		
	3072.624	-35.1		2.07 ± 0.62	75.1	7.33	
Ti II	3072.785	-19.4		6.84 ± 1.14	157.8	15.39	
	3072.885	-9.6		2.16 ± 0.15	50.5	4.93	
	3073.003	1.9		8.57 ± 1.09	140.3	13.69	
Ti II	3228.695	-46.7	[24.14 ± 6.56]	11.63 ± 14.99	50.2	4.66	
	3228.821	-35.1		0.84 ± 0.00	79.0	7.33	
	3228.990	-19.4		1.77 ± 0.05	165.8	15.39	
Ti II	3229.095	-9.6		0.65 ± 0.09	53.1	4.93	
	3229.219	1.9		4.59 ± 0.51	147.5	13.69	
			[6.58 ± 1.66]				
Ti II	3241.488	-46.7	[3.66]	3.39 ± 0.16	50.4	4.66	
	3241.614	-35.1		4.28 ± 0.22	79.3	7.33	
	3241.784	-19.4		11.54 ± 0.44	166.4	15.39	

TABLE 4 — *Continued*

Target	Species	λ_{helio} [Å]	v_{helio} [km s $^{-1}$]	W_λ [mÅ]	FWHM [mÅ]	FWHM [km s $^{-1}$]
HD110432	Ti II	3241.890	-9.6	2.95 ± 0.06	53.3	4.93
		3242.014	1.9	17.88 ± 0.49	148.1	13.69
				[47.22 ± 2.28]		
		3383.242 ± 0.003	-46.6 ± 0.3	2.36 ± 0.45	66.0 ± 8.0	5.85 ± 0.70
		3383.371 ± 0.003	-35.2 ± 0.3	3.97 ± 0.17	82.9 ± 8.7	7.34 ± 0.77
	Na I	3383.548 ± 0.005	-19.5 ± 0.4	13.98 ± 0.44	177.5 ± 18.0	15.72 ± 1.60
		3383.659 ± 0.001	-9.6 ± 0.1	4.79 ± 0.05	55.3 ± 4.6	4.90 ± 0.41
		3383.790 ± 0.001	1.9 ± 0.1	29.13 ± 0.37	156.6 ± 3.3	13.87 ± 0.29
				[54.05 ± 2.21]		
		3302.441 ± 0.002	6.6 ± 0.2	39.36 ± 0.21	70.0 ± 0.4	6.35 ± 0.04
HD112244	Na I	3303.055 ± 0.002	7.0 ± 0.2	24.33 ± 0.10	62.4 ± 0.3	5.66 ± 0.03
		3241.922	-6.7	2.18 ± 0.23	98.2	9.08
	Ti II	3242.044	4.7	4.41 ± 0.16	82.4	7.62
				[7.43 ± 0.88]		
	Ti II	3383.692 ± 0.005	-6.7 ± 0.4	3.78 ± 0.19	102.6 ± 11.6	9.09 ± 1.03
		3383.821 ± 0.002	4.7 ± 0.2	7.33 ± 0.18	86.6 ± 4.4	7.67 ± 0.39
	CH	3143.226 ± 0.001	7.3 ± 0.1	5.54 ± 0.18	82.4 ± 3.5	7.86 ± 0.33
		3627.489 ± 0.016	7.1 ± 1.3	0.59 ± 0.26	115.4 ± 39.9	9.54 ± 3.30
		3633.376 ± 0.009	7.1 ± 0.7	0.61 ± 0.14	66.6 ± 21.5	5.49 ± 1.77
		3636.320 ± 0.012	8.1 ± 1.0	0.99 ± 0.34	115.9 ± 28.0	9.56 ± 2.31
		3579.094 ± 0.005	6.2 ± 0.4	1.40 ± 0.17	78.1 ± 10.6	6.55 ± 0.89
HD112842	Na I	3302.193 ± 0.002	-15.9 ± 0.2	9.52 ± 0.13	75.0 ± 1.5	6.81 ± 0.13
		3302.466 ± 0.002	8.9 ± 0.2	9.67 ± 0.19	97.1 ± 2.1	8.82 ± 0.19
	Na I	3302.803 ± 0.001	-15.9 ± 0.1	5.61 ± 0.21	77.3 ± 3.2	7.02 ± 0.29
		3303.080 ± 0.002	9.3 ± 0.2	5.60 ± 0.30	105.2 ± 5.0	9.55 ± 0.46
	Ti II	3072.810	-16.9	2.45 ± 0.33	80.4	7.84
		3072.926	-5.6	3.14 ± 0.30	87.0	8.49
		3073.046	6.1	3.14 ± 0.27	73.6	7.18
	Ti II	3229.017	-16.9	[7.29 ± 1.94]		
		3229.139	-5.6	1.02 ± 0.12	84.5	7.84
		3229.264	6.1	2.63 ± 0.15	91.5	8.49
HD114213	Ti II	3241.811	-16.9	[5.19 ± 0.71]		
		3241.933	-5.6	2.18 ± 0.14	77.3	7.18
		3242.060	6.1	7.89 ± 0.13	77.7	7.18
	Ti II	3383.577 ± 0.003	-16.9 ± 0.2	[19.48 ± 0.74]		
		3383.705 ± 0.002	-5.6 ± 0.2	7.57 ± 0.39	89.1 ± 6.5	7.90 ± 0.58
		3383.837 ± 0.001	6.1 ± 0.1	11.53 ± 0.27	95.7 ± 6.2	8.48 ± 0.55
	Na I	3302.451 ± 0.002	7.5 ± 0.2	13.61 ± 0.31	81.3 ± 2.8	7.21 ± 0.25
		3303.063 ± 0.002	7.7 ± 0.2	[33.62 ± 1.51]		
HD114213	Ti II	3072.601	-37.4	7.98 ± 0.64	162.8	15.88
		3072.804	-17.5	10.09 ± 0.41	124.0	12.10
		3072.952	-3.1	6.39 ± 0.36	113.5	11.07
		3073.037	5.1	4.80 ± 0.25	70.5	6.88
				[30.35 ± 2.07]		
	Ti II	3228.796	-37.4	2.59 ± 0.54	171.1	15.88
		3229.010	-17.5	4.34 ± 0.34	130.3	12.10
		3229.166	-3.1	3.94 ± 0.27	119.2	11.07
		3229.254	5.1	2.76 ± 0.19	74.1	6.88
HD114213	Ti II	3241.589	-37.4	[13.65 ± 1.62]		
		3241.805	-17.5	13.78 ± 0.63	171.7	15.88
		3241.961	-3.1	16.67 ± 0.42	130.9	12.10
		3242.049	5.1	15.13 ± 0.35	119.7	11.07
	Ti II	3383.346 ± 0.002	-37.4 ± 0.2	8.35 ± 0.24	74.4	6.88
		3383.570 ± 0.002	-17.5 ± 0.2	[58.93 ± 2.59]		
		3383.733 ± 0.002	-3.1 ± 0.2	16.79 ± 0.48	179.1 ± 5.1	15.86 ± 0.45
	Na I	3383.826 ± 0.002	5.1 ± 0.2	24.25 ± 0.19	136.7 ± 4.6	12.11 ± 0.41
				21.41 ± 0.21	125.1 ± 7.0	11.08 ± 0.62
HD114213	CH	3143.240 ± 0.003	8.6 ± 0.3	12.85 ± 0.11	77.8 ± 1.6	6.89 ± 0.14
		3146.065 ± 0.008	5.2 ± 0.7	2.55 ± 0.21	63.7 ± 6.4	6.08 ± 0.61
		3579.120 ± 0.004	8.4 ± 0.4	1.88 ± 0.43	70.6 ± 18.4	6.72 ± 1.75
		3440.398 ± 0.004	-18.1 ± 0.3	1.32 ± 0.12	72.9 ± 10.4	6.11 ± 0.87
		3440.566 ± 0.004	-3.4 ± 0.4	2.61 ± 0.41	87.3 ± 8.6	7.61 ± 0.75
	Fe I	3302.174 ± 0.002	-17.6 ± 0.2	0.58 ± 0.07	35.3 ± 0.2	3.08 ± 0.02
		3302.418 ± 0.002	4.6 ± 0.2	[3.82 ± 1.00]		
				55.07 ± 0.13	79.5 ± 0.3	7.21 ± 0.02
HD114213	Na I			39.32 ± 0.15	75.1 ± 0.3	6.82 ± 0.03
				[95.51 ± 0.97]		

TABLE 4 — *Continued*

Target	Species	λ_{helio} [Å]	v_{helio} [km s $^{-1}$]	W_λ [mÅ]	FWHM	
					[mÅ]	[km s $^{-1}$]
Na I	3302.782 ± 0.002	-17.8 ± 0.2	38.06 ± 0.30	78.4 ± 0.7	7.12 ± 0.06	
	3303.027 ± 0.002	4.4 ± 0.2	26.68 ± 0.26	78.8 ± 1.0	7.15 ± 0.09	
Ti II			[65.13 ± 1.39]			
	3065.906	-43.8	2.11 ± 1.12	95.6	9.35	
	3066.045	-30.2	3.23 ± 0.83	66.9	6.54	
	3066.179	-17.2	5.78 ± 1.77	140.4	13.73	
	3066.336	-1.8	2.96 ± 0.92	86.6	8.47	
Ti II	3066.419	6.4	2.08 ± 0.97	81.9	8.01	
			[16.71 ± 9.27]			
	3072.535	-43.8	2.06 ± 1.00	95.8	9.35	
	3072.675	-30.2	5.08 ± 0.62	67.0	6.54	
	3072.808	-17.2	15.81 ± 1.29	140.7	13.73	
Ti II	3072.966	-1.8	6.14 ± 0.65	86.8	8.47	
	3073.049	6.4	3.12 ± 0.77	82.1	8.01	
			[33.49 ± 6.22]			
	3228.727	-43.8	1.10 ± 0.08	100.7	9.35	
	3228.874	-30.2	3.30 ± 0.20	70.5	6.54	
Ti II	3229.014	-17.2	9.73 ± 0.41	147.9	13.73	
	3229.180	-1.8	2.88 ± 0.20	91.2	8.47	
	3229.268	6.4	2.95 ± 0.23	86.3	8.01	
			[19.94 ± 2.56]			
	3241.520	-43.8	6.25 ± 0.31	101.1	9.35	
Ti II	3241.668	-30.2	12.04 ± 0.16	70.7	6.54	
	3241.808	-17.2	32.84 ± 0.35	148.5	13.73	
	3241.975	-1.8	10.66 ± 0.17	91.6	8.47	
	3242.063	6.4	8.58 ± 0.19	86.6	8.01	
			[76.39 ± 2.00]			
Ti II	3383.274 ± 0.005	-43.8 ± 0.4	4.61 ± 0.45	103.6 ± 11.4	9.18 ± 1.01	
	3383.428 ± 0.001	-30.2 ± 0.1	15.44 ± 0.14	73.8 ± 2.6	6.54 ± 0.23	
	3383.574 ± 0.001	-17.2 ± 0.1	45.93 ± 0.42	154.9 ± 4.7	13.73 ± 0.42	
	3383.748 ± 0.002	-1.8 ± 0.2	16.05 ± 0.14	95.7 ± 5.9	8.48 ± 0.52	
	3383.840 ± 0.002	6.4 ± 0.2	13.30 ± 0.33	90.4 ± 3.7	8.01 ± 0.33	
CH			[96.44 ± 2.11]			
	3137.360 ± 0.002	-16.2 ± 0.2	4.48 ± 0.27	57.4 ± 4.9	5.48 ± 0.46	
CH	3137.593 ± 0.004	6.0 ± 0.4	1.43 ± 0.17	40.7 ± 8.8	3.89 ± 0.84	
			[7.15 ± 1.90]			
CH	3142.967 ± 0.001	-17.5 ± 0.1	10.64 ± 0.42	60.1 ± 3.0	5.73 ± 0.29	
	3143.216 ± 0.005	6.3 ± 0.5	5.46 ± 0.56	92.0 ± 11.1	8.78 ± 1.06	
CH			[15.76 ± 2.14]			
	3145.796 ± 0.005	-20.4 ± 0.5	9.57 ± 1.63	71.4 ± 12.7	6.81 ± 1.21	
	3627.156 ± 0.005	-20.4 ± 0.4	1.24 ± 0.18	81.3 ± 11.4	6.72 ± 0.94	
CH	3627.460 ± 0.005	4.7 ± 0.4	0.51 ± 0.08	45.4 ± 10.6	3.76 ± 0.87	
			[2.05 ± 0.58]			
	3633.056 ± 0.004	-19.3 ± 0.3	1.86 ± 0.23	64.0 ± 8.6	5.28 ± 0.71	
CH	3633.336 ± 0.006	3.9 ± 0.5	0.33 ± 0.10	31.2 ± 6.2	2.57 ± 0.51	
			[1.71 ± 0.77]			
CH	3635.993 ± 0.005	-18.8 ± 0.4	1.35 ± 0.16	65.7 ± 11.2	5.41 ± 0.92	
	3636.321 ± 0.007	8.1 ± 0.5	1.10 ± 0.41	102.0 ± 22.8	8.41 ± 1.88	
CN			[1.94 ± 0.88]			
	3579.216 ± 0.002	-19.9 ± 0.1	3.68 ± 0.16	62.0 ± 3.7	5.20 ± 0.31	
	3579.721 ± 0.002	-20.2 ± 0.2	10.16 ± 0.07	55.8 ± 0.6	4.67 ± 0.05	
	3580.701 ± 0.002	-19.8 ± 0.2	1.91 ± 0.12	52.8 ± 5.7	4.42 ± 0.48	
NH	3353.699 ± 0.007	-20.2 ± 0.6	2.70 ± 0.52	76.4 ± 16.4	6.83 ± 1.47	
	3357.839 ± 0.002	-19.1 ± 0.1	2.10 ± 0.08	52.0 ± 3.7	4.64 ± 0.33	
OH	3078.266 ± 0.002	-16.9 ± 0.2	9.86 ± 0.96	102.6 ± 8.4	9.99 ± 0.82	
	3078.475 ± 0.003	3.4 ± 0.3	2.18 ± 0.44	31.5 ± 7.6	3.07 ± 0.74	
			[14.72 ± 1.89]			
OH	3081.461 ± 0.004	-19.8 ± 0.4	8.30 ± 0.87	81.0 ± 9.5	7.88 ± 0.92	
	3081.668 ± 0.008	0.3 ± 0.7	4.29 ± 0.73	79.3 ± 17.9	7.71 ± 1.74	
HD115363	Na I	3302.133 ± 0.002	-21.3 ± 0.2	45.30 ± 0.71	87.2 ± 1.6	7.91 ± 0.15
		3302.422 ± 0.002	4.9 ± 0.2	53.11 ± 0.66	67.2 ± 0.9	6.10 ± 0.09
	Na I	3302.744 ± 0.002	-21.2 ± 0.2	[97.44 ± 4.02]		
Ti II	3228.976	-20.7	22.67 ± 0.46	79.8 ± 1.8	7.25 ± 0.16	
	3229.215	1.5	37.14 ± 0.31	61.1 ± 0.7	5.55 ± 0.07	
Ti II	3241.770	-20.7	[28.58 ± 7.90]			
	3242.010	1.5	35.44 ± 0.72	112.8	10.43	
Ti II	3383.534 ± 0.002	-20.7 ± 0.2	[62.54 ± 5.23]			
	3383.785 ± 0.002	1.5 ± 0.2	59.32 ± 0.46	117.8 ± 0.2	10.43 ± 0.02	
			30.88 ± 0.43	117.8 ± 0.2	10.43 ± 0.02	
			[113.64 ± 3.25]			

TABLE 4 — *Continued*

Target	Species	λ_{helio} [Å]	v_{helio} [km s $^{-1}$]	W_λ [mÅ]	FWHM [mÅ]	FWHM [km s $^{-1}$]	
HD115842	Na I	CH	3137.599 ± 0.016	6.5 ± 1.6	12.22 ± 5.28	247.4 ± 40.2	
		CH	3143.214 ± 0.004	6.1 ± 0.4	7.87 ± 1.37	75.6 ± 10.2	
		CH	3146.044 ± 0.006	3.3 ± 0.5	4.84 ± 0.88	51.8 ± 13.2	
		OH	3081.721 ± 0.005	5.6 ± 0.5	5.64 ± 0.71	41.8 ± 10.8	
		3302.207 ± 0.002	-14.6 ± 0.2	28.04 ± 0.18	51.8 ± 1.3	4.70 ± 0.12	
		3302.264 ± 0.002	-9.5 ± 0.2	34.08 ± 0.14	53.7 ± 1.2	4.88 ± 0.11	
		3302.423 ± 0.001	5.0 ± 0.1	9.77 ± 0.35	81.7 ± 3.5	7.42 ± 0.32	
				[69.66 ± 1.90]			
		Na I	3302.818 ± 0.002	-14.6 ± 0.2	18.72 ± 0.15	51.3 ± 1.3	
	Ti II	3302.875 ± 0.002	-9.3 ± 0.2	25.88 ± 0.05	50.1 ± 0.9	4.55 ± 0.08	
		3303.029 ± 0.002	4.7 ± 0.2	8.22 ± 0.33	109.7 ± 4.6	9.96 ± 0.42	
				[52.95 ± 1.09]			
		3072.814	-16.6	9.05 ± 0.60	109.1	10.64	
		3072.878	-10.3	0.17 ± 0.04	23.1	2.25	
		3072.946	-3.7	11.30 ± 1.69	203.7	19.87	
				[21.95 ± 4.59]			
		Ti II	3229.021	-16.6	1.84 ± 0.33	114.6	10.64
		3229.088	-10.3	0.47 ± 0.02	24.2	2.25	
	Ti II	3229.159	-3.7	7.13 ± 0.88	214.0	19.87	
				[9.45 ± 1.81]			
		3241.815	-16.6	11.86 ± 0.33	115.1	10.64	
		3241.882	-10.3	1.54 ± 0.03	24.3	2.25	
		3241.954	-3.7	22.48 ± 0.84	214.9	19.87	
				[37.69 ± 2.65]			
		Ti II	3383.581 ± 0.003	-16.6 ± 0.3	17.29 ± 1.46	120.1 ± 6.4	
		3383.652 ± 0.002	-10.3 ± 0.1	2.13 ± 0.20	25.0 ± 4.6	2.22 ± 0.41	
		3383.726 ± 0.005	-3.8 ± 0.4	39.33 ± 2.40	226.2 ± 4.0	20.04 ± 0.36	
HD136239	Fe I	CH	3137.449 ± 0.008	-7.7 ± 0.8	2.70 ± 1.06	88.7 ± 19.3	
		CH	3143.052 ± 0.003	-9.4 ± 0.3	6.91 ± 0.56	79.0 ± 6.4	
		CH	3145.880 ± 0.004	-12.4 ± 0.4	4.36 ± 0.58	54.3 ± 9.9	
		CH	3633.161 ± 0.010	-10.6 ± 0.8	1.29 ± 0.30	77.8 ± 23.6	
		CH	3636.074 ± 0.007	-12.2 ± 0.5	1.11 ± 0.20	67.7 ± 15.9	
		3440.124 ± 0.015	-42.0 ± 1.3	1.65 ± 0.76	82.6 ± 18.5	7.20 ± 1.61	
		3440.376 ± 0.018	-20.0 ± 1.6	0.74 ± 0.18	47.1 ± 0.2	4.10 ± 0.02	
		3440.447 ± 0.005	-13.9 ± 0.4	3.12 ± 0.34	56.6 ± 11.9	4.93 ± 1.04	
				[59.94 ± 1.66]			
	Na I	CH	3301.818 ± 0.006	-49.9 ± 0.5	19.79 ± 4.15	63.6 ± 13.0	
		CH	3302.143 ± 0.010	-20.4 ± 0.9	12.49 ± 3.62	53.2 ± 3.0	
		CH	3302.211 ± 0.004	-14.3 ± 0.3	44.08 ± 3.16	63.9 ± 8.6	
		CH	3302.327 ± 0.015	-3.8 ± 1.4	10.06 ± 3.96	68.7 ± 32.3	
				[6.74 ± 3.69]			
		Na I	3302.415 ± 0.003	-51.1 ± 0.2	13.89 ± 3.57	84.8 ± 5.5	
		Na I	3302.753 ± 0.003	-20.5 ± 0.3	5.98 ± 0.26	47.1 ± 0.2	
		Na I	3302.821 ± 0.002	-14.2 ± 0.2	31.65 ± 0.47	60.1 ± 2.2	
		Na I	3302.938 ± 0.006	-3.7 ± 0.6	3.93 ± 0.53	64.0 ± 14.7	
	Ti II			[83.32 ± 27.24]			
		3072.469	-50.2	16.48 ± 4.43	160.2	15.63	
		3072.657	-31.9	11.96 ± 2.58	131.8	12.86	
		3072.806	-17.4	14.18 ± 2.59	132.5	12.93	
		3072.976	-0.8	7.96 ± 2.66	116.4	11.35	
				[50.75 ± 4.94]			
		Ti II	3241.451	-50.2	33.91 ± 1.00	169.0	15.63
		3241.649	-31.9	20.08 ± 0.67	139.1	12.86	
		3241.806	-17.4	27.05 ± 0.79	139.8	12.93	
		3241.985	-0.8	10.25 ± 0.93	122.7	11.35	
	Ti II			[62.39 ± 24.06]			
		3383.202 ± 0.003	-50.1 ± 0.2	51.18 ± 2.70	179.0 ± 6.0	15.86 ± 0.54	
		3383.408 ± 0.004	-31.9 ± 0.4	32.07 ± 1.04	143.8 ± 12.7	12.74 ± 1.12	
		3383.571 ± 0.004	-17.5 ± 0.3	45.77 ± 0.88	146.3 ± 7.2	12.96 ± 0.63	
		3383.759 ± 0.002	-0.8 ± 0.2	20.38 ± 0.94	128.0 ± 6.4	11.34 ± 0.57	
				[103.02 ± 4.48]			
		CN	3579.775 ± 0.006	-15.7 ± 0.5	1.70 ± 0.34	53.8 ± 14.0	
	Na I	Na I	3301.897 ± 0.002	-42.7 ± 0.2	4.94 ± 0.29	45.1 ± 4.2	
		3302.254 ± 0.002	-10.3 ± 0.2	15.17 ± 0.45	54.3 ± 1.8		
		3302.412 ± 0.002	4.0 ± 0.2	7.27 ± 0.52	60.7 ± 4.4		
				[154.92 ± 4.59]			
		Na I	3302.499 ± 0.002	-43.5 ± 0.2	3.38 ± 0.21	47.1 ± 0.2	
		Na I	3302.866 ± 0.002	-10.2 ± 0.2	9.13 ± 0.24	55.2 ± 1.9	
		Na I	3303.025 ± 0.002	4.3 ± 0.2	4.02 ± 0.30	59.4 ± 4.8	
				[27.24 ± 2.89]			
		Ti II	3072.452	-51.9	10.26 ± 1.79	187.2	18.26
HD142758	Na I	3072.549	-42.4	0.06 ± 0.03	42.6	4.16	
		3072.673	-30.3	21.52 ± 1.34	192.4	18.77	
		3072.836	-14.4	11.67 ± 0.94	116.2	11.34	

TABLE 4 — *Continued*

Target	Species	λ_{helio} [Å]	v_{helio} [km s $^{-1}$]	W_λ [mÅ]	FWHM [mÅ]	FWHM [km s $^{-1}$]
Ti II	3072.999	1.5	3.08 ± 0.82 [58.51 ± 7.23]	72.9	7.11	
	3228.640	-51.9	7.20 ± 0.95	196.7	18.26	
	3228.742	-42.4	0.38 ± 0.01	44.8	4.16	
	3228.872	-30.3	14.08 ± 0.68	202.2	18.77	
	3229.043	-14.4	8.11 ± 0.43	122.2	11.34	
	3229.215	1.5	2.74 ± 0.36	76.6	7.11	
			[35.89 ± 3.68]			
	3241.433	-51.9	20.24 ± 1.02	197.5	18.26	
	3241.536	-42.4	2.05 ± 0.02	45.0	4.16	
	3241.666	-30.3	34.95 ± 0.78	203.0	18.77	
Ti II	3241.838	-14.4	23.25 ± 0.58	122.6	11.34	
	3242.010	1.5	5.84 ± 0.53	76.9	7.11	
			[91.96 ± 3.11]			
	3383.183 ± 0.002	-51.9 ± 0.2	36.98 ± 0.89	206.9 ± 3.7	18.33 ± 0.33	
	3383.290 ± 0.001	-42.4 ± 0.1	3.66 ± 0.08	47.1 ± 0.7	4.17 ± 0.06	
	3383.426 ± 0.002	-30.3 ± 0.2	63.74 ± 0.26	212.0 ± 0.2	18.78 ± 0.02	
	3383.605 ± 0.002	-14.4 ± 0.2	39.37 ± 0.25	127.9 ± 1.9	11.33 ± 0.17	
	3383.785 ± 0.001	1.5 ± 0.1	9.98 ± 0.22	80.1 ± 2.7	7.09 ± 0.24	
			[155.38 ± 1.53]			
	CH	3143.031 ± 0.004	-11.3 ± 0.4	1.88 ± 0.22	38.8 ± 8.8	3.70 ± 0.84
HD143448	Na I	3302.403 ± 0.002	3.2 ± 0.2	5.56 ± 0.30	79.3 ± 5.0	7.20 ± 0.45
	Na I	3303.018 ± 0.002	3.6 ± 0.2	4.00 ± 0.35	71.5 ± 5.8	6.49 ± 0.53
	Ti II	3242.010 ± 0.002	1.5 ± 0.2	8.77 ± 0.49	102.5 ± 5.7	9.48 ± 0.53
	Ti II	3383.781 ± 0.001	1.2 ± 0.1	12.69 ± 0.39	95.9 ± 3.1	8.50 ± 0.27
	Cr I	3578.592 ± 0.003	-7.6 ± 0.3	1.94 ± 0.38	109.6 ± 7.4	9.18 ± 0.62
	Fe I	3440.536 ± 0.002	-6.1 ± 0.2	7.30 ± 0.18	61.4 ± 2.1	5.35 ± 0.19
	Fe I	3679.841 ± 0.002	-5.9 ± 0.1	2.08 ± 0.07	85.9 ± 4.1	7.00 ± 0.34
	Na I	3302.301 ± 0.002	-6.0 ± 0.2	43.11 ± 0.22	62.9 ± 0.5	5.71 ± 0.04
	Na I	3302.911 ± 0.002	-6.1 ± 0.2	36.34 ± 0.19	62.3 ± 0.5	5.65 ± 0.05
	Ti II	3072.721	-25.6	3.17 ± 0.91	213.4	20.82
HD147701		3072.902	-8.0	3.63 ± 0.26	79.3	7.74
		3073.055	6.9	4.80 ± 1.16	192.3	18.76
			[11.67 ± 2.95]			
	Ti II	3241.717	-25.6	7.37 ± 0.64	225.2	20.82
		3241.907	-8.0	4.91 ± 0.11	83.7	7.74
		3242.069	6.9	3.56 ± 0.52	202.9	18.76
			[14.98 ± 1.28]			
	Ti II	3383.479 ± 0.003	-25.6 ± 0.3	8.37 ± 0.46	235.4 ± 0.8	20.86 ± 0.07
		3383.678 ± 0.002	-8.0 ± 0.2	6.61 ± 0.10	87.5 ± 5.3	7.75 ± 0.47
		3383.846 ± 0.013	6.9 ± 1.1	4.97 ± 0.56	208.0 ± 25.9	18.43 ± 2.29
HD147889	CH	3137.494 ± 0.002	-3.5 ± 0.2	3.71 ± 0.22	49.3 ± 5.2	4.71 ± 0.50
	CH	3143.104 ± 0.002	-4.4 ± 0.2	13.52 ± 0.26	61.0 ± 2.0	5.82 ± 0.19
	CH	3145.932 ± 0.005	-7.4 ± 0.5	9.72 ± 1.25	66.2 ± 12.4	6.31 ± 1.18
	CH	3627.345 ± 0.005	-4.8 ± 0.5	1.46 ± 0.14	84.4 ± 12.8	6.98 ± 1.06
	CH	3633.217 ± 0.003	-6.0 ± 0.3	2.47 ± 0.14	67.8 ± 7.4	5.59 ± 0.61
	CH	3636.148 ± 0.002	-6.1 ± 0.2	1.43 ± 0.08	49.1 ± 5.8	4.05 ± 0.48
	CH ⁺	3578.949 ± 0.025	-5.9 ± 2.1	1.35 ± 0.41	68.3 ± 34.7	5.72 ± 2.90
	CN	3579.398 ± 0.010	-4.6 ± 0.8	2.26 ± 0.40	99.8 ± 23.5	8.36 ± 1.97
	CN	3579.891 ± 0.002	-6.0 ± 0.2	3.86 ± 0.19	56.0 ± 5.1	4.69 ± 0.43
	Cr I	3578.594 ± 0.002	-7.5 ± 0.2	2.74 ± 0.15	81.9 ± 5.4	6.86 ± 0.45
Ti II	Cr I	3593.395 ± 0.003	-7.3 ± 0.2	0.74 ± 0.05	43.6 ± 6.3	3.64 ± 0.53
	Fe I	3440.525 ± 0.002	-7.0 ± 0.2	9.58 ± 0.13	52.4 ± 1.1	4.56 ± 0.10
	Fe I	3679.826 ± 0.003	-7.1 ± 0.2	1.27 ± 0.08	45.7 ± 6.2	3.72 ± 0.51
	Na I	3302.291 ± 0.002	-6.9 ± 0.2	37.39 ± 0.16	60.9 ± 0.4	5.53 ± 0.04
	Na I	3302.903 ± 0.002	-6.8 ± 0.2	32.74 ± 0.15	55.5 ± 0.4	5.03 ± 0.04
	Ti II	3228.869	-30.6	0.13 ± 0.13	93.6	8.69
		3228.993	-19.1	0.42 ± 0.16	85.2	7.91
		3229.111	-8.2	1.00 ± 0.10	50.1	4.65
			[1.15 ± 0.64]			
	Ti II	3241.663	-30.6	1.78 ± 0.29	94.0	8.69
Ti II		3241.787	-19.1	2.05 ± 0.23	85.5	7.91
		3241.905	-8.2	3.20 ± 0.15	50.3	4.65
			[7.88 ± 1.36]			
	Ti II	3383.422 ± 0.004	-30.7 ± 0.4	3.31 ± 0.30	99.6 ± 10.3	8.82 ± 0.91
		3383.552 ± 0.006	-19.1 ± 0.5	2.04 ± 0.11	89.3 ± 14.9	7.91 ± 1.32
		3383.675 ± 0.002	-8.2 ± 0.2	5.03 ± 0.10	52.6 ± 2.0	4.66 ± 0.17
			[10.70 ± 0.65]			
	CH	3137.485 ± 0.002	-4.3 ± 0.2	10.80 ± 0.24	48.6 ± 1.7	4.65 ± 0.16
	CH	3143.089 ± 0.002	-5.8 ± 0.2	22.48 ± 0.20	52.5 ± 0.7	5.01 ± 0.06
	CH	3145.920 ± 0.004	-8.6 ± 0.4	16.11 ± 2.07	52.2 ± 9.3	4.97 ± 0.89
CH	3627.312 ± 0.001	-7.5 ± 0.1	2.38 ± 0.07	60.8 ± 2.6	5.02 ± 0.22	
	CH	3633.201 ± 0.001	-7.3 ± 0.1	6.63 ± 0.20	69.2 ± 2.7	5.71 ± 0.22
	CH	3636.134 ± 0.002	-7.3 ± 0.2	3.39 ± 0.05	52.0 ± 1.5	4.29 ± 0.12

TABLE 4 — *Continued*

Target	Species	λ_{helio} [Å]	v_{helio} [km s $^{-1}$]	W_λ [mÅ]	FWHM [mÅ]	FWHM [km s $^{-1}$]
HD147933	CH $^+$	3446.982 ± 0.009	-8.1 ± 0.8	1.69 ± 0.29	95.5 ± 20.8	8.30 ± 1.81
	CH $^+$	3578.933 ± 0.008	-7.2 ± 0.7	3.03 ± 0.63	82.8 ± 19.7	6.94 ± 1.65
	CN	3579.365 ± 0.009	-7.4 ± 0.7	1.35 ± 0.32	48.7 ± 19.4	4.08 ± 1.62
	CN	3579.871 ± 0.003	-7.7 ± 0.2	4.73 ± 0.34	61.6 ± 6.7	5.16 ± 0.56
	NH	3353.846 ± 0.007	-6.9 ± 0.6	2.12 ± 0.43	82.7 ± 17.2	7.39 ± 1.54
	NH	3357.971 ± 0.002	-7.3 ± 0.2	1.98 ± 0.15	47.3 ± 5.9	4.22 ± 0.53
	OH	3071.979 ± 0.005	-3.0 ± 0.5	6.31 ± 0.71	90.2 ± 11.2	8.80 ± 1.09
	OH	3078.375 ± 0.002	-6.3 ± 0.2	12.19 ± 0.45	69.8 ± 3.8	6.79 ± 0.37
	OH	3081.594 ± 0.001	-6.8 ± 0.1	5.38 ± 0.20	41.7 ± 3.2	4.06 ± 0.31
	Cr I	3578.575 ± 0.001	-9.1 ± 0.1	2.23 ± 0.06	114.8 ± 3.5	9.62 ± 0.29
	Fe I	3440.518 ± 0.002	-7.6 ± 0.2	6.31 ± 0.14	57.0 ± 2.1	4.97 ± 0.19
	Fe I	3679.817 ± 0.002	-7.8 ± 0.1	0.93 ± 0.04	48.0 ± 3.7	3.91 ± 0.30
	Na I	3302.281 ± 0.002	-7.9 ± 0.2	35.03 ± 0.13	55.5 ± 0.3	5.04 ± 0.03
	Na I	3302.892 ± 0.002	-7.8 ± 0.2	26.29 ± 0.07	51.2 ± 0.3	4.64 ± 0.02
	Ti II	3072.688	-28.8	1.26 ± 0.36	77.5	7.56
		3072.788	-19.1	1.26 ± 0.44	106.9	10.43
		3072.889	-9.3	3.21 ± 0.26	47.2	4.60
				[8.77 ± 3.59]		
	Ti II	3228.888	-28.8	0.50 ± 0.08	81.4	7.56
		3228.993	-19.1	0.73 ± 0.14	112.4	10.43
		3229.099	-9.3	1.76 ± 0.10	49.6	4.60
				[5.81 ± 1.42]		
	Ti II	3241.682	-28.8	1.07 ± 0.14	81.8	7.56
		3241.787	-19.1	2.96 ± 0.17	112.8	10.43
		3241.894	-9.3	5.65 ± 0.08	49.7	4.60
				[13.24 ± 1.45]		
	Ti II	3383.430 ± 0.004	-30.0 ± 0.4	2.62 ± 0.22	83.2 ± 9.5	7.37 ± 0.84
		3383.550 ± 0.007	-19.3 ± 0.6	3.16 ± 0.13	117.8 ± 0.2	10.43 ± 0.02
		3383.663 ± 0.002	-9.3 ± 0.2	8.70 ± 0.07	50.7 ± 1.2	4.49 ± 0.10
				[15.16 ± 1.21]		
HD148184	CH	3137.477 ± 0.003	-5.1 ± 0.2	3.14 ± 0.28	61.9 ± 6.0	5.91 ± 0.57
	CH	3143.081 ± 0.002	-6.6 ± 0.2	5.69 ± 0.12	42.3 ± 1.7	4.03 ± 0.17
	CH	3145.909 ± 0.004	-9.6 ± 0.4	5.33 ± 0.75	57.1 ± 10.4	5.44 ± 0.99
	CH	3627.307 ± 0.006	-7.9 ± 0.5	0.62 ± 0.11	66.5 ± 13.8	5.49 ± 1.14
	CH	3633.188 ± 0.003	-8.3 ± 0.3	1.23 ± 0.09	53.2 ± 7.2	4.39 ± 0.60
	CH	3636.127 ± 0.005	-7.8 ± 0.4	0.63 ± 0.07	51.3 ± 11.9	4.23 ± 0.98
	CH $^+$	3578.929 ± 0.012	-7.6 ± 1.0	1.71 ± 0.41	99.5 ± 29.0	8.33 ± 2.43
	OH	3078.367 ± 0.004	-7.1 ± 0.4	3.63 ± 0.27	82.4 ± 8.9	8.02 ± 0.87
	OH	3081.583 ± 0.005	-7.9 ± 0.4	2.02 ± 0.31	64.1 ± 10.7	6.24 ± 1.04
	Fe I	3440.480 ± 0.001	-10.9 ± 0.1	2.80 ± 0.09	50.3 ± 2.7	4.39 ± 0.23
	Na I	3302.251 ± 0.002	-10.7 ± 0.2	33.04 ± 0.11	55.6 ± 0.3	5.05 ± 0.03
	Na I	3302.860 ± 0.002	-10.8 ± 0.2	24.84 ± 0.07	51.1 ± 0.3	4.64 ± 0.03
	Ti II	3228.916	-26.3	2.53 ± 0.17	112.4	10.43
		3229.079	-11.1	0.46 ± 0.00	87.8	8.15
				[2.62 ± 0.37]		
	Ti II	3241.710	-26.3	7.13 ± 0.20	112.8	10.43
		3241.874	-11.1	1.63 ± 0.17	88.1	8.15
				[10.26 ± 0.64]		
	Ti II	3383.471 ± 0.001	-26.3 ± 0.1	10.96 ± 0.18	117.8 ± 0.2	10.43 ± 0.02
		3383.642 ± 0.005	-11.1 ± 0.5	1.96 ± 0.28	96.0 ± 12.8	8.50 ± 1.14
				[13.18 ± 0.51]		
HD148379	CH	3137.442 ± 0.002	-8.4 ± 0.2	3.85 ± 0.21	50.6 ± 4.3	4.84 ± 0.41
	CH	3143.048 ± 0.002	-9.7 ± 0.2	9.79 ± 0.17	52.5 ± 1.5	5.01 ± 0.14
	CH	3145.878 ± 0.005	-12.6 ± 0.4	7.58 ± 1.34	54.3 ± 10.6	5.17 ± 1.01
	CH	3627.264 ± 0.004	-11.5 ± 0.3	0.75 ± 0.08	45.3 ± 8.3	3.74 ± 0.69
	CH	3633.152 ± 0.002	-11.3 ± 0.2	1.79 ± 0.11	57.6 ± 5.9	4.76 ± 0.48
	CH	3636.079 ± 0.003	-11.8 ± 0.2	1.35 ± 0.11	60.8 ± 6.9	5.01 ± 0.57
	Fe I	3440.318 ± 0.007	-25.1 ± 0.6	2.23 ± 0.44	153.4 ± 16.4	13.37 ± 1.43
		3440.636 ± 0.006	2.6 ± 0.5	1.56 ± 0.24	110.6 ± 14.4	9.64 ± 1.25
				[4.08 ± 0.73]		
	Na I	3302.126 ± 0.002	-21.9 ± 0.2	44.14 ± 0.26	94.3 ± 0.5	8.56 ± 0.04
		3302.372 ± 0.002	0.4 ± 0.2	19.30 ± 0.21	63.0 ± 0.6	5.72 ± 0.05
				[68.78 ± 0.71]		
	Na I	3302.736 ± 0.002	-22.0 ± 0.2	24.26 ± 0.27	85.0 ± 0.8	7.71 ± 0.07
		3302.982 ± 0.002	0.4 ± 0.2	10.60 ± 0.16	60.6 ± 1.1	5.50 ± 0.10
				[37.43 ± 0.94]		
	Ti II	3072.772	-20.7	14.48 ± 0.78	180.5	17.61
		3072.979	-0.5	9.52 ± 0.42	99.1	9.67
				[21.42 ± 3.81]		
	Ti II	3228.976	-20.7	9.69 ± 0.48	189.7	17.61
		3229.194	-0.5	6.89 ± 0.28	104.2	9.67
				[18.89 ± 1.69]		
	Ti II	3241.770	-20.7	24.91 ± 0.60	190.5	17.61
		3241.989	-0.5	15.60 ± 0.32	104.6	9.67
				[38.90 ± 1.80]		

TABLE 4 — *Continued*

Target	Species	λ_{helio} [Å]	v_{helio} [km s $^{-1}$]	W_λ [mÅ]	FWHM		
				[mÅ]	[km s $^{-1}$]		
HD149404	Ti II	3383.535 ± 0.001	-20.7 ± 0.1	44.20 ± 0.59	198.9 ± 3.0	17.62 ± 0.27	
		3383.763 ± 0.002	-0.5 ± 0.2	27.68 ± 0.27	109.2 ± 1.8	9.67 ± 0.16	
				[73.54 ± 2.68]			
	Na I	3302.171 ± 0.002	-17.9 ± 0.2	24.75 ± 0.17	54.5 ± 0.6	4.94 ± 0.06	
		3302.289 ± 0.002	-7.1 ± 0.2	27.03 ± 0.16	71.9 ± 1.3	6.53 ± 0.12	
		3302.375 ± 0.002	0.7 ± 0.2	29.23 ± 0.19	57.7 ± 0.8	5.24 ± 0.07	
	Na I	3302.776 ± 0.002	-18.3 ± 0.2	15.31 ± 0.11	52.6 ± 0.6	4.77 ± 0.05	
		3302.900 ± 0.002	-7.1 ± 0.2	14.97 ± 0.12	67.9 ± 1.3	6.16 ± 0.11	
		3302.985 ± 0.002	0.7 ± 0.2	21.00 ± 0.10	55.5 ± 0.6	5.04 ± 0.06	
	Ti II	3066.219	-13.2	2.55 ± 1.05	106.7	10.43	
		3066.275	-7.8	1.20 ± 0.03	47.2	4.61	
		3066.342	-1.2	3.12 ± 1.02	106.7	10.43	
HD149757	Ti II	3072.849	-13.2	[10.89 ± 8.62]			
		3072.904	-7.8	6.24 ± 0.61	106.9	10.43	
		3072.972	-1.2	2.66 ± 0.01	47.3	4.61	
	Ti II	3229.057	-13.2	[13.88 ± 2.63]			
		3229.115	-7.8	7.40 ± 0.65	106.9	10.43	
		3229.187	-1.2	5.05 ± 0.35	112.4		
	Ti II	3241.852	-13.2	[10.70 ± 1.33]			
		3241.910	-7.8	12.27 ± 0.23	112.8	10.43	
		3241.981	-1.2	5.39 ± 0.00	49.9	4.61	
	Ti II	3383.620 ± 0.002	-13.1 ± 0.2	[13.13 ± 0.23]			
		3383.680 ± 0.002	-7.8 ± 0.2	19.96 ± 0.03	117.8 ± 0.2	10.43 ± 0.02	
		3383.755 ± 0.001	-1.2 ± 0.1	8.41 ± 0.29	51.8 ± 2.5	4.59 ± 0.22	
HD150136	CH	3137.375 ± 0.006	-14.8 ± 0.6	[23.50 ± 0.19]			
		3137.483 ± 0.003	-4.5 ± 0.2	19.96 ± 0.03	117.8 ± 0.2	10.43 ± 0.02	
		3137.559 ± 0.005	2.7 ± 0.4	2.43 ± 0.23	51.8 ± 0.2	4.59 ± 0.22	
	CH	3142.971 ± 0.005	-17.0 ± 0.5	[55.46 ± 1.56]			
		3143.097 ± 0.006	-5.0 ± 0.6	1.09 ± 0.53	44.0 ± 7.0	4.21 ± 0.66	
		3143.170 ± 0.002	1.9 ± 0.2	0.90 ± 0.07	24.0 ± 2.1	2.29 ± 0.20	
	CH	3145.993 ± 0.005	-1.6 ± 0.5	2.43 ± 0.23	67.2 ± 6.8	6.42 ± 0.65	
		3633.291 ± 0.006	0.2 ± 0.5	[4.60 ± 1.46]			
		3633.110 ± 0.003	0.0 ± 0.4	1.78 ± 0.29	49.0 ± 11.6	4.68 ± 1.11	
HD150136	CH ⁺	3579.020 ± 0.005	0.0 ± 0.4	2.04 ± 0.24	54.7 ± 15.3	5.21 ± 1.46	
		Na I	3302.209 ± 0.002	-14.4 ± 0.2	3.90 ± 0.17	42.9 ± 5.2	4.09 ± 0.50
		Na I	3302.821 ± 0.002	-14.3 ± 0.2	[7.65 ± 2.12]		
	Ti II	3241.677	-29.3	29.47 ± 0.10	52.8 ± 0.3	4.79 ± 0.02	
		3241.829	-15.2	21.95 ± 0.11	49.9 ± 0.4	4.53 ± 0.03	
				4.83 ± 0.19	81.4	7.53	
	Ti II	3383.438 ± 0.001	-29.3 ± 0.1	2.46 ± 0.22	90.0	8.32	
		3383.596 ± 0.002	-15.2 ± 0.2	[8.18 ± 0.89]			
				8.07 ± 0.30	85.8 ± 3.5	7.61 ± 0.31	
HD150136	CH	3137.404 ± 0.002	-12.1 ± 0.2	2.18 ± 0.26	93.9 ± 2.4	8.32 ± 0.21	
		3143.010 ± 0.002	-13.4 ± 0.2	[10.18 ± 0.81]			
		3145.843 ± 0.004	-15.9 ± 0.4	3.54 ± 0.30	59.5 ± 4.7	5.69 ± 0.45	
	CH	3145.843 ± 0.004	-15.9 ± 0.4	6.52 ± 0.17	44.4 ± 1.8	4.23 ± 0.17	
		3633.110 ± 0.003	-14.7 ± 0.2	5.35 ± 0.79	55.8 ± 10.3	5.32 ± 0.98	
		3636.050 ± 0.006	-14.2 ± 0.5	1.56 ± 0.10	65.2 ± 7.0	5.38 ± 0.58	
	CH ⁺	3578.843 ± 0.003	-14.8 ± 0.3	1.19 ± 0.15	73.5 ± 14.2	6.06 ± 1.17	
		3578.843 ± 0.003	-14.8 ± 0.3	2.01 ± 0.14	62.7 ± 7.6	5.25 ± 0.64	
		OH	3078.302 ± 0.005	-13.4 ± 0.5	2.90 ± 0.37	70.1 ± 12.6	6.83 ± 1.23
HD150136	Cr I	3578.599 ± 0.012	-7.0 ± 1.0	1.33 ± 0.24	136.8 ± 29.3	11.46 ± 2.46	
		Fe I	3440.604 ± 0.008	-0.1 ± 0.7	0.97 ± 0.42	75.8 ± 19.5	6.60 ± 1.70
		Na I	3302.240 ± 0.002	-11.6 ± 0.2	15.38 ± 0.15	63.4 ± 0.9	5.75 ± 0.08
	Na I	3302.375 ± 0.002	0.7 ± 0.2	12.07 ± 0.12	47.3 ± 0.7	4.29 ± 0.07	
				[27.97 ± 0.75]			
		3302.850 ± 0.002	-11.6 ± 0.2	8.58 ± 0.18	65.4 ± 1.9	5.94 ± 0.17	
HD150136	Ti II	3302.988 ± 0.002	0.9 ± 0.2	7.40 ± 0.13	47.3 ± 1.4	4.29 ± 0.12	
				[16.06 ± 0.85]			
		3072.820	-16.0	6.44 ± 0.62	145.2	14.16	
	Ti II	3072.975	-0.9	5.09 ± 0.42	107.6	10.50	
				[11.88 ± 2.14]			
		3229.027	-16.0	4.14 ± 0.47	152.5	14.16	
HD150136	Ti II	3229.189	-0.9	3.10 ± 0.29	113.1	10.50	
				[7.54 ± 1.46]			
		3241.821	-16.0	15.02 ± 0.29	153.1	14.16	
	Ti II	3241.984	-0.9	9.03 ± 0.22	113.6	10.50	
				[25.54 ± 1.17]			
		3383.588 ± 0.001	-16.0 ± 0.1	23.12 ± 0.39	160.3 ± 3.6	14.20 ± 0.32	

TABLE 4 — *Continued*

Target	Species	λ_{helio} [Å]	v_{helio} [km s $^{-1}$]	W_λ [mÅ]	FWHM [mÅ]	FWHM [km s $^{-1}$]
HD152003		3383.779 ± 0.002	0.9 ± 0.1	14.14 ± 0.27 [38.70 ± 0.96]	118.9 ± 3.5	10.53 ± 0.31
	CH	3143.031 ± 0.007	-11.3 ± 0.6	1.90 ± 0.54	80.2 ± 15.7	7.65 ± 1.49
		3143.172 ± 0.003	2.1 ± 0.3	2.05 ± 0.20	47.1 ± 6.5	4.50 ± 0.62
				[4.66 ± 1.08]		
	CH $^+$	3578.898 ± 0.014	-10.2 ± 1.2	2.37 ± 0.61	175.4 ± 34.9	14.69 ± 2.92
	NH	3353.828 ± 0.001	-8.5 ± 0.1	1.55 ± 1.73	33.3 ± 14.5	2.98 ± 1.29
	Fe I	3440.598 ± 0.003	-0.7 ± 0.3	1.99 ± 0.19	49.6 ± 7.1	4.32 ± 0.62
	Na I	3302.374 ± 0.002	0.6 ± 0.2	72.21 ± 0.42	83.7 ± 0.5	7.60 ± 0.04
	Na I	3302.988 ± 0.002	0.9 ± 0.2	50.89 ± 0.44	72.4 ± 0.6	6.57 ± 0.06
	Ti II	3066.221 ± 0.033	-13.0 ± 3.3	18.08 ± 10.98	460.5 ± 84.5	45.02 ± 8.26
HD152235	Ti II	3072.875 ± 0.003	-10.6 ± 0.3	22.76 ± 1.22	203.0 ± 7.9	19.81 ± 0.77
	Ti II	3229.092 ± 0.008	-9.9 ± 0.8	12.93 ± 1.71	239.7 ± 19.1	22.26 ± 1.77
	Ti II	3241.893 ± 0.001	-9.3 ± 0.1	37.50 ± 0.97	200.6 ± 3.3	18.55 ± 0.31
	Ti II	3383.661 ± 0.002	-9.5 ± 0.2	60.33 ± 0.91	222.4 ± 2.1	19.70 ± 0.18
	CH	3137.562 ± 0.006	3.0 ± 0.6	3.15 ± 0.47	67.3 ± 13.7	6.43 ± 1.31
	CH	3143.171 ± 0.001	2.1 ± 0.1	9.72 ± 0.36	65.8 ± 3.3	6.28 ± 0.32
	CH	3146.002 ± 0.005	-0.8 ± 0.5	7.81 ± 1.20	70.2 ± 12.8	6.69 ± 1.22
	CH	3633.284 ± 0.003	-0.4 ± 0.3	2.88 ± 0.24	104.7 ± 8.0	8.64 ± 0.66
	CH	3636.225 ± 0.008	0.2 ± 0.7	1.45 ± 0.22	78.8 ± 19.0	6.49 ± 1.56
	Fe I	3440.595 ± 0.004	-0.9 ± 0.4	4.05 ± 0.79	120.7 ± 9.7	10.52 ± 0.84
HD152236	Na I	3302.314 ± 0.002	-4.9 ± 0.2	25.25 ± 9.02	44.3 ± 2.9	4.02 ± 0.26
		3302.370 ± 0.002	0.2 ± 0.2	53.75 ± 6.87 [79.18 ± 2.55]	79.1 ± 4.2	7.18 ± 0.38
	Na I	3302.927 ± 0.002	-4.7 ± 0.2	22.47 ± 0.15	46.8 ± 1.0	4.25 ± 0.09
		3302.985 ± 0.002	0.7 ± 0.2	30.86 ± 0.31 [54.30 ± 0.68]	66.3 ± 1.6	6.02 ± 0.15
	Ti II	3072.481	-49.1	0.82 ± 0.34	55.6	5.42
		3072.683	-29.3	3.52 ± 1.06	159.4	15.55
		3072.807	-17.3	4.45 ± 0.37	80.5	7.85
		3072.932	-5.1	11.20 ± 0.83	109.1	10.64
				[19.12 ± 3.31]		
	Ti II	3228.670	-49.1	1.07 ± 0.28	58.4	5.42
HD152236		3228.883	-29.3	4.50 ± 0.64	167.5	15.55
		3229.013	-17.3	1.84 ± 0.21	84.6	7.85
		3229.144	-5.1	7.12 ± 0.45	114.6	10.64
				[15.81 ± 3.27]		
	Ti II	3241.463	-49.1	2.98 ± 0.18	58.6	5.42
		3241.677	-29.3	11.20 ± 0.44	168.2	15.55
		3241.807	-17.3	7.05 ± 0.16	84.9	7.85
		3241.939	-5.1	19.29 ± 0.36	115.1	10.64
				[44.75 ± 2.40]		
	Ti II	3383.214 ± 0.002	-49.1 ± 0.2	2.57 ± 0.19	61.8 ± 5.5	5.47 ± 0.49
HD152236		3383.437 ± 0.002	-29.3 ± 0.2	15.20 ± 0.35	175.9 ± 6.2	15.59 ± 0.55
		3383.573 ± 0.001	-17.3 ± 0.1	11.08 ± 0.07	88.6 ± 3.1	7.85 ± 0.27
		3383.711 ± 0.002	-5.1 ± 0.2	33.11 ± 0.37	120.4 ± 1.7	10.66 ± 0.15
				[65.42 ± 1.34]		
	CH	3137.514 ± 0.005	-1.5 ± 0.4	3.05 ± 0.70	61.0 ± 10.6	5.83 ± 1.01
	CH	3143.132 ± 0.002	-1.7 ± 0.2	12.13 ± 0.74	98.0 ± 5.0	9.35 ± 0.47
	CH	3145.945 ± 0.004	-6.2 ± 0.4	5.61 ± 0.76	47.1 ± 0.2	4.49 ± 0.02
	CH $^+$	3578.969 ± 0.007	-4.3 ± 0.6	3.76 ± 0.85	71.3 ± 15.5	5.97 ± 1.30
	Na I	3302.191 ± 0.002	-16.1 ± 0.2	7.71 ± 0.08	42.2 ± 1.2	3.83 ± 0.11
HD152236		3302.273 ± 0.002	-8.6 ± 0.2	29.29 ± 0.10	66.6 ± 0.7	6.05 ± 0.07
		3302.375 ± 0.002	0.7 ± 0.2	34.99 ± 0.12 [69.84 ± 0.75]	59.0 ± 0.4	5.36 ± 0.04
	Na I	3302.800 ± 0.001	-16.2 ± 0.1	4.21 ± 0.09	42.4 ± 2.7	3.85 ± 0.24
		3302.883 ± 0.002	-8.6 ± 0.2	18.21 ± 0.15	69.7 ± 1.6	6.33 ± 0.15
		3302.988 ± 0.002	0.9 ± 0.2	24.55 ± 0.15 [46.56 ± 1.21]	56.9 ± 0.7	5.17 ± 0.06
	Ti II	3072.788	-19.1	4.49 ± 0.35	58.7	5.73
		3072.909	-7.3	7.47 ± 0.37	73.4	7.16
		3073.068	8.2	3.75 ± 0.74	314.0	30.63
				[16.83 ± 3.35]		
	Ti II	3228.993	-19.1	2.42 ± 0.24	61.7	5.73
HD152236		3229.121	-7.3	4.06 ± 0.15	77.1	7.16
		3229.288	8.2	5.20 ± 1.16	329.9	30.63
				[10.59 ± 1.12]		
	Ti II	3241.787	-19.1	7.89 ± 0.13	61.9	5.73
		3241.915	-7.3	13.56 ± 0.08	77.4	7.16
		3242.083	8.2	5.20 ± 0.76	331.2	30.63
				[30.63 ± 1.11]		
	Ti II	3383.552 ± 0.004	-19.2 ± 0.3	16.33 ± 0.47 [53.01 ± 0.93]	117.5 ± 5.7	10.41 ± 0.51
		3383.686 ± 0.002	-7.3 ± 0.2	32.64 ± 0.43	138.4 ± 7.2	12.26 ± 0.63
		3383.861 ± 0.016	8.3 ± 1.4	3.95 ± 0.50	150.7 ± 30.8	13.35 ± 2.73

TABLE 4 — *Continued*

Target	Species	λ_{helio} [Å]	v_{helio} [km s $^{-1}$]	W_λ [mÅ]	[mÅ]	FWHM [km s $^{-1}$]	
HD154368	CH	3143.174 ± 0.002	2.3 ± 0.2	4.19 ± 0.27	46.8 ± 4.9	4.46 ± 0.47	
	CH	3146.010 ± 0.003	0.0 ± 0.3	2.15 ± 0.18	45.3 ± 8.0	4.31 ± 0.76	
	Fe I	3440.580 ± 0.002	-2.2 ± 0.2	2.48 ± 0.14	65.1 ± 5.1	5.68 ± 0.45	
	Na I	3302.137 ± 0.002	-21.0 ± 0.2	16.60 ± 0.16	52.8 ± 0.6	4.79 ± 0.06	
		3302.336 ± 0.002	-2.9 ± 0.2	63.56 ± 0.24	74.7 ± 0.2	6.78 ± 0.02	
				[88.20 ± 0.94]			
	Na I	3302.752 ± 0.002	-20.5 ± 0.2	8.91 ± 0.21	54.5 ± 1.3	4.94 ± 0.12	
		3302.948 ± 0.002	-2.8 ± 0.2	50.25 ± 0.17	65.7 ± 0.3	5.96 ± 0.03	
				[61.74 ± 1.02]			
	Ti II	3072.800	-17.9	2.97 ± 1.26	147.4	14.38	
		3072.927	-5.6	4.77 ± 0.61	72.9	7.11	
		3073.043	5.8	2.50 ± 1.16	113.0	11.02	
				[9.51 ± 3.66]			
	Ti II	3229.006	-17.9	1.83 ± 0.23	154.9	14.38	
		3229.139	-5.6	2.49 ± 0.14	76.6	7.11	
		3229.261	5.8	1.98 ± 0.27	118.7	11.02	
				[6.08 ± 1.27]			
	Ti II	3241.800	-17.9	7.91 ± 0.36	155.5	14.38	
		3241.933	-5.6	8.16 ± 0.12	76.9	7.11	
		3242.056	5.8	4.40 ± 0.30	119.2	11.02	
				[18.99 ± 1.22]			
	Ti II	3383.566 ± 0.002	-17.9 ± 0.2	14.11 ± 0.33	161.9 ± 2.5	14.35 ± 0.22	
		3383.705 ± 0.002	-5.6 ± 0.2	14.20 ± 0.09	80.4 ± 1.6	7.13 ± 0.14	
		3383.833 ± 0.002	5.8 ± 0.2	10.69 ± 0.33	123.4 ± 4.4	10.93 ± 0.39	
				[39.08 ± 0.68]			
	HD154811	CH	3137.535 ± 0.001	0.5 ± 0.1	5.73 ± 0.26	47.6 ± 3.2	4.55 ± 0.31
		CH	3143.140 ± 0.002	-1.0 ± 0.2	14.79 ± 0.24	52.7 ± 1.2	5.03 ± 0.11
		CH	3145.968 ± 0.004	-4.0 ± 0.4	10.34 ± 1.30	51.3 ± 9.0	4.89 ± 0.86
		CH	3627.373 ± 0.004	-2.5 ± 0.3	1.36 ± 0.10	77.8 ± 8.4	6.43 ± 0.70
		CH	3633.259 ± 0.002	-2.5 ± 0.2	3.52 ± 0.24	69.5 ± 5.8	5.73 ± 0.48
		CH	3636.193 ± 0.002	-2.4 ± 0.1	2.45 ± 0.14	61.7 ± 4.2	5.08 ± 0.34
		CN	3579.424 ± 0.003	-2.4 ± 0.3	1.94 ± 0.18	54.7 ± 7.2	4.58 ± 0.60
		CN	3579.930 ± 0.002	-2.7 ± 0.2	5.42 ± 0.11	47.4 ± 1.7	3.97 ± 0.14
		CN	3580.912 ± 0.004	-2.1 ± 0.3	1.05 ± 0.42	52.5 ± 10.0	4.40 ± 0.84
		NH	3353.904 ± 0.009	-1.8 ± 0.8	2.62 ± 0.84	100.5 ± 20.7	8.98 ± 1.85
	Na I	NH	3358.031 ± 0.002	-2.0 ± 0.1	2.04 ± 0.10	38.6 ± 4.0	3.45 ± 0.36
		OH	3078.427 ± 0.003	-1.3 ± 0.3	9.25 ± 0.58	62.9 ± 6.1	6.13 ± 0.59
		OH	3081.639 ± 0.002	-2.4 ± 0.2	4.01 ± 0.31	40.5 ± 5.0	3.94 ± 0.49
	Na I	Na I	3302.230 ± 0.002	-12.5 ± 0.2	47.07 ± 0.65	146.4 ± 1.9	13.29 ± 0.17
		Na I	3302.281 ± 0.002	-7.8 ± 0.2	9.82 ± 0.06	57.3 ± 1.9	5.20 ± 0.18
		Na I	3302.408 ± 0.002	3.6 ± 0.2	13.77 ± 0.19	79.0 ± 2.0	7.17 ± 0.18
				[72.96 ± 1.45]			
	Na I	Na I	3302.840 ± 0.002	-12.5 ± 0.2	22.39 ± 0.49	136.0 ± 3.2	12.34 ± 0.29
		Na I	3302.890 ± 0.001	-8.0 ± 0.1	6.14 ± 0.06	59.7 ± 2.9	5.42 ± 0.27
		Na I	3303.018 ± 0.001	3.6 ± 0.1	6.72 ± 0.17	75.6 ± 3.4	6.87 ± 0.30
				[34.97 ± 0.84]			
	Ti II	3072.820	-16.0	8.40 ± 0.59	106.3	10.37	
		3072.965	-1.9	7.62 ± 0.81	136.9	13.35	
		3073.003	1.8	0.55 ± 0.01	37.4	3.65	
				[18.23 ± 3.70]			
	Ti II	3229.027	-16.0	4.36 ± 0.32	111.7	10.37	
		3229.179	-1.9	4.86 ± 0.42	143.8	13.35	
		3229.219	1.8	0.41 ± 0.00	39.3	3.65	
				[10.53 ± 1.27]			
	Ti II	3241.821	-16.0	14.42 ± 0.32	112.2	10.37	
		3241.974	-1.9	13.82 ± 0.40	144.4	13.35	
		3242.014	1.8	0.92 ± 0.00	39.5	3.65	
				[33.48 ± 1.96]			
	Ti II	3383.587 ± 0.002	-16.0 ± 0.2	21.18 ± 0.62	117.0 ± 3.0	10.37 ± 0.26	
		3383.747 ± 0.003	-1.9 ± 0.2	21.26 ± 0.48	150.9 ± 4.7	13.37 ± 0.41	
		3383.789 ± 0.002	1.8 ± 0.2	2.19 ± 0.11	41.1 ± 7.8	3.65 ± 0.69	
				[46.58 ± 1.43]			
	HD154873	CH	3146.014 ± 0.002	0.4 ± 0.2	6.76 ± 0.61	37.5 ± 5.2	3.58 ± 0.50
		Na I	3302.164 ± 0.002	-18.5 ± 0.2	29.21 ± 0.21	87.1 ± 0.7	7.90 ± 0.07
		Na I	3302.323 ± 0.002	-4.1 ± 0.2	11.53 ± 0.12	54.2 ± 0.9	4.92 ± 0.08
		Na I	3302.407 ± 0.002	3.5 ± 0.2	24.18 ± 0.09	54.0 ± 0.5	4.90 ± 0.05
				[66.30 ± 1.16]			
	Na I	Na I	3302.774 ± 0.002	-18.5 ± 0.2	15.59 ± 0.26	82.9 ± 1.3	7.53 ± 0.12
		Na I	3302.940 ± 0.002	-3.5 ± 0.2	4.06 ± 0.03	19.1 ± 0.3	1.73 ± 0.03
		Na I	3303.017 ± 0.002	3.5 ± 0.2	15.10 ± 0.13	57.9 ± 0.8	5.25 ± 0.07
				[34.84 ± 1.91]			
	Ti II	3072.813	-16.7	4.80 ± 0.58	114.4	11.16	
		3072.931	-5.2	1.18 ± 0.12	40.2	3.92	
		3072.994	1.0	4.00 ± 0.36	81.4	7.94	
				[7.63 ± 4.97]			

TABLE 4 — *Continued*

Target	Species	λ_{helio} [Å]	v_{helio} [km s $^{-1}$]	W_λ [mÅ]	FWHM [mÅ]	FWHM [km s $^{-1}$]
	Ti II	3229.019	-16.7	3.27 ± 0.53	120.2	11.16
		3229.143	-5.2	0.75 ± 0.11	42.2	3.92
		3229.209	1.0	3.75 ± 0.33	85.5	7.94
				[9.55 ± 3.51]		
	Ti II	3241.814	-16.7	7.18 ± 0.31	120.7	11.16
		3241.938	-5.2	1.28 ± 0.06	42.4	3.92
		3242.004	1.0	7.05 ± 0.18	85.9	7.94
				[13.03 ± 1.54]		
	Ti II	3383.580 ± 0.002	-16.7 ± 0.2	16.98 ± 0.27	125.8 ± 2.1	11.14 ± 0.19
		3383.710 ± 0.001	-5.2 ± 0.1	3.06 ± 0.06	44.4 ± 3.2	3.93 ± 0.28
		3383.779 ± 0.001	1.0 ± 0.1	15.38 ± 0.23	89.6 ± 2.5	7.94 ± 0.22
				[38.24 ± 1.33]		
	CH	3145.899 ± 0.004	-10.6 ± 0.4	4.10 ± 0.27	23.6 ± 2.5	2.25 ± 0.24
		3145.961 ± 0.013	-4.7 ± 1.3	6.72 ± 2.82	92.1 ± 55.7	8.78 ± 5.31
		3146.047 ± 0.003	3.5 ± 0.3	11.68 ± 0.46	39.1 ± 6.8	3.73 ± 0.65
				[19.63 ± 16.85]		
HD156575	Na I	3302.208 ± 0.002	-14.5 ± 0.2	12.68 ± 0.29	71.2 ± 2.2	6.46 ± 0.20
		3302.323 ± 0.002	-4.1 ± 0.2	12.83 ± 0.02	44.0 ± 1.7	3.99 ± 0.15
		3302.378 ± 0.002	0.9 ± 0.2	18.61 ± 0.32	53.4 ± 1.8	4.84 ± 0.17
				[45.80 ± 2.79]		
	Na I	3302.828 ± 0.002	-13.6 ± 0.2	8.20 ± 0.49	92.5 ± 5.2	8.39 ± 0.48
		3302.931 ± 0.001	-4.3 ± 0.1	5.94 ± 0.16	34.5 ± 3.6	3.13 ± 0.33
		3302.986 ± 0.001	0.7 ± 0.1	13.00 ± 0.34	59.2 ± 2.9	5.37 ± 0.26
				[29.32 ± 1.43]		
	Ti II	3072.830	-15.0	5.25 ± 0.83	85.5	8.34
		3072.920	-6.2	5.07 ± 0.63	85.0	8.29
		3073.011	2.6	4.43 ± 0.93	85.0	8.29
				[15.85 ± 5.96]		
	Ti II	3229.037	-15.0	3.05 ± 0.26	89.8	8.34
		3229.132	-6.2	2.99 ± 0.18	89.3	8.29
		3229.227	2.6	2.86 ± 0.26	89.3	8.29
				[10.05 ± 1.27]		
	Ti II	3241.831	-15.0	8.72 ± 0.28	90.2	8.34
		3241.927	-6.2	8.20 ± 0.19	89.7	8.29
		3242.022	2.6	8.20 ± 0.26	89.7	8.29
				[25.29 ± 1.72]		
	Ti II	3383.598 ± 0.002	-15.0 ± 0.2	15.55 ± 0.22	94.2 ± 0.2	8.35 ± 0.02
		3383.698 ± 0.002	-6.2 ± 0.2	15.26 ± 0.18	93.6 ± 3.0	8.29 ± 0.27
		3383.797 ± 0.002	2.6 ± 0.2	16.04 ± 0.19	94.2 ± 0.2	8.35 ± 0.02
				[53.61 ± 1.25]		
	CH	3145.858 ± 0.002	-14.5 ± 0.2	3.53 ± 1.24	72.8 ± 24.6	6.94 ± 2.35
		3145.970 ± 0.022	-3.8 ± 2.1	4.35 ± 2.55	67.9 ± 47.4	6.47 ± 4.51
		3146.019 ± 0.002	0.9 ± 0.2	6.35 ± 0.20	33.2 ± 6.1	3.16 ± 0.58
				[15.07 ± 2.83]		
HD157038	Na I	3302.086 ± 0.005	-25.6 ± 0.5	6.92 ± 1.23	96.0 ± 11.0	8.72 ± 1.00
		3302.199 ± 0.001	-15.4 ± 0.1	22.73 ± 0.39	82.5 ± 3.9	7.49 ± 0.35
		3302.289 ± 0.001	-7.1 ± 0.1	14.22 ± 0.19	54.8 ± 3.6	4.97 ± 0.33
		3302.351 ± 0.001	-1.5 ± 0.1	12.92 ± 0.23	50.1 ± 2.4	4.55 ± 0.22
				[56.25 ± 2.14]		
	Na I	3302.689 ± 0.006	-26.3 ± 0.6	5.14 ± 0.85	131.3 ± 12.8	11.91 ± 1.16
		3302.811 ± 0.001	-15.2 ± 0.1	11.63 ± 0.22	78.8 ± 4.3	7.15 ± 0.39
		3302.900 ± 0.001	-7.1 ± 0.1	8.10 ± 0.13	61.3 ± 5.2	5.57 ± 0.47
		3302.962 ± 0.001	-1.4 ± 0.1	6.49 ± 0.12	46.9 ± 2.3	4.25 ± 0.21
				[31.51 ± 0.93]		
	Ti II	3072.543	-43.1	4.62 ± 0.68	106.9	10.43
		3072.646	-33.0	7.50 ± 0.43	96.0	9.36
		3072.728	-25.0	6.15 ± 0.34	71.0	6.93
		3072.824	-15.6	13.12 ± 0.49	90.9	8.87
		3072.933	-5.0	15.20 ± 0.62	101.5	9.90
		3073.077	9.1	5.42 ± 0.75	97.6	9.52
				[56.82 ± 5.46]		
	Ti II	3228.735	-43.1	2.11 ± 0.43	112.4	10.43
		3228.844	-33.0	3.83 ± 0.26	100.8	9.36
		3228.930	-25.0	5.06 ± 0.20	74.7	6.93
		3229.031	-15.6	6.78 ± 0.30	95.6	8.87
		3229.145	-5.0	9.96 ± 0.39	106.6	9.90
		3229.297	9.1	2.50 ± 0.49	102.6	9.52
				[30.30 ± 2.67]		
	Ti II	3241.528	-43.1	9.14 ± 0.28	112.8	10.43
		3241.637	-33.0	12.04 ± 0.18	101.2	9.36
		3241.724	-25.0	13.55 ± 0.15	74.9	6.93
		3241.826	-15.6	19.35 ± 0.23	95.9	8.87
		3241.940	-5.0	25.21 ± 0.30	107.1	9.90
		3242.092	9.1	5.95 ± 0.37	103.0	9.52
				[100.65 ± 2.54]		

TABLE 4 — *Continued*

Target	Species	λ_{helio} [Å]	v_{helio} [km s $^{-1}$]	W_λ [mÅ]	FWHM	
				[mÅ]	[km s $^{-1}$]	
HD161056	Ti II	3383.279 ± 0.002	-43.3 ± 0.2	6.50 ± 1.06	117.8 ± 0.2	10.43 ± 0.02
		3383.396 ± 0.005	-33.0 ± 0.4	18.23 ± 3.05	109.0 ± 2.4	9.66 ± 0.21
		3383.487 ± 0.003	-24.9 ± 0.2	19.69 ± 1.29	77.5 ± 7.5	6.87 ± 0.67
		3383.592 ± 0.003	-15.6 ± 0.2	30.49 ± 0.82	100.6 ± 10.8	8.92 ± 0.95
		3383.712 ± 0.003	-5.0 ± 0.3	41.07 ± 0.54	111.7 ± 5.7	9.90 ± 0.51
		3383.871 ± 0.002	9.1 ± 0.2	11.75 ± 0.75	108.2 ± 8.2	9.59 ± 0.73
				[129.47 ± 3.92]		
	CH	3145.994 ± 0.004	-1.5 ± 0.3	9.18 ± 6.72	73.9 ± 8.4	7.04 ± 0.80
	CH $^+$	3578.891 ± 0.003	-10.8 ± 0.3	5.16 ± 0.26	148.7 ± 8.1	12.45 ± 0.68
	Fe I	3440.459 ± 0.003	-12.8 ± 0.3	2.40 ± 0.73	79.6 ± 7.9	6.93 ± 0.69
	Na I	3302.219 ± 0.002	-13.5 ± 0.2	88.40 ± 0.29	103.6 ± 0.4	9.41 ± 0.03
HD163758	Na I	3302.835 ± 0.002	-12.9 ± 0.2	59.75 ± 0.28	89.7 ± 0.5	8.15 ± 0.05
	Ti II	3072.659	-31.7	3.59 ± 0.71	148.5	14.49
		3072.829	-15.1	4.91 ± 0.43	91.2	8.90
				[11.06 ± 3.92]		
	Ti II	3228.857	-31.7	2.27 ± 0.48	156.1	14.49
		3229.036	-15.1	3.11 ± 0.28	95.9	8.90
				[6.67 ± 1.79]		
	Ti II	3241.651	-31.7	2.10 ± 0.31	156.7	14.49
		3241.830	-15.1	9.02 ± 0.18	96.3	8.90
				[11.13 ± 1.65]		
	Ti II	3383.410 ± 0.002	-31.7 ± 0.2	5.75 ± 0.31	159.8 ± 11.3	14.16 ± 1.00
		3383.597 ± 0.002	-15.2 ± 0.2	15.28 ± 0.20	99.2 ± 1.8	8.79 ± 0.16
HD163800	CH	3137.432 ± 0.002	-9.4 ± 0.1	5.63 ± 0.30	64.5 ± 3.6	6.17 ± 0.34
	CH	3143.035 ± 0.001	-11.0 ± 0.1	14.23 ± 0.45	74.1 ± 2.6	7.07 ± 0.25
	CH	3145.866 ± 0.004	-13.8 ± 0.4	11.56 ± 1.83	85.7 ± 10.0	8.17 ± 0.96
	CH	3627.242 ± 0.006	-13.3 ± 0.5	0.83 ± 0.13	55.5 ± 13.7	4.58 ± 1.13
	CH	3633.143 ± 0.003	-12.0 ± 0.3	1.76 ± 0.14	58.5 ± 7.6	4.83 ± 0.63
	CH	3636.062 ± 0.003	-13.1 ± 0.2	2.05 ± 0.15	94.4 ± 6.4	7.78 ± 0.53
	CH $^+$	3578.878 ± 0.007	-11.9 ± 0.6	1.99 ± 0.35	116.7 ± 16.9	9.78 ± 1.41
	CN	3579.214 ± 0.002	-20.0 ± 0.2	0.45 ± 0.07	42.5 ± 0.2	3.56 ± 0.02
		3579.298 ± 0.002	-13.0 ± 0.2	0.38 ± 0.07	35.5 ± 0.2	2.97 ± 0.02
				[1.51 ± 0.49]		
	CN	3579.724 ± 0.022	-20.0 ± 1.8	0.76 ± 0.27	66.9 ± 42.8	5.61 ± 3.58
		3579.808 ± 0.025	-13.0 ± 2.1	1.60 ± 0.39	106.7 ± 41.3	8.93 ± 3.46
HD166734	OH	3078.310 ± 0.003	-12.7 ± 0.3	10.71 ± 0.61	113.2 ± 7.2	11.03 ± 0.70
	OH	3081.520 ± 0.003	-14.0 ± 0.3	6.78 ± 0.50	99.9 ± 7.2	9.72 ± 0.70
	Na I	3302.241 ± 0.002	-11.5 ± 0.2	20.18 ± 0.12	45.9 ± 0.6	4.16 ± 0.05
		3302.354 ± 0.001	-1.3 ± 0.1	8.38 ± 0.25	78.7 ± 3.3	7.14 ± 0.30
				[26.33 ± 1.01]		
	Na I	3302.853 ± 0.002	-11.4 ± 0.2	13.47 ± 0.09	46.3 ± 0.7	4.20 ± 0.06
		3302.963 ± 0.002	-1.4 ± 0.2	3.71 ± 0.15	69.7 ± 3.7	6.33 ± 0.33
				[15.99 ± 0.58]		
	Ti II	3072.915 ± 0.006	-6.7 ± 0.6	34.73 ± 4.54	236.5 ± 15.3	23.07 ± 1.50
	Ti II	3229.136 ± 0.004	-5.8 ± 0.4	25.15 ± 1.49	283.6 ± 9.8	26.33 ± 0.91
	Ti II	3241.914 ± 0.002	-7.4 ± 0.2	73.04 ± 1.04	283.8 ± 2.1	26.25 ± 0.20
HD166734	Ti II	3383.689 ± 0.001	-7.0 ± 0.1	111.60 ± 1.92	296.6 ± 2.7	26.28 ± 0.24
	Cr I	3593.418 ± 0.005	-5.3 ± 0.4	0.65 ± 0.13	49.5 ± 11.5	4.13 ± 0.96
	Fe I	3440.545 ± 0.002	-5.3 ± 0.1	3.06 ± 0.14	54.0 ± 3.5	4.71 ± 0.31
	Na I	3302.305 ± 0.002	-5.7 ± 0.2	36.54 ± 0.10	51.2 ± 0.2	4.65 ± 0.02
	Na I	3302.916 ± 0.002	-5.7 ± 0.2	29.42 ± 0.14	49.1 ± 0.4	4.46 ± 0.03
	Ti II	3072.897 ± 0.002	-8.5 ± 0.2	10.37 ± 0.58	106.5 ± 5.5	10.39 ± 0.53
	Ti II	3229.125 ± 0.002	-6.9 ± 0.2	6.14 ± 0.26	107.9 ± 4.3	10.02 ± 0.40
	Ti II	3241.909 ± 0.002	-7.8 ± 0.2	18.15 ± 0.25	101.5 ± 1.2	9.38 ± 0.11
	Ti II	3383.683 ± 0.002	-7.6 ± 0.2	31.59 ± 0.30	116.8 ± 0.9	10.34 ± 0.08
	CH	3137.498 ± 0.002	-3.0 ± 0.2	3.42 ± 0.15	53.0 ± 3.9	5.07 ± 0.38
	CH	3143.106 ± 0.002	-4.2 ± 0.2	7.97 ± 0.09	44.9 ± 0.8	4.28 ± 0.08
HD166734	CH	3146.010 ± 0.001	-0.0 ± 0.1	22.87 ± 1.22	47.8 ± 3.4	4.55 ± 0.32
	CH	3627.328 ± 0.005	-6.2 ± 0.4	1.00 ± 0.17	61.3 ± 10.8	5.07 ± 0.89
	CH	3633.215 ± 0.002	-6.1 ± 0.1	1.41 ± 0.05	47.6 ± 3.8	3.93 ± 0.31
	CH	3636.148 ± 0.004	-6.1 ± 0.4	1.30 ± 0.61	68.3 ± 10.3	5.63 ± 0.85
	CH $^+$	3578.951 ± 0.004	-5.8 ± 0.3	1.24 ± 0.17	59.1 ± 9.8	4.95 ± 0.82
	CN	3579.367 ± 0.008	-7.2 ± 0.7	1.42 ± 0.61	100.5 ± 20.4	8.42 ± 1.71
	CN	3579.888 ± 0.006	-6.3 ± 0.5	1.07 ± 0.19	52.5 ± 13.6	4.40 ± 1.14
	OH	3078.388 ± 0.002	-5.1 ± 0.2	2.00 ± 0.17	38.9 ± 6.2	3.79 ± 0.61
	OH	3081.609 ± 0.002	-5.4 ± 0.2	1.85 ± 0.12	41.3 ± 4.7	4.02 ± 0.46
Na I	Na I	3302.239 ± 0.002	-11.7 ± 0.2	69.65 ± 0.29	81.8 ± 0.4	7.43 ± 0.04
		3302.333 ± 0.002	-3.1 ± 0.2	39.16 ± 0.07	60.0 ± 0.5	5.44 ± 0.05
		3302.453 ± 0.002	7.8 ± 0.2	23.49 ± 0.23	75.8 ± 1.0	6.88 ± 0.09
				[138.89 ± 1.24]		
	Na I	3302.847 ± 0.002	-11.9 ± 0.2	49.00 ± 0.16	78.2 ± 0.5	7.10 ± 0.04
Na I		3302.943 ± 0.002	-3.2 ± 0.2	33.56 ± 0.07	70.1 ± 0.6	6.37 ± 0.06
		3303.068 ± 0.002	8.1 ± 0.2	13.70 ± 0.12	69.2 ± 1.0	6.28 ± 0.09

TABLE 4 — *Continued*

Target	Species	λ_{helio} [Å]	v_{helio} [km s $^{-1}$]	W_λ [mÅ]	FWHM [mÅ]	FWHM [km s $^{-1}$]	
Ti II	3066.216	-13.5	[96.46 ± 0.59]	4.17 ± 0.66	89.1	8.71	
	3066.311	-4.2	1.41 ± 0.38	78.7		7.69	
	3066.418	6.2	7.33 ± 0.91	109.5		10.70	
Ti II	3072.845	-13.5	[15.24 ± 5.91]	6.77 ± 0.37	89.3	8.71	
	3072.941	-4.2	5.56 ± 0.24	78.8		7.69	
	3073.048	6.2	14.44 ± 0.50	109.7		10.70	
Ti II	3229.053	-13.5	[25.35 ± 3.41]	5.48 ± 0.26	93.8	8.71	
	3229.154	-4.2	2.35 ± 0.16	82.8		7.69	
	3229.266	6.2	11.08 ± 0.30	115.3		10.70	
Ti II	3241.848	-13.5	[23.56 ± 2.20]	14.06 ± 0.17	94.2	8.71	
	3241.948	-4.2	9.63 ± 0.11	83.2		7.69	
	3242.061	6.2	28.49 ± 0.23	115.7		10.70	
Ti II	3383.615 ± 0.001	-13.5 ± 0.1	[52.92 ± 1.21]	22.01 ± 0.47	98.3 ± 2.0	8.71 ± 0.18	
	3383.721 ± 0.002	-4.2 ± 0.2	14.79 ± 0.38	87.0 ± 4.4	7.71 ± 0.39		
	3383.839 ± 0.002	6.3 ± 0.2	45.09 ± 0.48	120.7 ± 1.5	10.70 ± 0.14		
HD167971	Na I	3302.239 ± 0.002	-11.7 ± 0.2	[86.20 ± 1.29]	49.86 ± 0.17	79.8 ± 0.5	7.24 ± 0.05
	3302.364 ± 0.002	-0.3 ± 0.2	29.03 ± 0.16	95.7 ± 1.6	8.69 ± 0.15		
	3302.495 ± 0.002	11.5 ± 0.2	41.18 ± 0.18	75.9 ± 0.6	6.89 ± 0.05		
	Na I	3302.848 ± 0.002	-11.8 ± 0.2	[116.34 ± 1.07]	31.89 ± 0.24	77.8 ± 1.2	7.06 ± 0.10
	3302.978 ± 0.001	-0.0 ± 0.1	18.64 ± 0.27	108.3 ± 4.4	9.83 ± 0.40		
	3303.109 ± 0.002	11.9 ± 0.2	25.37 ± 0.23	67.0 ± 1.1	6.08 ± 0.10		
	Ti II	3072.872	-10.9	[73.51 ± 1.51]	9.95 ± 1.01	114.3	11.15
	3072.983	-0.1	5.75 ± 0.45	89.9		8.77	
	3073.074	8.8	6.64 ± 0.89	105.4		10.28	
Ti II	3229.082	-10.9	[22.08 ± 5.45]	6.75 ± 0.30	120.1	11.15	
	3229.198	-0.1	3.66 ± 0.13	94.5		8.77	
	3229.294	8.8	4.09 ± 0.27	110.7		10.28	
Ti II	3241.876	-10.9	[14.58 ± 0.94]	20.58 ± 0.26	120.6	11.15	
	3241.993	-0.1	12.44 ± 0.11	94.8		8.77	
	3242.089	8.8	12.51 ± 0.22	111.2		10.28	
Ti II	3383.645 ± 0.002	-10.9 ± 0.2	[46.00 ± 1.16]	30.58 ± 0.64	125.7 ± 3.4	11.14 ± 0.30	
	3383.767 ± 0.003	-0.1 ± 0.2	20.36 ± 0.87	99.0 ± 6.8	8.77 ± 0.60		
	3383.868 ± 0.005	8.8 ± 0.4	19.73 ± 0.88	115.9 ± 6.3	10.27 ± 0.56		
HD169454	CH	3143.038 ± 0.002	-10.6 ± 0.2	[72.66 ± 1.02]	4.42 ± 0.26	62.4 ± 4.6	5.95 ± 0.44
	Fe I	3440.503 ± 0.003	-9.0 ± 0.2	1.61 ± 0.20	79.7 ± 6.3	6.95 ± 0.55	
	Na I	3302.262 ± 0.002	-9.6 ± 0.2	74.99 ± 0.18	93.1 ± 0.2	8.45 ± 0.02	
	Na I	3302.876 ± 0.002	-9.2 ± 0.2	50.76 ± 0.41	79.0 ± 0.7	7.17 ± 0.06	
	Ti II	3066.213	-13.8	[12.53 ± 4.42]	2.62 ± 0.75	104.9	10.26
	3066.271	-8.1	1.18 ± 0.00	55.6		5.44	
	3066.363	0.9	9.23 ± 1.09	145.3		14.20	
	Ti II	3072.842	-13.8	[31.36 ± 3.55]	7.02 ± 0.61	105.2	10.26
	3072.901	-8.1	2.28 ± 0.00	55.8		5.44	
	3072.993	0.9	22.91 ± 0.75	145.6		14.20	
Ti II	3229.050	-13.8	[105.37 ± 2.56]	5.04 ± 0.22	110.5	10.26	
	3229.112	-8.1	1.58 ± 0.00	58.6		5.44	
	3229.209	0.9	15.26 ± 0.31	153.0		14.20	
Ti II	3241.844	-13.8	[23.25 ± 0.93]	22.20 ± 0.22	111.0	10.26	
	3241.906	-8.1	3.65 ± 0.00	58.8		5.44	
	3242.004	0.9	49.83 ± 0.32	153.6		14.20	
Ti II	3383.612 ± 0.001	-13.8 ± 0.1	[102.54 ± 1.12]	25.12 ± 5.43	114.1 ± 1.7	10.11 ± 0.15	
	3383.678 ± 0.001	-8.0 ± 0.1	6.52 ± 1.68	60.0 ± 2.9	5.31 ± 0.26		
	3383.779 ± 0.002	0.9 ± 0.2	67.90 ± 0.86	160.1 ± 1.4	14.18 ± 0.13		
CH	3137.467 ± 0.001	-6.0 ± 0.1	[102.54 ± 1.12]	4.52 ± 0.27	60.6 ± 3.3	5.79 ± 0.31	
	3143.070 ± 0.002	-7.6 ± 0.2	11.01 ± 0.30	58.9 ± 1.7	5.62 ± 0.16		
	3145.899 ± 0.006	-10.6 ± 0.6	10.08 ± 1.53	88.5 ± 2.9	8.43 ± 0.28		
	3627.292 ± 0.003	-9.1 ± 0.3	0.54 ± 0.05	49.7 ± 7.8	4.11 ± 0.64		
	3633.179 ± 0.002	-9.1 ± 0.2	1.73 ± 0.10	56.1 ± 4.4	4.63 ± 0.36		
	3636.110 ± 0.004	-9.2 ± 0.3	1.16 ± 0.13	60.3 ± 9.6	4.97 ± 0.79		

TABLE 4 — *Continued*

Target	Species	λ_{helio} [Å]	v_{helio} [km s $^{-1}$]	W_λ [mÅ]	[mÅ]	FWHM [km s $^{-1}$]
HD170235	CN	3579.344 ± 0.002	-9.1 ± 0.2	2.97 ± 0.07	47.5 ± 1.9	3.98 ± 0.16
	CN	3579.852 ± 0.002	-9.3 ± 0.2	7.65 ± 0.11	47.3 ± 1.2	3.96 ± 0.10
	CN	3580.835 ± 0.003	-8.5 ± 0.3	1.84 ± 0.19	66.5 ± 7.3	5.57 ± 0.61
	NH	3353.828 ± 0.006	-8.6 ± 0.5	1.79 ± 0.41	47.8 ± 15.7	4.27 ± 1.40
	NH	3357.954 ± 0.002	-8.8 ± 0.2	2.72 ± 0.04	48.1 ± 1.5	4.29 ± 0.13
	OH	3071.942 ± 0.008	-6.6 ± 0.8	2.65 ± 0.44	97.9 ± 19.1	9.56 ± 1.86
	OH	3078.353 ± 0.001	-8.4 ± 0.1	6.24 ± 0.25	60.0 ± 3.5	5.84 ± 0.34
	OH	3081.577 ± 0.002	-8.5 ± 0.2	2.90 ± 0.22	42.6 ± 5.8	4.14 ± 0.56
	Na I	3302.345 ± 0.002	-2.1 ± 0.2	30.23 ± 0.60	98.7 ± 2.1	8.96 ± 0.20
	Na I	3302.953 ± 0.001	-2.3 ± 0.1	16.32 ± 0.41	95.4 ± 3.1	8.66 ± 0.28
	Ti II	3072.877 ± 0.005	-10.4 ± 0.5	13.01 ± 1.35	116.4 ± 12.7	11.36 ± 1.24
	Ti II	3229.088 ± 0.006	-10.3 ± 0.5	9.84 ± 1.30	170.3 ± 13.5	15.81 ± 1.25
	Ti II	3241.884 ± 0.002	-10.2 ± 0.2	19.27 ± 0.49	102.5 ± 2.2	9.47 ± 0.20
	Ti II	3383.656 ± 0.002	-10.0 ± 0.2	34.91 ± 0.58	122.9 ± 1.6	10.89 ± 0.14
HD170740	Na I	3302.258 ± 0.002	-10.0 ± 0.2	39.08 ± 0.13	68.5 ± 0.3	6.22 ± 0.03
	Na I	3302.871 ± 0.002	-9.7 ± 0.2	27.19 ± 0.17	70.4 ± 0.6	6.39 ± 0.05
	Ti II	3228.956	-22.6	0.83 ± 0.13	68.6	6.37
		3229.052	-13.7	1.87 ± 0.18	65.0	6.03
				[2.27 ± 0.72]		
HD171432	Ti II	3241.750	-22.6	3.61 ± 0.16	68.9	6.37
		3241.846	-13.7	6.29 ± 0.16	65.2	6.03
	Ti II	3383.513 ± 0.003	-22.6 ± 0.2	4.15 ± 0.31	73.1 ± 6.7	6.48 ± 0.59
		3383.614 ± 0.002	-13.7 ± 0.2	10.87 ± 0.18	68.0 ± 2.3	6.02 ± 0.20
				[14.92 ± 0.62]		
	CH	3137.464 ± 0.003	-6.3 ± 0.3	2.16 ± 0.16	48.5 ± 6.4	4.64 ± 0.61
	CH	3143.064 ± 0.002	-8.2 ± 0.2	6.56 ± 0.22	61.3 ± 2.2	5.85 ± 0.21
	CH	3145.903 ± 0.003	-10.2 ± 0.3	4.49 ± 0.48	61.8 ± 8.0	5.89 ± 0.76
	CH	3633.167 ± 0.005	-10.1 ± 0.4	0.84 ± 0.09	52.6 ± 11.2	4.34 ± 0.93
	CN	3579.858 ± 0.002	-8.8 ± 0.1	2.09 ± 0.12	54.0 ± 4.2	4.52 ± 0.35
HD172028	Na I	3302.121 ± 0.002	-22.4 ± 0.2	8.53 ± 0.11	55.5 ± 1.4	5.04 ± 0.13
		3302.301 ± 0.002	-6.1 ± 0.2	37.61 ± 0.19	91.3 ± 0.7	8.29 ± 0.06
		3302.198 ± 0.002	-15.4 ± 0.2	4.85 ± 0.05	50.0 ± 2.4	4.54 ± 0.21
				[45.48 ± 1.63]		
	Na I	3302.731 ± 0.002	-22.4 ± 0.2	3.71 ± 0.09	50.1 ± 2.3	4.55 ± 0.21
		3302.913 ± 0.002	-5.9 ± 0.2	19.60 ± 0.13	85.7 ± 1.0	7.78 ± 0.09
		3302.812 ± 0.002	-15.1 ± 0.2	1.95 ± 0.05	-47.1 ± 4.5	-4.28 ± 0.41
				[17.32 ± 1.45]		
	Ti II	3072.831	-14.9	15.83 ± 0.81	173.7	16.94
		3072.931	-5.2	6.05 ± 0.28	105.8	10.32
HD172028	Ti II	3229.038	-14.9	7.13 ± 0.33	182.5	16.94
		3229.143	-5.2	4.00 ± 0.18	111.2	10.32
				[11.44 ± 0.90]		
	Ti II	3241.833	-14.9	33.49 ± 0.31	183.2	16.94
		3241.938	-5.2	12.77 ± 0.12	111.6	10.32
				[64.31 ± 1.75]		
	Ti II	3383.600 ± 0.002	-14.9 ± 0.2	38.68 ± 0.36	191.7 ± 1.6	16.98 ± 0.14
		3383.710 ± 0.002	-5.2 ± 0.2	16.68 ± 0.20	116.9 ± 1.7	10.36 ± 0.15
				[55.46 ± 0.70]		
	CH	3143.089 ± 0.004	-5.8 ± 0.4	3.39 ± 0.53	78.1 ± 9.8	7.45 ± 0.93
HD172028	CH	3145.894 ± 0.005	-11.1 ± 0.4	11.00 ± 1.37	40.5 ± 11.8	3.86 ± 1.13
		3145.958 ± 0.045	-4.9 ± 4.3	3.39 ± 1.76	66.1 ± 19.0	6.29 ± 1.81
		3146.040 ± 0.004	2.9 ± 0.4	8.65 ± 1.23	33.0 ± 9.9	3.15 ± 0.94
				[22.22 ± 7.10]		
	CH	3633.192 ± 0.007	-8.0 ± 0.5	0.77 ± 0.13	74.1 ± 15.7	6.12 ± 1.29
	OH	3078.380 ± 0.003	-5.9 ± 0.3	2.51 ± 0.18	55.9 ± 6.5	5.45 ± 0.63
	Cr I	3593.383 ± 0.006	-8.2 ± 0.5	1.71 ± 0.22	119.5 ± 14.2	9.97 ± 1.19
	Fe I	3440.485 ± 0.002	-10.5 ± 0.2	8.08 ± 0.16	93.9 ± 2.2	8.18 ± 0.19
	Na I	3302.257 ± 0.002	-10.1 ± 0.2	107.48 ± 0.41	107.9 ± 0.5	9.79 ± 0.04
	Na I	3302.868 ± 0.002	-10.0 ± 0.2	81.63 ± 0.21	92.9 ± 0.3	8.43 ± 0.03
HD172028	Ti II	3229.025	-16.2	2.96 ± 0.83	130.2	12.09
		3229.107	-8.5	0.68 ± 0.16	60.1	5.58
				[3.32 ± 0.86]		
	Ti II	3241.819	-16.2	11.68 ± 0.37	130.8	12.09
		3241.902	-8.5	3.15 ± 0.13	60.3	5.58
				[15.43 ± 1.04]		
	Ti II	3383.585 ± 0.003	-16.2 ± 0.3	19.46 ± 0.58	135.2 ± 5.5	11.98 ± 0.48
		3383.672 ± 0.002	-8.5 ± 0.2	3.66 ± 0.24	63.7 ± 6.8	5.64 ± 0.60
				[23.18 ± 0.52]		
	CH	3137.457 ± 0.002	-7.0 ± 0.2	5.81 ± 0.35	68.3 ± 4.6	6.53 ± 0.44
HD172028	CH	3143.057 ± 0.002	-8.8 ± 0.2	15.59 ± 0.30	67.1 ± 1.7	6.40 ± 0.16
	CH	3145.887 ± 0.006	-11.7 ± 0.6	11.46 ± 1.67	78.1 ± 13.9	7.44 ± 1.32
	CH	3627.252 ± 0.011	-12.5 ± 0.9	1.88 ± 0.44	144.2 ± 25.1	11.92 ± 2.08
	CH	3633.165 ± 0.002	-10.2 ± 0.2	2.92 ± 0.16	76.6 ± 5.6	6.32 ± 0.46

TABLE 4 — *Continued*

Target	Species	λ_{helio} [Å]	v_{helio} [km s $^{-1}$]	W_λ [mÅ]	[mÅ]	FWHM [km s $^{-1}$]
HD182985	CH	3636.085 ± 0.004	-11.3 ± 0.3	1.79 ± 0.16	69.3 ± 8.6	5.71 ± 0.71
	CN	3579.333 ± 0.004	-10.0 ± 0.3	1.18 ± 0.12	48.9 ± 9.0	4.10 ± 0.76
	CN	3579.842 ± 0.002	-10.1 ± 0.1	4.92 ± 0.19	72.0 ± 4.2	6.03 ± 0.35
	OH	3071.912 ± 0.006	-9.6 ± 0.6	7.27 ± 0.98	119.6 ± 14.3	11.67 ± 1.40
	OH	3078.355 ± 0.004	-8.3 ± 0.4	5.05 ± 0.50	71.8 ± 10.5	6.99 ± 1.03
	OH	3081.562 ± 0.003	-10.0 ± 0.3	4.09 ± 0.35	65.5 ± 7.9	6.37 ± 0.77
	Na I	3302.346 ± 0.002	-2.0 ± 0.2	14.10 ± 0.22	54.6 ± 1.3	4.96 ± 0.12
	Na I	3302.958 ± 0.002	-1.8 ± 0.2	8.58 ± 0.13	55.9 ± 1.3	5.07 ± 0.12
	Ti II	3241.766	-21.0	0.66 ± 0.02	61.6	5.70
		3241.864	-12.0	0.53 ± 0.00	50.3	4.65
		3241.967	-2.5	2.28 ± 0.17	59.9	5.54
				[5.11 ± 1.28]		
	Ti II	3383.531 ± 0.003	-21.0 ± 0.3	1.15 ± 0.06	65.1 ± 7.0	5.77 ± 0.62
		3383.633 ± 0.003	-12.0 ± 0.3	0.82 ± 0.04	52.9 ± 7.5	4.68 ± 0.66
		3383.740 ± 0.002	-2.5 ± 0.2	3.12 ± 0.07	62.8 ± 2.4	5.57 ± 0.21
HD183143	CH	3143.139 ± 0.002	-1.0 ± 0.2	5.09 ± 0.35	74.8 ± 5.7	7.14 ± 0.55
	CH	3145.975 ± 0.004	-3.3 ± 0.4	2.89 ± 0.37	59.9 ± 9.6	5.70 ± 0.91
	CN	3579.928 ± 0.003	-3.0 ± 0.2	1.48 ± 0.10	56.2 ± 6.7	4.70 ± 0.56
	OH	3078.423 ± 0.005	-1.6 ± 0.5	2.75 ± 0.45	60.5 ± 12.4	5.90 ± 1.21
	Fe I	3440.482 ± 0.006	-10.8 ± 0.5	2.09 ± 0.23	92.6 ± 13.6	8.07 ± 1.19
		3440.676 ± 0.007	6.2 ± 0.6	2.31 ± 0.28	116.3 ± 2.4	10.13 ± 0.21
				[5.17 ± 1.48]		
	Na I	3302.259 ± 0.002	-9.9 ± 0.2	51.33 ± 0.26	81.1 ± 0.5	7.36 ± 0.05
		3302.429 ± 0.002	5.5 ± 0.2	48.68 ± 0.26	74.1 ± 0.5	6.73 ± 0.04
				[90.99 ± 3.12]		
	Na I	3302.870 ± 0.002	-9.8 ± 0.2	34.37 ± 0.45	84.8 ± 1.2	7.70 ± 0.11
		3303.039 ± 0.002	5.6 ± 0.2	34.73 ± 0.36	72.7 ± 0.9	6.60 ± 0.08
				[58.22 ± 6.45]		
	Ti II	3072.879	-10.2	10.11 ± 1.00	145.7	14.21
		3072.981	-0.2	2.81 ± 0.15	62.3	6.08
		3073.063	7.7	10.21 ± 0.78	106.9	10.43
HD188220	Ti II	3229.089	-10.2	5.82 ± 0.85	153.1	14.21
		3229.196	-0.2	2.44 ± 0.12	65.5	6.08
		3229.282	7.7	5.24 ± 0.62	112.4	10.43
				[26.38 ± 4.31]		
	Ti II	3241.883	-10.2	19.86 ± 0.32	153.7	14.21
		3241.991	-0.2	8.36 ± 0.04	65.8	6.08
		3242.077	7.7	16.17 ± 0.22	112.8	10.43
				[45.30 ± 1.60]		
	Ti II	3383.653 ± 0.002	-10.2 ± 0.2	33.94 ± 0.87	160.1 ± 4.1	14.19 ± 0.37
		3383.765 ± 0.002	-0.2 ± 0.2	12.40 ± 0.38	68.9 ± 2.5	6.10 ± 0.22
		3383.855 ± 0.002	7.7 ± 0.2	28.05 ± 0.23	117.8 ± 0.2	10.43 ± 0.02
				[86.06 ± 1.69]		
	CH	3137.434 ± 0.024	-9.1 ± 2.3	0.93 ± 0.64	60.6 ± 20.9	5.79 ± 2.00
		3137.610 ± 0.002	7.6 ± 0.2	2.60 ± 0.52	52.2 ± 16.8	4.99 ± 1.61
				[2.28 ± 3.44]		
HD205637	CH	3143.062 ± 0.006	-8.4 ± 0.6	5.45 ± 1.15	84.7 ± 14.3	8.08 ± 1.37
		3143.225 ± 0.003	7.1 ± 0.2	8.44 ± 0.59	61.0 ± 6.0	5.82 ± 0.57
				[14.07 ± 2.59]		
	CH	3145.884 ± 0.009	-12.0 ± 0.9	7.08 ± 1.12	107.7 ± 12.4	10.26 ± 1.18
		3146.054 ± 0.006	4.2 ± 0.6	9.58 ± 1.14	98.6 ± 13.6	9.40 ± 1.29
				[17.62 ± 3.74]		
	CH	3633.362 ± 0.004	6.0 ± 0.4	2.13 ± 0.22	77.9 ± 10.5	6.43 ± 0.87
	CH ⁺	3578.892 ± 0.009	-10.7 ± 0.7	2.37 ± 0.49	80.0 ± 20.2	6.70 ± 1.70
		3579.081 ± 0.006	5.1 ± 0.5	3.02 ± 0.47	77.8 ± 15.2	6.52 ± 1.27
				[5.67 ± 1.60]		
	Na I	3302.284 ± 0.002	-7.6 ± 0.2	26.97 ± 0.20	58.6 ± 0.6	5.32 ± 0.05
	Na I	3302.894 ± 0.002	-7.6 ± 0.2	18.33 ± 0.12	62.9 ± 0.6	5.71 ± 0.05
	Ti II	3066.167 ± 0.007	-18.3 ± 0.7	111.50 ± 7.59	509.8 ± 17.7	49.84 ± 1.73
	Ti II	3241.844 ± 0.002	-13.9 ± 0.2	73.39 ± 1.44	526.9 ± 5.6	48.73 ± 0.52
	Ti II	3383.598 ± 0.002	-15.1 ± 0.2	78.94 ± 1.22	529.4 ± 4.4	46.91 ± 0.39
	CH	3137.479 ± 0.002	-4.9 ± 0.2	1.10 ± 0.08	34.1 ± 5.5	3.26 ± 0.53
	CH	3143.080 ± 0.002	-6.7 ± 0.2	5.65 ± 0.26	56.9 ± 4.0	5.43 ± 0.38
	CH	3145.905 ± 0.006	-10.0 ± 0.6	3.73 ± 0.55	58.1 ± 14.2	5.53 ± 1.35
	CH	3627.305 ± 0.005	-8.1 ± 0.4	0.90 ± 0.10	67.3 ± 12.2	5.56 ± 1.01
	CH	3633.180 ± 0.003	-9.0 ± 0.3	1.64 ± 0.15	84.8 ± 7.4	7.00 ± 0.61
	CN	3579.856 ± 0.010	-8.9 ± 0.8	0.96 ± 0.21	58.6 ± 22.6	4.91 ± 1.89
	Na I	3302.244 ± 0.003	-11.2 ± 0.3	1.92 ± 0.28	73.9 ± 8.2	6.71 ± 0.74
	Ti II	3072.777	-20.2	3.47 ± 0.21	66.5	6.49
		3072.927	-5.6	3.74 ± 0.43	119.6	11.67
				[8.00 ± 1.50]		
	Ti II	3241.776	-20.2	3.27 ± 0.17	70.2	6.49
		3241.933	-5.6	4.85 ± 0.29	126.2	11.67

TABLE 4 — *Continued*

Target	Species	λ_{helio} [Å]	v_{helio} [km s $^{-1}$]	W_λ [mÅ]	FWHM	
				[mÅ]	[km s $^{-1}$]	
HD210121	Ti II	3383.541 ± 0.001	-20.2 ± 0.1	[8.49 ± 1.16] 5.60 ± 0.13	73.3 ± 3.1	6.49 ± 0.27
		3383.705 ± 0.002	-5.6 ± 0.2	9.01 ± 0.29 [14.52 ± 0.82]	130.9 ± 4.8	11.60 ± 0.42
	Fe I	3440.436 ± 0.005	-14.8 ± 0.4	1.13 ± 0.24	69.6 ± 12.1	6.06 ± 1.06
	Na I	3302.213 ± 0.002	-14.0 ± 0.2	48.38 ± 0.15	66.9 ± 0.3	6.08 ± 0.03
	Na I	3302.826 ± 0.002	-13.8 ± 0.2	38.64 ± 0.10	65.0 ± 0.2	5.90 ± 0.02
	Ti II	3072.835	-14.5	4.06 ± 0.43	71.6	6.98
		3072.948	-3.5	5.58 ± 0.70	105.1	10.25
	Ti II	3229.043	-14.5	[14.06 ± 3.50] 1.95 ± 0.15	75.2	6.98
		3229.161	-3.5	2.03 ± 0.27	110.4	10.25
	Ti II	3241.837	-14.5	[3.59 ± 0.73] 5.12 ± 0.13	75.5	6.98
		3241.956	-3.5	7.59 ± 0.19	110.9	10.25
HD36861	Ti II	3383.605 ± 0.001	-14.5 ± 0.1	[12.07 ± 0.82] 9.13 ± 0.10	78.9 ± 2.3	6.99 ± 0.20
		3383.728 ± 0.001	-3.5 ± 0.1	15.60 ± 0.27 [25.31 ± 0.68]	115.5 ± 2.7	10.23 ± 0.24
	CH	3137.414 ± 0.002	-11.1 ± 0.2	3.31 ± 0.24	49.6 ± 4.6	4.73 ± 0.44
	CH	3143.018 ± 0.002	-12.5 ± 0.2	8.31 ± 0.19	57.6 ± 2.0	5.49 ± 0.19
	CH	3145.852 ± 0.005	-15.0 ± 0.4	6.13 ± 0.96	64.0 ± 10.9	6.10 ± 1.03
	CH	3627.215 ± 0.014	-15.5 ± 1.2	1.15 ± 0.26	138.3 ± 33.9	11.43 ± 2.80
	CH	3633.116 ± 0.002	-14.3 ± 0.2	1.28 ± 0.06	61.9 ± 5.2	5.11 ± 0.43
	CH	3636.071 ± 0.004	-12.4 ± 0.3	1.23 ± 0.13	102.1 ± 8.6	8.42 ± 0.71
	CN	3579.282 ± 0.003	-14.3 ± 0.2	2.10 ± 0.14	93.1 ± 6.2	7.80 ± 0.52
	CN	3579.797 ± 0.002	-13.9 ± 0.2	4.42 ± 0.10	68.1 ± 2.1	5.70 ± 0.17
HD67536	NH	3357.908 ± 0.003	-12.9 ± 0.2	1.77 ± 0.17	61.6 ± 6.6	5.50 ± 0.59
	OH	3078.314 ± 0.002	-12.3 ± 0.2	4.45 ± 0.28	66.4 ± 5.6	6.46 ± 0.55
	OH	3081.519 ± 0.003	-14.1 ± 0.3	3.03 ± 0.23	51.9 ± 6.2	5.05 ± 0.60
	Na I	3302.646 ± 0.002	25.2 ± 0.2	12.83 ± 0.13	58.4 ± 0.9	5.30 ± 0.08
	Na I	3303.257 ± 0.002	25.3 ± 0.2	7.79 ± 0.15	65.4 ± 1.6	5.94 ± 0.15
	Ti II	3073.038	5.3	0.18 ± 0.15	52.8	5.15
		3073.131	14.3	2.23 ± 0.18	64.6	6.30
		3073.219	23.0	2.70 ± 0.18	64.3	6.27
	Ti II	3229.256	5.3	[5.38 ± 1.18] 0.27 ± 0.12	55.5	5.15
		3229.354	14.3	0.85 ± 0.11	67.9	6.30
HD68761	Ti II	3229.446	23.0	2.07 ± 0.11 [3.22 ± 0.37]	67.5	6.27
	Ti II	3242.052	5.3	0.82 ± 0.15	55.7	5.15
		3242.149	14.3	3.48 ± 0.15	68.1	6.30
		3242.242	23.0	6.06 ± 0.15	67.8	6.27
	Ti II	3383.828 ± 0.002	5.3 ± 0.2	[10.36 ± 0.74] 1.81 ± 0.07	58.4 ± 4.5	5.18 ± 0.39
		3383.930 ± 0.002	14.3 ± 0.2	6.05 ± 0.05	71.2 ± 2.7	6.31 ± 0.24
		3384.027 ± 0.002	23.0 ± 0.2	10.98 ± 0.10	75.8 ± 1.4	6.71 ± 0.12
	NH	3354.172 ± 0.002	22.1 ± 0.2	[18.89 ± 0.31] 1.48 ± 0.24	11.8 ± 0.2	1.05 ± 0.02
		3354.222 ± 0.002	26.6 ± 0.2	2.43 ± 0.04	33.2 ± 0.5	2.97 ± 0.04
HD94963	Na I	3302.528 ± 0.002	14.6 ± 0.2	[5.34 ± 0.85] 4.86 ± 0.23	95.0 ± 5.6	8.63 ± 0.51
	Na I	3303.132 ± 0.004	14.0 ± 0.4	4.56 ± 0.29	140.1 ± 11.5	12.71 ± 1.04
	Ti II	3073.148 ± 0.006	16.0 ± 0.6	12.33 ± 1.75	226.5 ± 14.9	22.10 ± 1.45
	Ti II	3229.364 ± 0.005	15.3 ± 0.5	2.91 ± 0.41	128.9 ± 12.9	11.97 ± 1.20
	Ti II	3242.159 ± 0.001	15.2 ± 0.1	9.74 ± 0.25	106.1 ± 2.8	9.81 ± 0.26
	Ti II	3383.937 ± 0.002	15.0 ± 0.2	14.38 ± 0.18	113.9 ± 1.5	10.09 ± 0.13
	CH	3146.202 ± 0.002	18.3 ± 0.2	4.61 ± 0.11	40.4 ± 1.7	3.85 ± 0.16
		3146.350 ± 0.002	32.4 ± 0.2	11.97 ± 0.13	38.6 ± 0.7	3.68 ± 0.06
	Ti II	3229.464 ± 0.005	24.6 ± 0.5	[16.07 ± 0.87] 5.95 ± 0.53	162.0 ± 12.5	15.04 ± 1.16
	Ti II	3242.300 ± 0.001	28.3 ± 0.1	21.69 ± 0.57	186.6 ± 3.4	17.25 ± 0.31
HD94963	Ti II	3384.061 ± 0.002	26.0 ± 0.2	23.72 ± 0.82	141.8 ± 4.3	12.57 ± 0.38
	CH	3137.745 ± 0.005	20.5 ± 0.5	1.17 ± 0.15	48.5 ± 11.1	4.64 ± 1.06
	CH	3143.355 ± 0.002	19.6 ± 0.2	2.92 ± 0.29	52.3 ± 5.7	4.99 ± 0.54
	CH	3146.102 ± 0.005	8.7 ± 0.4	4.97 ± 1.54	47.4 ± 10.5	4.51 ± 1.00
		3146.226 ± 0.002	20.6 ± 0.2	8.34 ± 0.67	35.8 ± 4.2	3.41 ± 0.40
HD94963	Na I	3302.481 ± 0.002	10.2 ± 0.2	[13.48 ± 4.66] 10.55 ± 0.19	50.3 ± 1.3	4.57 ± 0.12
	Na I	3303.092 ± 0.002	10.4 ± 0.2	5.55 ± 0.14	45.5 ± 2.0	4.13 ± 0.18
	Ti II	3072.899	-8.3	16.04 ± 1.10	200.3	19.54
		3073.091	10.5	3.98 ± 0.32	64.1	6.25

TABLE 4 — *Continued*

Target	Species	λ_{helio} [Å]	v_{helio} [km s $^{-1}$]	W_{λ} [mÅ]	FWHM [mÅ]	FWHM [km s $^{-1}$]
Ti II	3229.109	-8.3	[21.18 ± 4.79]	10.52 ± 1.36	210.5	19.54
	3229.312	10.5		2.99 ± 0.41	67.3	6.25
Ti II	3241.904	-8.3	[13.89 ± 4.12]	33.98 ± 0.79	211.3	19.54
	3242.107	10.5		8.83 ± 0.25	67.6	6.25
Ti II	3383.674 ± 0.002	-8.3 ± 0.2	[42.56 ± 3.03]	52.85 ± 0.63	220.6 ± 2.4	19.54 ± 0.21
	3383.886 ± 0.002	10.5 ± 0.2		13.92 ± 0.14	70.6 ± 0.2	6.26 ± 0.02
HD96917	Na I	3302.197 ± 0.002	-15.5 ± 0.2	[67.30 ± 1.29]	61.6 ± 0.4	5.59 ± 0.04
		3302.285 ± 0.002	-7.5 ± 0.2	42.18 ± 0.13	57.9 ± 1.3	5.26 ± 0.12
		3302.373 ± 0.001	0.5 ± 0.1	15.67 ± 0.09	56.9 ± 3.0	5.16 ± 0.27
		3302.460 ± 0.002	8.4 ± 0.2	6.75 ± 0.10	62.8 ± 6.1	5.70 ± 0.56
		3302.647 ± 0.002	25.4 ± 0.1	3.19 ± 0.15	91.1 ± 3.7	8.27 ± 0.34
	Na I	3302.806 ± 0.002	-15.6 ± 0.2	[66.31 ± 2.53]	6.88 ± 0.26	
		3302.893 ± 0.003	-7.7 ± 0.2	27.85 ± 0.45	54.9 ± 1.8	4.98 ± 0.16
		3302.990 ± 0.005	1.1 ± 0.5	9.82 ± 0.43	64.9 ± 7.2	5.89 ± 0.66
		3303.066 ± 0.018	8.0 ± 1.6	2.76 ± 0.28	45.4 ± 13.5	4.12 ± 1.22
		3303.260 ± 0.008	25.6 ± 0.7	1.10 ± 0.35	54.4 ± 41.3	4.94 ± 3.75
Ti II	3066.239	-11.2	[44.07 ± 5.02]	5.34 ± 1.63	170.5	16.67
	3066.302	-5.1		3.25 ± 0.16	81.8	8.00
	3066.404	4.9		4.90 ± 1.17	130.3	12.74
Ti II	3072.869	-11.2	[14.92 ± 7.15]	10.03 ± 1.23	170.9	16.67
	3072.932	-5.1		10.26 ± 0.13	82.0	8.00
	3073.034	4.9		13.84 ± 0.82	130.6	12.74
Ti II	3229.078	-11.2	[33.21 ± 4.91]	5.53 ± 0.66	179.6	16.67
	3229.144	-5.1		5.56 ± 0.08	86.2	8.00
	3229.251	4.9		10.04 ± 0.39	137.2	12.74
Ti II	3241.873	-11.2	[20.65 ± 2.08]	18.39 ± 0.56	180.3	16.67
	3241.939	-5.1		17.10 ± 0.06	86.5	8.00
	3242.047	4.9		29.45 ± 0.34	137.8	12.74
Ti II	3383.641 ± 0.002	-11.2 ± 0.2	[67.58 ± 2.44]	28.96 ± 1.65	188.7 ± 9.7	16.72 ± 0.86
	3383.710 ± 0.002	-5.1 ± 0.2		25.18 ± 0.97	90.4 ± 5.0	8.01 ± 0.44
	3383.823 ± 0.003	4.9 ± 0.3		47.82 ± 1.75	143.9 ± 6.0	12.75 ± 0.53
CH	3142.995 ± 0.002	-14.7 ± 0.2	[106.15 ± 2.24]	3.21 ± 0.14	53.9 ± 4.5	5.14 ± 0.43
	3145.822 ± 0.005	-17.9 ± 0.5		3.28 ± 0.63	54.1 ± 11.7	5.16 ± 1.11

The equivalent widths listed are determined analytically from the Gaussian parameters. However, for multi-component features, we also integrate across the entire profile – this value is enclosed in square parentheses. In the case of the Ti II lines, we have first measured the strongest feature at 3383.768Å, and then fixed the widths and central velocities of components when fitting the other Ti II transitions. For these lines, the uncertainties will correspond to the uncertainties of the 3383.768Å feature, and therefore are not repeated in the table. The measurements of the 3146.010Å CH line should be taken with caution – we noticed systematic issues here: the wavelength calibration, and perhaps other reduction issues have compromised this region.

Fig. Set 14. Comparison of geocentric, heliocentric, interstellar, and stellar rest frame superspectra

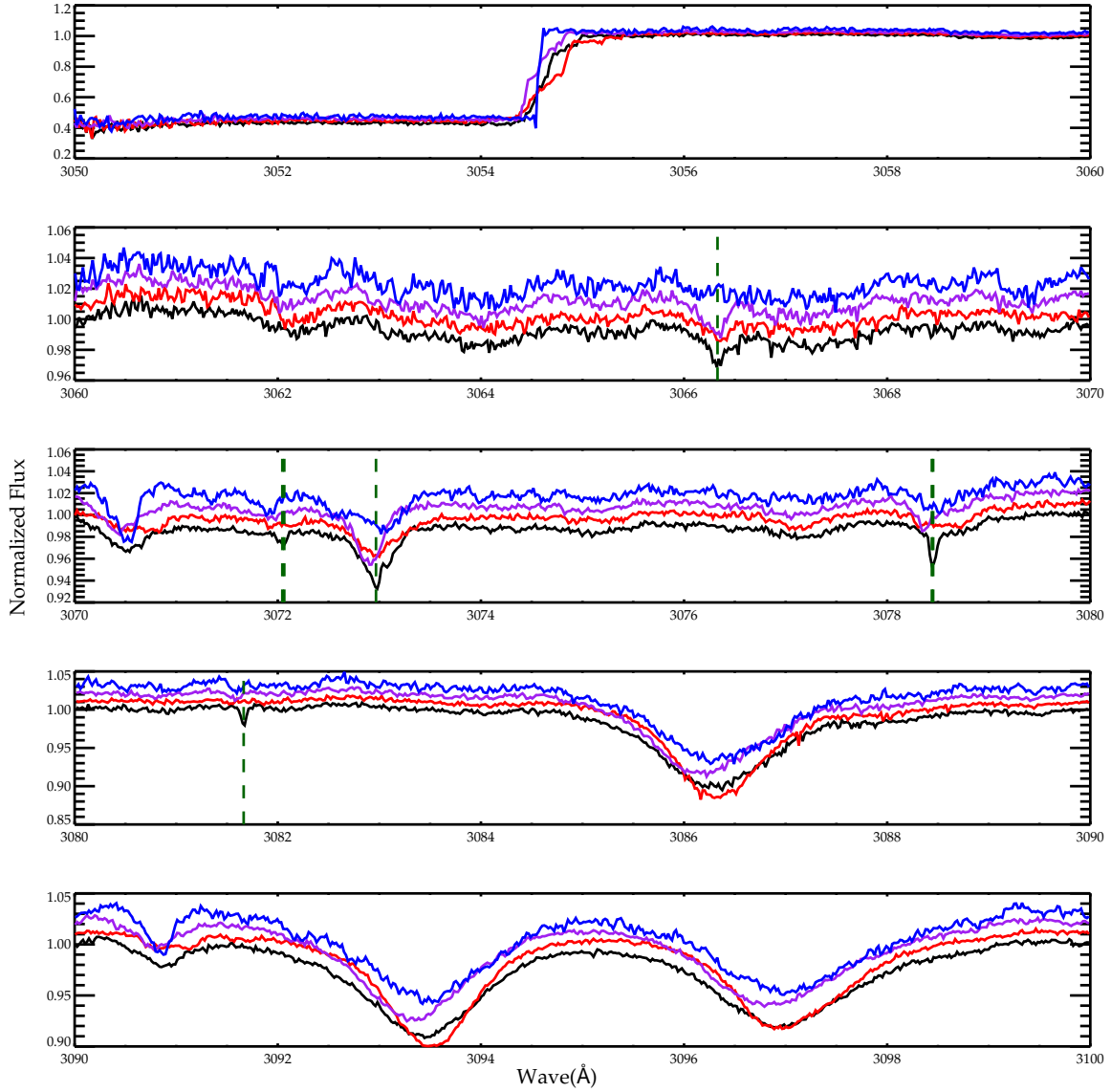


FIG. 14.— From top to bottom, the reddened superspectra (comprised of all 51 targets) are compared: geocentric (top; blue); heliocentric (purple); stellar (red); interstellar (bottom; black). Known interstellar lines (if any) are indicated with green vertical line, and features which appear interstellar in nature (if any) are shown with a red vertical line. Figures 14.1–14.13 are available in the online version of the Journal.

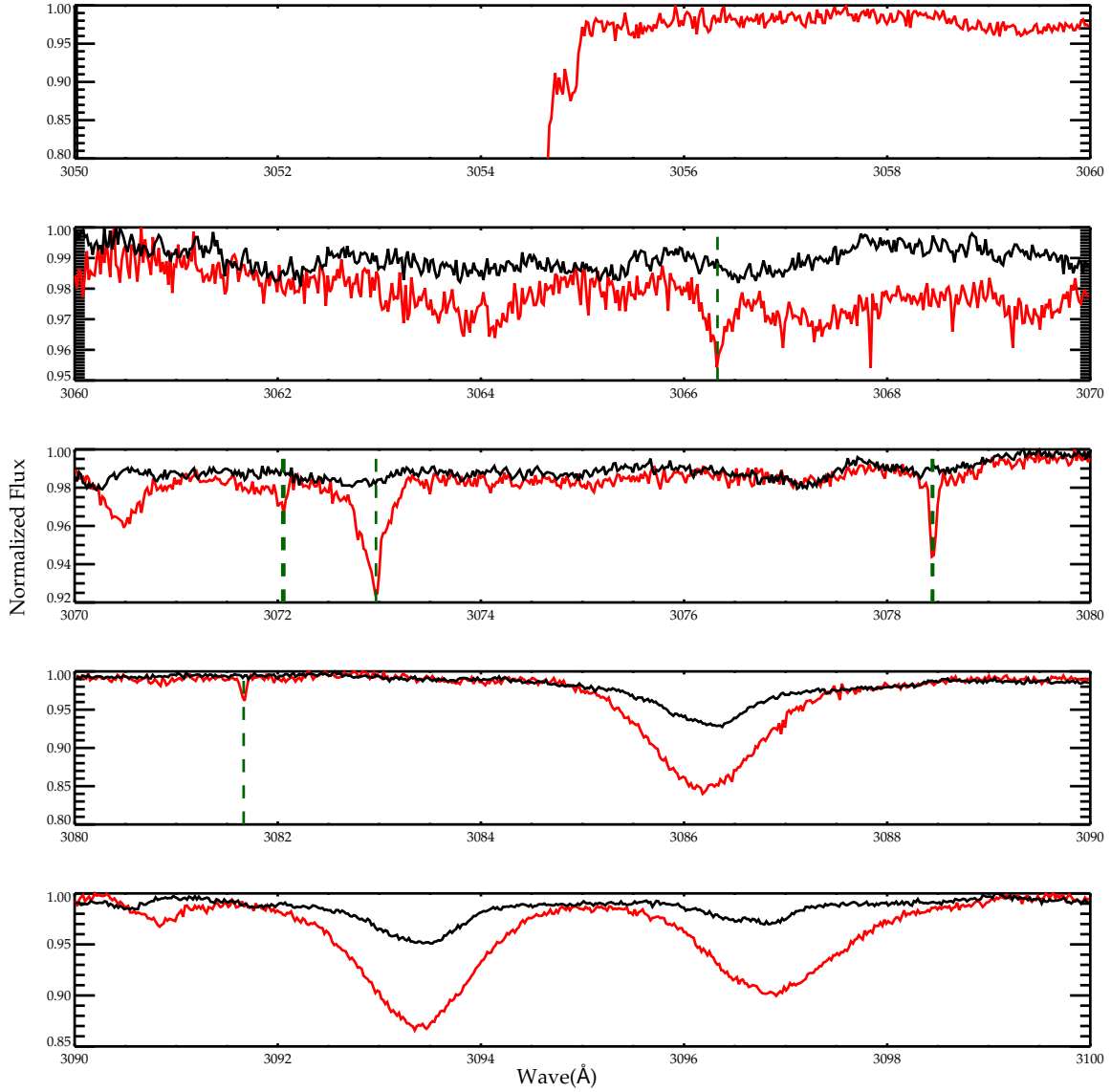
Fig. Set 15. Comparison of unreddened and reddened interstellar rest frame superspectra

FIG. 15.— A co-add of reddened targets (red) with good spectral standards (black) in steps of 10 \AA . Known interstellar lines (if any) are indicated with green vertical line, and features which appear interstellar in nature (if any) are shown with a red vertical line. Figures 15.1–15.13 are available in the online version of the Journal.

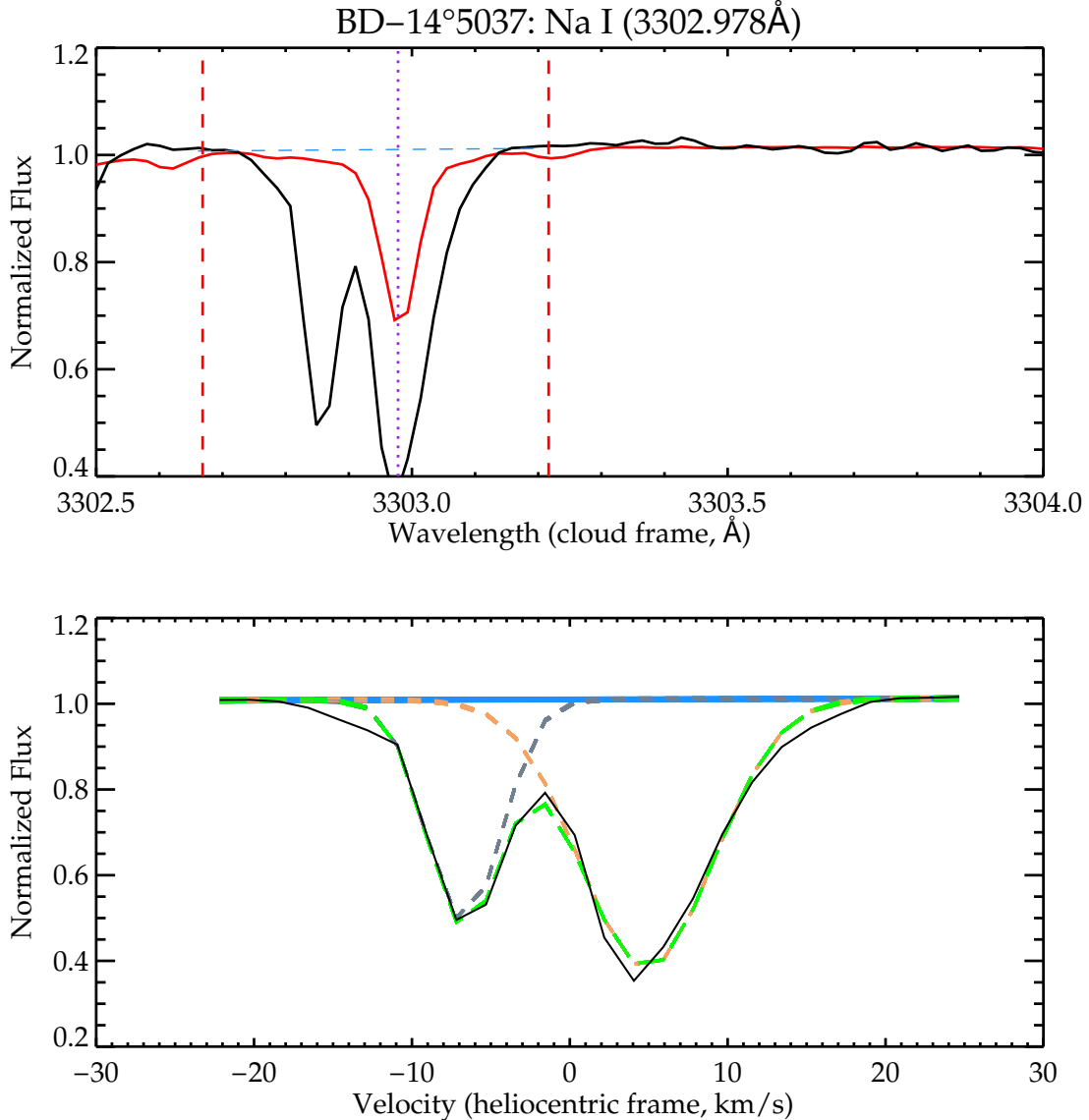
Fig. Set 16. Line of Sight Measurements

FIG. 16.— An example measurement of one of the Na I lines in BD-14°5037 is shown. The top panel shows the target spectrum (black), and the interstellar superspectrum of all 51 reddened targets (red), in the interstellar rest frame. The red vertical lines bracket the feature of interest, whose rest wavelength is shown with the dotted purple line. The continuum for the feature is shown with a horizontal blue line. The bottom panel depicts the Monte Carlo process on the region of interest in heliocentric velocity space of the target spectrum (black): the blue horizontal lines are the repositioned continua (based on the local S/N); the green swaths are the best fits; and the dashed neutral coloured swaths are the Gaussian decompositions. Figures 16.1-16.536 are available in the online version of the Journal.